OZONE DYNAMICS AND SEASONAL VARIABILITY OVER AFRICA

By

Kassahun Ture

SUBMITTED IN PARTIAL FULFILLMENT OF THE
REQUIREMENTS FOR THE DEGREE OF
DOCTOR OF PHILOSOPHY IN PHYSICS
AT
ADDIS ABABA UNIVERSITY
ADDIS ABABA, ETHIOPIA
JULY 2011

ADDIS ABABA UNIVERSITY

DEPARTMENT OF PHYSCS

Ph.D. degree:

Supervisor:

Dr. Gizaw Mingistu
Department of Physics
Addis Ababa University

Examiners:

Dr. Xu Jiyao
National Space Science Center
Chianese Academy of Sciences

Dr. Elias Lewi
Institute of Geophysics, Space Science
and Astronomy (IGSSA)
Addis Ababa University

Chairman:

Dr. Lemi Demeyu
Department of Physics
Addis Ababa University

ADDIS ABABA UNIVERSITY

Date: **July 2011**

Author: **Kassahun Ture**

Title: **Ozone dynamics and seasonal variability over Africa**

Department: **Physics**

Degree: **Ph.D** Convocation: **November 8** Year: **2011**

Permission is herewith granted to Addis Ababa University to circulate and to have copied for non-commercial purposes, at its discretion, the above title upon the request of individuals or institutions.

Signature of Author

Dedicated with Love to:

My Wife Yeshumnesh Belete

Daughter Lidya Kassahun and

Son Nahom Kassahun.

Table of Contents

List of Figures

List of Abbreviations

DU	Dobson Unit
ECMWF	European Center for Medium-range Weather Forecast
GLDAS	Global Land Data Assimilation System
GOME	Global Ozone Monitoring Experiment
ICAO	International Civil Aviation Organization
IPV	Isentropic Potential Vorticity
ITCZ	Inner Tropical Convergence Zone
MOZAIC	**M**easurement of **OZ**one by Inservice **AI**r**C**raft
NASA	National Aeronautics and Space Administration
NCAR	National Center for Atmospheric Research
OLR	Outgoing Long-wave Radiation
ppmv	Parts per million by volume
ppbv	parts per billion by volume
pptv	Parts per trillion by volume
PV	Potential Vorticity
PVEL	PV area equivalent latitude
PVU	Potential vorticity units, 1 PVU = $1.10^{-6} K m^2 s^{-1} kg^{-1}$
PSCs	Polar Stratospheric Clouds
STE	Stratosphere-Troposphere Exchange
TOC	Total Ozone Column
TOMS	Total Ozone Mapping Spectrometer
UTC	Coordinated Universal Time
VMR	Volume Mixing Ratio
VOCs	Volatile Organic Compounds
WMO	The World Meteorological Organisation

Abstract

In this thesis results of satellite and in-situ airplane ozone data analysis are presented. Total Ozone Column (TOC) from Total Ozone Mapping Spectrometer (TOMS), and ozone enhancements sampled on the cruise flight route from Johannesburg to Vienna by **M**easurement of **OZ**one by Inservice **AI**r**C**raft (MOZAIC) at Equatorial Africa and North Africa are investigated. The work in this thesis is focused on the study of ozone transport during stratosphere-troposphere exchange (STE) events over intense STE areas, and seasonal variability of ozone over Africa. On very few occasions, at upper troposphere Equatorial Africa ozone spikes are observed at a flying altitude of 250-200 hPa. To understand the events that attribute to spiky MOZAIC ozone and relative humidity observations, additional data sets from different data sources were used to examine the observed events. Vertical wind fields in the regions of low Outgoing Long-wave Radiation (OLR), very high latent heat and cloud liquid water content transport have indicated presence of convection and thunderstorm events. Potential vorticity intrusion over equatorial region introduced enhanced ozone of stratospheric origin, as revealed by ERA-interim ozone data. Both downwelling and upwelling induced by convection and intrusion transported enhanced ozone from the stratosphere all the way down to the boundary layer.

We have distinguished source and regions of discharge of MOZAIC ozone enhancements observed at a flying altitude of 250-200 hPa over North Africa. Different data sets from ECMWF-ERA-Interim are used to examine the dynamics associated with the events. Relative humidity from MOZAIC measurement, longitudinal cross-section of potential vorticity (PV) and ozone volume mixing ratio (VMR) over the region of MOZAIC ozone enhancements confirmed that the observed enhancements are measured within lower stratosphere. This is mainly due to massive shift in the tropopause level. Longitudinal cross-section of PV, potential vorticity in isentropic surfaces (IPV) and ozone VMR revealed that the first mode of transport is large scale airmass subsidence from the stratosphere over mid-latitude. Some of these events lead to cross tropopause ozone transport

to upper troposphere North Africa. The second case is subsidence at polar regions during North hemisphere winter seasons. IPV is strongly modified as revealed by wind fields. In addition zonal winds and Rossby waves, which are active during winter seasons, have strong contribution in modifying potential vorticity and ozone spatial and temporal distribution.

TOC is analyzed from TOMS satellite data to study its seasonal variability over Africa. The seasonal variability comparisons in the latitude regions 0-34.5^0 N and 0-34.5^0 S show that ozone concentration peaks shift from April at North Africa to September near the equator. Ozone concentration begins to raise from May to October, and decreasing afterwards in the Southern part of Africa with highest peaks only between September to October. This result shows that ozone concentration seasonal duration is longer in the Northern part of Africa than the South. Low total column ozone concentration around 20^0 N and 20^0 S was observed which could be related to dynamical factors such as convection while the seasonal variability of very high ozone VMR is related to photochemical production.

Acknowledgements

I feel great pleasure and honor in writing these words of acknowledgement and appreciation for individuals and institutes who have made great contribution for the successful accomplishment of my study.

I would like to express my sincere heart felt gratitude to my advisor Dr.Gizaw Mengistu. First, for his kind interest to accept me as his PhD student especially during those challenging hectic moments. I am greatly benefited from his rich research expertise knowledge and experience. Material support and his kind cooperation in facilitating my participation in workshop and training in Italy and Germany respectively greatly acknowledged. I am also indebt for his priceless support in publishing my PhD work in international Journals and his great contribution that enables me to present at international conferences held in Greece, USA and South Africa. Many thanks to Addis Ababa University for responding to every support that I stand in need. Special thanks goes to Madawelabu University for sponsoring my study.

I thank research partner from Council for Scientific and Industrial Research, CSIR, South Africa, Prof. Sivakumar Venkataraman, who got the MOZAIC data from the MOZAIC team, provides valuable comments in the research results and invitation for a research visit at CSIR.

Many thanks to institutes who provide the data and services for free. MOZAIC team for the data set. NASA/Goddard Ozone Processing Team (OPT) for TOMS ozone data, ECMWF and NOAA for the various data sets used in this thesis. I would like to acknowledge Institute of Geophysics, Space Science and Astronomy (IGSSA, AAU) for the study rooms and facilities (computer and internate services).

I am grateful to my family members especially my mother Abebech Tsega, wife Yeshumnesh Belete, daughter Lidiya and son Nahom Kassahun and my sister Almaz Girma for their patience and strong support during my study period.

I would like to acknowledge Prof. A.V. Golap for his constructive comments and all

my friends, especially Abebe Belay, Tadesse Trefe, Samuel Takele and Titkie Kassa for nobel ideas and the colorful time I spent with them. Last but not least, I would like to acknowledge department head Dr. Lemi Demeyu and secretary W/ro Tslat Adnew who helped me a lot in facilitation of administrative affairs.

"For every house is builded by some man;**but he that built all things is God"**
Hebrew 3:4

Chapter 1

Introduction

Ever since the formation of our planet its atmosphere was subject to changes concerning composition, temperature, and self-purification power. However, during the last two centuries especially the atmospheric composition is shifting faster than ever before in the history of mankind [e.g. IPCC, 2001; World Meteorological Organisation (WMO), 2004]. The quasi-exponential growth in the world population and the industrialization have led to a strong growth in fossil fuel and biomass burning emissions of trace gases such as carbon dioxide (CO_2), carbon monoxide (CO), nitrogen oxides (NO_x), methane (CH_4), and other hydrocarbons [Van Aardenne et al., 2001]. The effects of these changes are getting more and more distinct as can be seen in acid rain, corrosion processes, smog, and depletion of the ozone layer. Another well-known effect is the global warming by greenhouse gases, which is at least partially counterbalanced by the emission of particulate matter and the formation of aerosols.

Remarkably, these aggravating effects are not based on a shift of the major atmospheric components except for the strongly variable content of water vapor, the concentration of the gases which amount to more than 99.9% remained almost constant for a much longer time than mankind exists on the planet. Responsible for the outlined effects are the mostly increasing contents of the so- called trace gases. For example, sulphur dioxide SO_2 maximum volume mixing ratio (50 ppbv) and nitrogen oxides NO_x (mixing ratio 0.1 ppmv - 1pptv) are responsible for photochemical smog, and the chloroflourocarbons CFC

(mixing ratio 1 ppbv) deplete the stratospheric ozone layer. Furthermore, together with CH_4 , dinitrogen monoxide (N_2O), the predominant trace gas in the atmosphere carbon dioxide (CO_2), mixing ratio of 350 ppmv and Chlorofluorocarbons(CFCs) enhance the greenhouse. The hydroxyl-radical, which plays a main role as atmospheric detergent even shows mixing ratios of less than 0.1 ptv [Gracdel and Crutzen, 1990].

The unique role of ozone in absorbing certain wavelengths of incoming solar ultraviolet light was recognized in the latter part of the nineteenth century by Cornu [1879] and Hartley [1880]. Interest in ozone stems from the fact that such absorption of solar radiation is important in determining not only the thermal structure of the stratosphere [e.g., Andrews et al., 1987] but also the ecological framework for life on the earth surface. Ozone has different impacts depending on where it resides. Stratospheric ozone, where approximately 90% of the atmospheric ozone is found, prevents the suns ultraviolet radiation reaching the surface of the earth. In the troposphere, ozone is direct green house gas while in the boundary layer, it is a pollutant, which has harmful effect on human, animal and crops [Prather, 2001].

Ozone depletion in the stratosphere results in enhanced levels of solar UV radiation at the earth surface. UV radiation has the potential to damage DNA in living cells, damage animal and human skin, increases the likelihood of especially skin cancer, damage eye cornea, affects the immune system and reduce plant growth. Most relevant to living organisms is the radiation in the UV-B (280-315 nm) and UV-A (315-400 nm) ranges. The biological effect of the solar radiation is generally expressed in terms of the UV-dose, taking into account the wavelength dependence of the sensitivity of a particular biological system to UV radiation, e.g. erythema induction (sunburn) [McKinlay and Diffey, 1987]. The Antarctic ozone hole resulted in strong increases in the UV-dose in the polar region of the Southern Hemisphere in October and November. A positive trend in the UV-dose is also found at the Northern mid-latitudes in winter and spring [WMO, 2003]. The total increase of tropospheric ozone since pre-industrial times has led to a globally averaged

positive radiative forcing of about 0.35 W/m^2 [IPCC, 2001; Hansen et al., 1997].

With regards to the sources of ozone at a given area; it is determined by transportation and/or in-situ production by different mechanisms. Photochemical production is the dominant source of ozone in the stratosphere. Most ozone is produced in the tropics, where the solar irradiance is highest. However, the highest ozone abundances in the troposhere are found at mid and high-latitudes as a result of the poleward transport of ozone-rich air in the stratosphere by the Brewer-Dobson circulation [Brewer, 1949; Dobson, 1956]. In the troposphere, ozone is produced from biomass burning, natural emission from vegetation and soil, lightning, NO_x emissions, and other anthropogenic sources such as emissions related to the combustion of fossil-fuel for energy, industrial, transport and domestic uses. Over the tropics, Africa is an important reservoir of ozone precursor sources allowing ozone to build up through active photochemistry exacerbated by high solar radiation. Africa contributes a significant amount to the global emissions from the first four categories listed above, while emissions from fossil fuel combustion are important only on the regional scale [Sauvage et al, 2007]. Thunderstorms inject NO_x mainly into the relatively clean upper troposphere. Measurements of O_3 in clouds indicate that both production and loss mechanisms exist. Locally within the cloud the concentrated NO reacts with ambient O_3 to produce NO_2 which reduces the O_3 abundance accordingly. Lightning NO_x is also responsible for a large fraction of the O_3 produced in the troposphere [Grewe, 2007].

The most important sources of ozone precursors over equatorial Africa are biomass burning, biogenic and lightning. African biomass burning activities, generally categorized as savanna, forest and agricultural waste burning, are driven by the slash and burn agricultural practices that take place during the dry seasons (late November to early March) in the northern hemisphere (NH), and July to October in the southern hemispheric (SH)[Aghedo et al., 2007]. The dynamic processes allow redistribution of such emissions on a more global scale. During the TRACE-A campaign, plumes loaded with

high O_3 over the Atlantic were attributed to biomass burning emissions from Africa. More recently high CO mixing ratios over the Indian Ocean have been attributed to African biomass burning [Sauvage et al, 2007]. Surface ozone concentration may rise by up to 50 ppbv during the biomass burning seasons. Biogenic emissions yield between 5-30 ppbv increase in the near surface ozone concentration over tropical Africa. The impact of lightning on surface ozone is negligible. Anthropogenic emissions yield a maximum of 7 ppbv increase in the annual-mean surface ozone concentration over Nigeria, South Africa and Egypt [Aghedo, 2007].

Stratosphere-troposphere exchange (STE) influences the chemical composition of both the stratosphere and the troposphere and represents an important aspect of global change [Butchart and Scaife, 2001]. It is also often associated with severe weather events [Goering et al., 2001]. Upper tropospheric ozone is an important greenhouse gas that affects global outgoing long wave radiations, chemistry, climate, and the radiation budget [Holton et al. 1995]. Upper troposphere changes have a great impact on the surface temperature [Forster and Shine, 1997].

Ozone is transported from the lower stratosphere into the upper troposphere through tropopause folding [Danielsen, 1968; Danielsen et al., 1987] and is exchanged with the troposphere via diabatic processes and turbulent diffusion [Lamarque and Hess, 1994], mixing processes and convective erosion during the breakup of stratospheric filaments [Appenzeller et al., 1996; Gouget et al., 2000]. Though stratosphere-troposphere exchange is limited by the large potential vorticity jump (>1PVU; 1 PVU=10^{-6}K kg^{-1} m^2 s^{-1}) associated with the subtropical jet, synoptic scale instabilities in the upper troposphere can induce transport across the tropopause [Chen, 1995]. Experimental evidence already exists of a two-way exchange, using e.g. the water vapor distribution in the lowermost stratosphere [Dessler et al., 1995] or ozone mixing ratios from aircraft observations [Gouget et al., 1996].

Air in the stratosphere has high static stability and, as a result, high IPV values greater

than 1.5 IPV units are typically found only in the stratosphere; thus IPV can be used to define the tropopause level. Because IPV is quasi-conservative (under adiabatic conditions), it can also be used to trace ozone-rich air which has moved from the stratosphere to the troposphere. Danielsen[1980] proposed that atmospheric chemists should be able to use positive correlations of ozone and potential vorticity and negative correlations of water vapor mixing ratio and potential vorticity to identify air of stratospheric origin.

Water vapor is frequently used as a chemical tracer in the vicinity of the tropopause because the stratosphere is much drier than the troposphere. Danielsen et al. [1987] further suggested that these correlations might be used to derive quantitative estimates of stratospheric-tropospheric exchange. A recent stratospheric origin ($\leqq$ 24 h) is allocated to an air parcel if three criteria are met: IPV $\geqq$ 1.5 PVU, altitude $>$ 2000 m and observed relative humidity (RH)$<$ 50 % [Zbinden et al., 2006].

The long-range transport of ozone and its precursor compounds allows pollution from one region to impact air quality in regions thousands of kilometers downwind. Several modelling studies have shown that pollution from one region can directly elevate the ozone in another, where the contribution of inter-continental transport is generally less than about 10% of the total ozone [Auvray and Bey, 2005]. However, Li et al. [2002] attributed 20% of the violations of the European ozone standard during summer 1997 to North American sources. European pollution has a much greater direct impact on air quality in downwind populated regions than pollution from either North America or East Asia. This is because it is largely exported near the surface over land to the Arctic and Russia in winter and to North Africa and to the Middle East in summer [Duncan and Bey, 2004; Stohl et al., 2002].

Duncan and Bey [2004] used a chemistry and transport model (CTM) to show that the long range transport of ozone generated from European pollution caused the European standard for ozone exceed regularly during the summer of 1994 over much of North Africa (i.e., countries bordering the Mediterranean Sea) and the Near East (i.e., Israel, Lebanon,

Syria, Jordan, Palestine and Iraq). About 200 million inhabitants live in these regions; they found that European sources contributed 5-20 ppbv ozone to these regions as a monthly mean. According to Duncan et al. [2008] European pollution regularly and significantly elevates surface ozone above the European health standard (i.e., 8-h average of 120 g/m3 or 60 ppbv) in North Africa and in the Near East regions, especially in summer when prevailing winds favor transport from Europe to these photochemically productive regions. In July, European pollution elevates average surface ozone in North Africa by 10-20 ppbv and by 5- 10 ppbv in the Near East. For the sake of comparison, European pollution elevates surface ozone by typically 10-30 ppbv over southern Europe and 10-20 ppbv over northern Europe.

European emissions cause 50-150 additional violations per year in northern Africa and the Near East. Estimated 19, 000 additional mortalities occur annually in these regions from exposure to European ozone pollution and 50,000 additional deaths globally; the majority of the additional deaths occurs outside of Europe [Duncan, 2008].

Stratospheric ozone over the northern mid latitude has significantly decreased compared with the pre 1970 values, with a large decrease occurring during winter and spring. Some of the observed trends could be caused by changes in the stratospheric dynamics, increase in the reactive chlorine produced from photodissociation of man made chlorofluorocarbon (CFCs) and halons under strong ultraviolet radiation in the stratosphere. Enhanced ozone depletion at mid latitude resulting from additional heterogeneous processes after large volcanic eruptions is an important factor in the observed long-term ozone changes [Shibata and Deushi, 2008]. Natural chemicals (emission and spray from microscopic sea organisms called phytoplankton) in the atmosphere west of equatorial Africa, Cape Verde, destroyed 50% more troposphere ozone in that region than expected. It also reduced methane [Katie, 2008].

As outlined above, atmospheric trace gases have significant influence on air quality and climate change. In spite of large research outputs pertaining to atmospheric trace

gases in general and ozone in particular, Africa still remains a poorly understood and documented continent [Sauvage, 2004].

Thus, the objective of this work is to study the impact of dynamical events to ozone distribution over equatorial and north Africa. In addition seasonal and spatial variability of ozone over Africa is investigated. In light of this, we used MOZAIC and TOMS ozone data as well as assimilated GOME ozone as main data sources. Supplementary data sets from different sources were used as diagnostic tools to address our objectives.

The dissertation is organized as follows. Chapter 2 describes atmospheric dynamics. In this chapter, a general description of atmospheric composition, global circulation, stratospheric circulation, stratospheric-tropospheric exchange, potential vorticity and Rossby waves explained in greater detail. In chapter 3, atmospheric chemistry of ozone and its precursors both within both the troposphere and the stratosphere are discussed. In chapter 4, data and methodologies are presented. In-situ airplane and instruments aboard satellite used for ozone measurement are discussed, followed by description of the data from MOZAIC, ECMWF-ERA intrim and TOMS in Section 4.2. Section 4.3 of this chapter discusses methodologies used to analyze the data. Chapter 5 presents results of the analysis. In this chapter ozone dynamics and seasonal variability of ozone over Africa are presented. Dynamical events such as convection, stratospheric intrusion and isentropic transport from high latitude regions that influence ozone distribution over equatorial Africa are discussed. Moreover, modes of ozone transport and impact of Robbsy waves on ozone distribution over north Africa are also discussed. Seasonal variability of ozone over Africa from TOMS total ozone column is presented and finally conclusions are given in Chapter 6.

Chapter 2

Atmospheric Dynamics

To understand observed distributions of ozone in the atmosphere, it is necessary to comprehend atmospheric dynamics especially those aspects pertaining to transport and dynamical mixing. Thus this chapter presents a brief overview of atmospheric composition and dynamics that influence the distribution of trace gases. Atmospheric dynamical parameters, such as potential vorticity, Outgoing Long-wave Radiation (OLR)(a proxy of convection) as well as atmospheric Rossby waves, which influences the distribution of atmospheric traces, are thoroughly discussed.

2.1 Atmospheric composition and vertical structure

Composition

The atmosphere (Greek: $\alpha\tau\mu\acute{o}\varsigma$, at$\acute{o}ms$, meaning vapor, haze, and $\sigma\varphi\alpha\iota\rho\alpha$, sphera, meaning sphere) is a layer of gases surrounding the earth, being retained by gravity. It is noticeable that among the permanent constituents like nitrogen, oxygen or noble gases, the greenhouse gases such as carbon dioxide (CO_2) and methane (CH_4) have obtained a prominent position. There are several other substances of minor abundance, but of major importance for atmospheric chemistry and climate, called trace substances or, when gaseous, trace gases. Apart from O_3, CO_2 and CH_4, the most important are carbon

monoxide (CO), halogen species (mostly bromine, chlorine or iodine compounds), compounds of nitrogen and sulphur and (volatile) organic compounds. 99% of all atmospheric gases are found below 40 km of altitude, which renders this region, i.e. troposphere and stratosphere (see Fig. 2.1), the main focus of atmospheric research [John and Peter, 2006; Hewitt and Jackson, 2003]

Vertical structure

The vertical structure of the atmosphere can be defined by the characteristics of the temperature profile. Accordingly, the atmosphere is subdivided into several layers with distinct boundaries, called pauses (see Fig. 2.1). In the lowermost layer, the troposphere, the temperature profile is dominated by adiabatic expansion and compression of rising and sinking air masses, driven by solar radiation. During the day the surface is heated, warm air elevates and is cooled by expansion, causing the temperature to decrease by 5 -10 ^0C per 1 km altitude and leading to a first temperature minimum, called the tropopause. An additional cooling occurs in the upper troposphere by radiative cooling of water in the infrared wavelength range (IR). The height of the tropopause is determined by the water vapor content of the troposphere, which itself is reigned by surface temperature. So the tropopause altitude ranges between 17 - 18 km in the tropics and between 9 - 13 km at higher latitudes, with the lowest tropopause heights occurring at polar winter latitudes. The above mentioned convective processes also lead to a steady mixing of the troposphere. In the stratosphere the conditions are vice versa. The heating in the upper stratosphere by absorption of solar radiation by ozone lead to an increase of temperature with altitude and thus to very little convection and mixing [Staehelin, et al., 2001]

In contrast to the troposphere, the radiative budget of the stratosphere is determined by absorption of solar radiation and emission of thermal IR radiation. Above the stratopause, which is given by a temperature maximum around 50 km altitude, is

the mesosphere where temperatures decrease again due to similar processes as in the troposphere. Thereafter, in the thermosphere, the temperature is again strongly increasing caused by absorption of solar UV radiation (mainly by oxygen) up to values of 1200 - 1500 K. At altitudes above 100 km, atmospheric constituents start to separate, according to their mass, e.g. above 1000 km, magnetosphere, there is only hydrogen left, which is why this region is also referred to as homosphere in contrast to the heterosphere below.

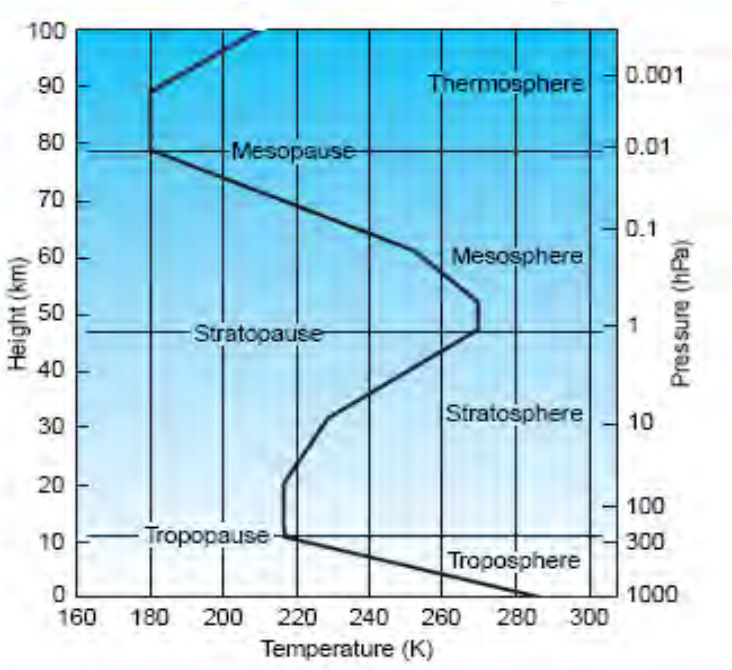

Figure 2.1: The vertical temperature and molecular density structure of the earth's Atmosphere. Adapted from Hewitt, C.N and Andrea Jackson, V, 2003.

2.2 Atmospheric dynamics at the global scale

Dynamics in the troposphere

The troposphere is subdivided into several layers according to their dynamics. The lower most millimeters form the molecular viscous layer. The name already implies that its dynamics are governed by molecular viscosity while above it is dominated by turbulent

diffusion. The next 20 - 200 m form the Prandtl layer where surface friction is the strongest force. The transition to the free troposphere above 1000 m, where dynamics are dominated by global circulation patterns, occurs in the Ekman layer. Here wind directions change steadily from the ground wind directions to the direction of the geostrophic winds of the free troposphere, i.e. isobaric wind stream caused by an equilibrium state between the forcing of pressure gradients and the Coriolis force. These layers combined form the planetary boundary layer or mixing layer, which is characterized by steady mixing. The planetary boundary layer is particularly interesting when studying the effects of emissions, either natural or anthropogenic, because most sources are ground-based. The global circulation patterns of the free troposphere are then responsible for the long-range transport of emitted trace gases and are briefly discussed in the following paragraphs.

Global circulation is driven by the strong differences in incoming solar radiation between the tropics and higher latitudes. Even though the radiative forcing provides on average zero net energy input, it produces entropy which drives the circulation. In the tropics, large scale tropospheric circulation is triggered by convective latent heat release, leading to deep vertical motion. This occurs primarily in the zone of the strongest incoming solar radiation, the Inner Tropical Convergence Zone (ITCZ).

The ITCZ is a narrow band of latitudes, moving back and forth across the equator, following the sun during the course of a seasonal cycle. There the uplift of hot humid air is most powerful. Once the convective air masses reach the level of neutral buoyancy at about 10 - 12 km, they cannot rise much further, start to flow poleward and typically descend at 30 - 35^0 degrees latitude in both hemispheres, since the poleward flow is constrained by conservation of angular momentum. This region is called the subtropical high pressure belt and is characterized by a downward wind component. The strong convection in the ITCZ leads to a rather low air pressure there, causing air near the ground to flow from higher latitudes towards the equator and simultaneously be deflected to the west by the Coriolis force: the trade winds. They are the dominating wind system in the tropics

up to about 30 - 35^0 of northern and southern latitude. The trade winds blow quite smoothly from northeast on the northern and from southeast on the southern hemisphere and converge in the ITCZ. This whole circulation pattern is referred to as Hadley cell. The descending branches of the Hadley circulation are undersaturated in water vapor and undergo adiabatic warming, because the moisture has largely been lost as rain during convection. This accounts for the hot, dry desert regions found in the subtropics and the humid green tropical regions. Embedded within the Hadley cell are longitudinal circulation cells, which result in a break up of almost any cross-equatorial flow. This explains why there are noticeable inter-hemispheric differences in the distribution of trace gases, e.g. CO_2, despite its long life time. While horizontal tropospheric mixing times range between days and several weeks within one hemisphere, global mixing times are extended to a year or even more.

In the extra-tropics, meridional circulation is driven by pressure instabilities, caused by the temperature gradient between (sub-)tropical and higher latitudes, with a poleward flow in the upper troposphere and a return flow in the surface layer (west wind drift zone). At the so called polar front cold air masses from high latitudes and warmer air masses from the mid-latitudes collide. This region is characterized by low pressure which increases again towards the poles. At high polar latitudes there are circumpolar east winds up to a height of about 3 km. The winds are caused by cooled air, "falling" downward (catabatic winds) and deflected eastward by the Coriolis force.

Dynamics in the stratosphere

While the tropospheric circulation is thermally driven, the radiative equilibrium of the stratosphere (and mesosphere) is dynamically very stable. Apart from zonal flows (i.e. flow along latitude circles), associated with temperature gradients and the Coriolis force, and the meridional circulation resulting from the slight radiative imbalance caused by the annual cycle, there is also a meridional circulation pattern in the stratosphere. This

circulation cannot be explained thermally, because persistent meridional motion requires a torque to move air masses across surfaces of constant angular momentum. As there are no external angular momentum sources in the atmosphere, such torques can only arise from angular momentum transfer by atmospheric motion. This transfer is induced by planetary waves and is also referred to as wave-drag.

Planetary waves are the propagation of a local disturbance in the atmosphere, e.g. caused by topography. Some of these waves reach up into the stratosphere, where they drive the meridional circulation. In the extra-tropical stratosphere, wave-drag comes mostly from planetary-scale Rossby waves. Rossby waves are caused in meridional flows by the rotation of the earth. These waves propagate into the stratosphere and drive a poleward circulation within the stratosphere, which leads to a descending motion in the extra-tropics and to an ascending motion in the tropics (Brewer-Dobson circulation).

To be precise, the above discussed tropospheric upward motion in the tropics is not because of "hot air rising", but is rather mechanically driven by stratospheric wave-drag. The meridional equatorward temperature gradient within the troposphere leads to an eastward zonal flow in both hemispheres. Maximum winds are achieved at the subtropical tropopause, which accounts for the rather famous jet streams.

Within the stratosphere, the temperature minimum over the winter pole also leads to eastward flows, parallel to the troposphere, except that in the stratosphere the temperature gradient is concentrated more in sub-polar latitudes, shifting the jet maximum poleward. This leads to the so called polar vortex, because the circumpolar flow constitutes a vortex. In the summer hemisphere, however, the temperature maximum over the pole leads to a change in wind direction in the stratosphere and the eastward zonal flows become westward winds. This is why there is hardly any meridional mixing in summer, where as it is rather intense during winter time. Consequences can, for example, be seen in the global ozone distribution: ozone produced in the tropical stratosphere is transported to higher latitudes during winter while this transport breaks down during

summer, causing lower ozone values in high latitudes during fall compared to spring. The zonal winds of the summer stratosphere also stop Rossby waves from propagating into the stratosphere. So the Brewer-Dobson circulation is mainly a wintertime phenomenon. Moreover it is stronger in the Northern Hemisphere, because the distribution of land masses in the North is such as to generate stronger planetary waves. Since stronger down welling at the pole implies warmer temperatures due to adiabatic warming, the Arctic winter stratosphere is usually warmer and has a weaker polar vortex than its Antarctic counterpart. In return the Antarctic polar vortex is typically very stable and colder. It confines polar air and provides the conditions for ozone hole chemistry. In spring, the vortex breaks down and the zonal wind pattern changes from winter to summer type (final warming). This causes fragments of the vortex to be transported to mid-latitudes, where e.g. ozone poor Antarctic air can reach the stratosphere over Australia and New Zealand.

In a simplified scheme it can be summarized that stratospheric circulation is driven by waves, while the temperature is determined by radiative equilibrium and circulation induced differences to that state. This renders the processes in the stratosphere a complex system of angular momentum and thermodynamical balances. For a detailed discussion see e.g. [Sheperd, 2003].

Stratosphere-troposphere exchange

Fig. 2.2 depicts the stratosphere-troposphere exchange events. The exchange processes between troposphere and stratosphere is of particular interest because all anthropogenic pollutants, except for e.g. exhaust gases of supersonic jets mainly flying in the extra-tropics, are emitted into the troposphere and hence enter the stratosphere from there. The low stratospheric water content suggests that the main entry to the stratosphere occurs via the very cold tropical tropopause which acts as a cold trap. This is explained by the ascent of air in the ITCZ which continues through the tropopause into the stratosphere. In the extratropical stratosphere, the air generally descends and, thus, can enter the troposphere.

This effect is strongest in the polar vortex and weakest in the summer hemisphere, and is, e.g., the origin of most of the ozone in the free troposphere. Additionally, there is dynamic mixing of stratospheric and tropospheric air by diabatic transport, i.e. transport of air masses with heat exchange. Adiabatic mixing between troposphere and stratosphere is also possible.

The characteristic exchange times between lower and middle stratosphere range between some months and two years, while timescales for stratosphere-troposphere exchange are in the order of 15 - 18 months. Further mechanisms for stratosphere-troposphere exchange are transports along isentropic (surface of constant potential temperature) and tropopause folding events. The dissipation of planetary-scale Rossby waves in the winter time stratosphere is known as "wave breaking" [Sheperd, 2003]: atmospheric waves grow in amplitude as they propagate upward and the density of the air decreases, which leads to intense mixing on isentropic surfaces. Stratospheric intrusions allows an air mass to sinks below the dynamical tropopause. They are directly associated with the strength of the horizontal temperature gradient at the tropopause level. In a tropopause fold, dry and clean stratospheric air, rich of ozone and potential vorticity, is transported downward to tropospheric levels.

Observations of the circulation near folding events reveal that tropospheric air is lifted upward as well. This tropospheric air usually contains larger amounts of water vapor, aerosols and CO as typical stratospheric air. Thus CO is also a good tracer for troposphere-stratosphere transport. In the subtropics, the probability of fold events is particularly high over the Asian continent.

The stratospheric circulation

The meridional circulation of the stratosphere, known as the "Brewer-Dobson" circulation, after the pioneering deductions of Brewer [1949] and Dobson [1956] from observations of stratospheric water vapor and ozone respectively. It comprises a two-cell structure in

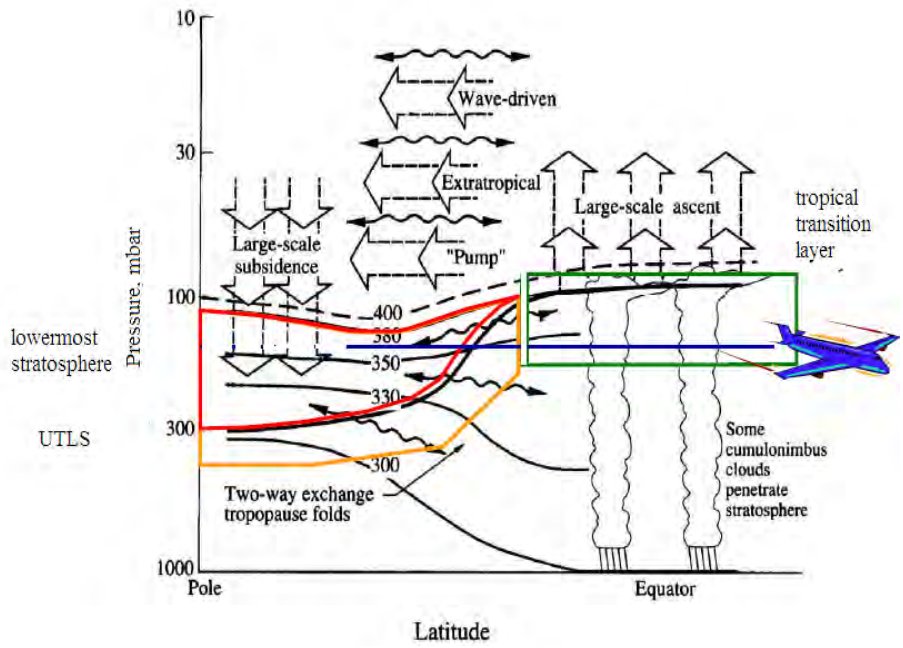

Figure 2.2: Simplified scheme of global circulation processes shown as latitudinal cross section. Main regions covered by the measurement flights of this work are highlighted with green red and yellow colors. Adapted from Holton et al., [1995].

the lower stratosphere, with upwelling in the tropics and subsidence in middle and high latitudes, and a single cell from the tropics into the winter hemisphere at higher altitudes. These characteristics have been confirmed from modern radiation calculations based on observed distributions of temperature and radiatively active constituents [Rosenlof, 1995; Eluszkiewicz et al., 1996], provided one interprets mean circulation as residual mean circulation, rather than the straightforward Eulerian mean (it is the residual mean that is relevant to tracer transport [Andrews et al., 1987].

A schematic of the residual circulation of the atmosphere (up to the mesopause) is depicted in Fig. 2.3. In the tropical troposphere, the well-known Hadley circulation can be understood, at least in its simplest form, as a nonlinear circulation driven by latitudinal gradients in thermal forcing [Held and Hou, 1980]. Despite the temptation to interpret the apparently thermally direct circulation of the stratosphere in the same way, it is clear

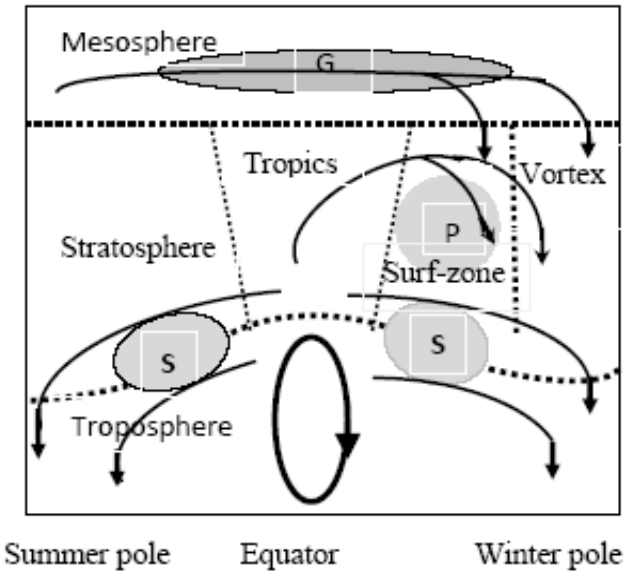

Figure 2.3: Schematic of the residual mean meridional circulation in the atmosphere. The heavy ellipse denotes the thermally-driven Hadley circulation of the troposphere. The shaded regions (labelled S, P, and G) denote regions of breaking waves (synoptic-scale, planetary-scale waves, and gravity waves, respectively), responsible for driving branches of the stratospheric and mesospheric circulation [Plumb, 2002].

that other processes must be involved, since air following the circulation must lose angular momentum as it moves poleward. The direct, large-scale, effects of friction being utterly negligible in the stratosphere, such loss of angular momentum can only be ascribed to the impact of waves: the presence of wave drag is thus crucial to the stratospheric circulation.

In contrast to the much more quiescent summer hemisphere, the wintertime stratosphere is dominated by large-amplitude, planetary-scale Rossby waves propagating upward from the troposphere. Intermittently, these waves break, stirring air more or less isentropically across large distances of the winter stratosphere within a region that has become known as the surf zone [McIntyre and Palmer, 1983], bounded by sharp gradients of potential vorticity (PV) and of tracers in the winter subtropics and at the edge of the polar vortex. Apart from the direct effects of this stirring on tracers, it has an indirect effect through the meridional circulation induced by the stirring of PV.

For adiabatic, inviscid flow, and assuming steady state (i.e. solstice conditions), the zonal mean momentum budget can be written [Andrews et al., 1987]

$$-\overline{\nu}^{*}\overline{P}^{*} = \overline{\hat{\nu}\hat{P}}^{*} \tag{2.2.1}$$

where P is Ertel PV, ν is northward velocity, the notation $\overline{\nu}^{*}$ denotes the mass-weighted zonal mean of ν along isentropic surfaces, and $\hat{\nu} = \nu - \overline{\nu}^{*}$ the departure from that mean.

Eq. (2.2.1) simply states the need for zero net flux of PV in a conservative steady mean state: mean and eddy fluxes must cancel. Therefore, a nonzero eddy flux of PV which will be present whenever waves are breaking, unless there is no background PV gradient requires a nonzero mean circulation in steady state. In fact, in the usual case of northward mean PV gradient and down gradient eddy flux,$-\overline{\nu}^{*}\overline{P}^{*} < 0$, and Eq. (2.2.1) implies a poleward circulation (since the sign of $\overline{P}^{*}$ has the same sign as latitude, except perhaps very close to the equator). Thus, the wave drag drives the flow poleward, through a mechanism we will here refer to as the Rossby wave pump, providing an explanation for the poleward flow in the winter stratosphere [Haynes et al., 1991; Holton et al., 1995].

There are outstanding issues, however, in our understanding of the latitudinal extent of the circulation. In the tropics, the observed circulation clearly extends far beyond the surf zone, deep into the tropics and even across the equator: issues involved in explaining this behavior are discussed in Plumb and Eluszkiewicz [1999]. At least a component of the tropical circulation may be a nonlinear, thermally driven circulation, analogous to the tropospheric Hadley cell [Dunkerton, 1989; Semeniuk and Shepherd, 2002a,b].

The component driven by wave drag may also extend into the tropics, either via a similar nonlinear mechanism or through the effects of other wave motions within the tropics [Plumb and Eluszkiewicz, 1999; Scott, 2002]. At the vortex edge, theoretical arguments lead us to expect little penetration of the steady circulation into the vortex, even under nonadiabatic conditions [Sobel and Plumb, 1999], despite the observational evidence there of strong descent of tracer isopleths.

In the lower stratosphere, the effects of synoptic-scale tropospheric disturbances, present throughout the year, are probably responsible for driving the strong two-cell circulation there and in the upper troposphere, through the same Rossby wave pumping mechanism (the local dynamics of these waves, away from their baroclinic sources, being just Rossby wave dynamics). Near the surface, these same baroclinic disturbances drive an equatorward return flow [Held and Schneider, 2000; Koh, 2001] in the form of cold air outbreaks.

The mesosphere is dominated by a strong global circulation (with $\overline{\nu}*$ of several ms^{-1}) from summer pole to winter pole, which manifests itself in the dramatic reversal of pole-to-pole temperature gradient in the upper mesosphere. This circulation is believed to be driven primarily by upward propagating inertia-gravity waves. Unlike Rossby waves, inertia-gravity waves can propagate through both mean easterlies and westerlies, and their effects on the mean zonal flow can be of either sign, depending on their phase velocities. Because of selective dissipation of these waves in the stratospheric winds, it turns out that their effect on the mesosphere through what we here call the gravity wave pump is such as to drive the flow generally equatorward in summer and poleward in winter, as observed. This mechanism is strong enough to pump significant descent of mesospheric air deep into the stratosphere, as we shall see below.

Rapid stirring in the surf zone

Within the surf zone of the midlatitude winter stratosphere, tracers are subjected to both isentropic stirring and diabatic advection. If the eddy motions are almost adiabatic, then, for a tracer with mixing ratio, χ

$$\frac{\partial\overline{\chi}^*}{\partial t} + \overline{\nu}^*\frac{\partial\overline{\chi}^*}{\partial y} + \overline{\dot{\theta}^*}\frac{\partial\overline{\chi}^*}{\partial\theta} = -\frac{1}{\bar{\sigma}}\frac{\partial}{\partial y}(\bar{\sigma}\overline{\hat{v}\hat{\chi}}^*) \tag{2.2.2}$$

where θ is potential temperature and $\sigma = -g^{-1}\frac{\partial P}{\partial\theta}$ is the isentropic density. Now, in Eq.(2.2.1), we saw that the dynamical balance is such that eddy and mean transport

of PV are of the same magnitude: is the same true of tracers? Suppose that the eddy fluxes (of PV and tracers) are such as to destroy the gross mean gradient across the surf zone in a characteristic time scale τ, so that the eddy flux of PV is $\overline{\hat{\nu}\hat{P}}^* \sim \frac{\Delta P}{\tau} L$, where L is the surf zone width, and ΔP the gross mPV gradient across the surf zone. Then, from Eq.(2.2.1), $\overline{\nu}^* \sim \frac{\Delta P}{P}\frac{L}{\tau}$, where P is a typical value of PV in the surf zone. Therefore the time scale τ for mean tracer advection horizontally across the surf zone, or vertically across a density scale height H, is T$\sim \frac{H}{\overline{\omega}^*} \sim \frac{L}{\overline{\nu}^*} \sim \tau\frac{P}{\Delta P}$,

Hence the ratio of eddy to mean tracer transport time scales is $\frac{\tau}{T} \sim \frac{\triangle P}{P}$. Now, suppose the surf-zone has width comparable with the Earth radius, but is weak enough that there is little tendency toward homogenization of PV within it; then $\triangle P \sim P$, and the two contributions to the tracer budget are comparable. However, the real stratospheric surf zone has weak PV gradients, a consequence of strong stirring such that $\Delta P \ll P$, implying that isentropic stirring dominates the tracer budgets within the surf zone. This fact, which is simply a consequence of the decreasing efficiency of the Rossby wave pump under strong stirring, has important consequences for stratospheric transport.

2.3 Potential vorticity

Potential vorticity is a dynamic tracer used mainly to indicate the direction of air mass transport within and across the stratosphere. The concept of PV was originally introduced by C.G Rossby. In 1930s he took a key step in realizing that the vertical component of absolute vorticity, ζ_a, is the most important for large-scale flow in the atmosphere. He further showed that $\frac{(f+\zeta_\theta)}{\Delta}$ = constant, where Δ is an expression for the thickness of a layer equal to $\frac{-\delta p}{g}$, ζ_θ is the relative 'isentropic vorticity' given by $(\frac{\partial V}{\partial x}\text{-}\frac{\partial U}{\partial y})_\theta$, i.e vorticity computed from winds along an isentropic surface, f is coriolis parameter. Ertel [1942 a, b, c], working independently derived a more general expression $PV = \frac{1}{\rho\zeta_a}.\nabla\theta$. PV is proportional to the absolute vorticity component normal to a potential temperature (θ)

surface, divided by the pressure difference (δp) between adjacent surfaces. In frictionless, adiabatic motion, PV is conserved on isentropic surface [Neeman and Alpert, 1990].

The isobaric coordinate of PV,

$$\text{PV} = \text{-g(fk} + \nabla_p \times \mathbf{V}).\nabla_p\theta \tag{2.3.1}$$

and isentropic versions assuming hydrostatic condition given by

$$\text{IPV} = \text{-g(f} + \text{k}.\nabla_\theta \times \mathbf{V})/(\tfrac{\partial P}{\partial \theta}) \tag{2.3.2}$$

PV is known as 'Ertel's potential vorticity', or simply potential vorticity, where **k** is the unit vertical vector, **V** the three-dimensional (3-D) wind vector and ∇_p and ∇_θ are the 3-D gradient operators in pressure and isentropic (θ) coordinates, respectively, g the gravity constant. For the vertical cross section Eq.(2.3.1) will be applied, while for the isentropic map Eq.(2.3.2) are adopted. IPV is used in some literatures to refer the isentropic coordinate PV, we will use IPV for PV in isentropic coordinate.

Potential vorticity increases with poleward propagation due to latitudinal variation in f, and increases somewhat with height due to variation in ρ. Much of the most marked change, though, occurs at the tropopause due to a rapid increase in static stability encountered on penetrating the stratosphere. Tropospheric values are generally less than 1.5 PV units and jump to values in excess of 4 PV units in the stratosphere.

2.4 Rossby waves

Vertically propagating waves have an important role in the dynamics of the stratosphere. The waves interact with the stratosphere's mean circulation, maintain the energy and momentum budget of the stratosphere, transport trace species (e.g. ozone) concentrations between the troposphere and stratosphere, and are the reason for the phenomena known as sudden stratospheric warming. The waves originate in the lower troposphere where they are forced to propagate vertically by topographic forcing or land-sea diabatic

heating differences. There are two distinct regions of vertically propagating waves, the extratropics and the tropics. Quasi-stationary Rossby waves are the most significant vertically propagating mode in the extratropics, while Kelvin and mixed Rossby-gravity waves are the most prominent vertically propagating waves in the tropics [Holton, 1980]. Charney and Drazin [1961] first explained the confinement of vertically propagating waves to the winter hemisphere. The lack of prominent vertically propagating extra-tropical waves in the southern hemisphere is most likely due to smaller difference in land-sea heating contrasts and difference in topographic forcing.

Rossby wave Structure in the Vertical

The amplitude of Rossby waves increases and shifts phase to the west with height. This is readily seen by examining the stream function,

$$\psi \propto e^{imz} e^{\frac{z}{2H}} \tag{2.4.1}$$

We see that ψ does not vary with height simply as e^{imz} but instead increases with height with the additional factor of $e^{\frac{z}{2H}}$. The reason for the increase in amplitude is simply the reduction of atmospheric density as height increases [Holton, 1975].

The deflection of jet known as the polar night jet, becomes the wave guide for vertically propagating Rossby waves. The waveguide should be thought of as a channel, which the waves are directed through and allowed to propagate higher than the troposphere. As Holton [1975] points out, the guiding of the Rossby waves into the region of strong mean zonal winds is one of the most important features to the dynamics of the winter stratosphere. Rossby-wave breaking is a concept basic to the theory of wave-induced forces. "Breaking" does not mean fracturing in any literal sense; rather, it refers to situations in which PV contours deform irreversibly, or fold sideways, on isentropic surfaces, instead of merely undulating as in a simple Rossby wave. These irreversible deformations may take place in a complicated, layerwise two-dimensional turbulent manner [Holton, 1995] and

the subsequent mixing of different air masses [Scott and Cammas, 2002].

2.5 Outgoing Long-wave Radiation

The planet Earth is in radiative equilibrium with its surroundings. It receives energy in the form of short-wave radiation from the sun and loses energy in the form of long-wave radiation to space. These two radiation streams can be represented approximately by black-body radiation of 6000 K for the solar short-wave radiation and 290 K for the terrestrial long-wave radiation. The balance between the incoming short-wave radiation and the outgoing long-wave radiation (OLR) determines the temperature in the atmosphere and on the Earth's surface [Salby 1996; Harries, 1996, 1997].

OLR is the emission to space of terrestrial radiation from the top of the earth's atmosphere [Salby, 1996]. The OLR originates partly from the surface and partly from higher levels of the atmosphere. Because of the lower temperature of these levels compared to the surface, the OLR is reduced compared to a hypothetical Earth without atmosphere. This is the atmospheric 'greenhouse' effect. From the known incoming solar short-wave radiation, we can easily infer the global average OLR to be close to 240 W m^{-2} because the incoming and outgoing radiation fluxes must balance [Harries, 1996]. However, there is considerable variability for different latitudes and weather conditions, so that local OLR values vary between about 160W m^{-2} and 320Wm^{-2}. Allan et al. [1999] showed that the clear-sky OLR variability is mostly due to temperature variability at high latitude and mostly due to humidity variability at low latitude. In physical terms OLR is strongly controlled by three main meteorological variables, namely the temperature of the earth and the atmosphere above it, the presence of water vapor in that atmosphere (which strongly absorbs infra-red radiation attenuating the terrestrial signal) and the presence of clouds (which may completely block all outgoing infra-red radiation from the surface). Thus, global maps of OLR averages and anomalies reveal information on the temperature,

humidity and cloudiness of the atmosphere. Clough et al. [1992] and Clough and Iacono [1995] showed that water vapour has a significant effect on OLR, not only in the pure rotational band from approximately 0 to 600 cm^{-1} and the vibrational-rotational band from approximately 1400 to 2100 cm^{-1}, but also in the continuum region between the bands. Moreover, these different frequency regions of water vapour absorption are responsible for OLR sensitivity to water vapour perturbations at different altitudes, a fact first pointed out by Sinha and Harries [1995], who particularly stressed the importance of the 0 to 500 cm^{-1} frequency region, where OLR is sensitive to perturbations in the middle and upper troposphere. Clouds reduce OLR in the same manner as other greenhouse gases and the magnitude of this impact depends on the cloud altitude. On average the cloud effect on OLR is 30 Wm^{-2} [Kiehl and Trenberth, 1997]

The highest OLR values are found above the hot, dry, cloud-free desert regions, where a lack of atmospheric water vapour permits the effective infra-red radiating temperature to originate from lower down in the atmosphere (i.e. warmer). High OLR values also occur above many ocean regions where there is a dry mid-to-upper troposphere (e.g. large areas of the sub-tropical Atlantic and Pacific Oceans).

Chapter 3

Atmospheric Chemistry

In the previous chapter we have seen some important dynamical events that influence traces distribution in the atmosphere. This chapter is devoted to atmospheric chemistry of ozone and its precursors. In addition chemical reaction pathways that affect ozone concentration and distribution are discussed.

3.1 Atmospheric nitrogen oxides and ozone

Human induced changes on atmospheric chemistry are not only seen in the stratosphere (e.g. the ozone hole), but also in the troposphere, e.g. in urban smog episodes due to anthropogenic emissions of nitrogen and sulfur compounds as well as hydrocarbons and other organic compounds. Of these species, many are involved in ozone chemistry and they all affect human health, as they attack the respiratory tract and can possibly cause nausea, headaches or worse health problems. So does ozone, which, in the boundary layer, is a product of specific smog conditions and commonly known as summer smog. With respect to atmospheric chemistry, the nitrogen compounds nitric oxide (NO) and nitrogen dioxide (NO_2) are among the most important trace gases, as both are radicals and thus highly reactive. The nitrogen radical budget, sum of NO and NO_2, often referred to as NO_x (see below), are involved in several chemical reactions and catalytic cycles that destroy ozone in the stratosphere, but they can also transfer ozone destructive halogen species

into passive reservoir products. In the troposphere, reactions involving NO_x are a key sequence for the formation and destruction of ozone, thus affecting the radiative budget and the oxidation capacity of the atmosphere. The term oxidation capacity denotes the capability of the atmosphere to oxidize or otherwise degrade trace species emitted into it. This ability is crucial for the removal of pollutants and is also referred to as the self-cleaning capacity of the atmosphere. Very often the oxidation capacity is associated with the abundance of OH. However, many other oxidants (including O_2 and O_3) can contribute to the oxidation capacity as well.

While tropospheric ozone formation is influenced by anthropogenic emissions, stratospheric ozone, which constitutes about 90% of the global ozone, is naturally formed. Lightning, biomass burning and soil releases constitute natural sources of NO_x, but today more than 50% of the total emissions are from fossil fuel combustion and biomass burning due to arson. In consequence, tropospheric levels of NO_x have likely doubled over the last hundred years in the northern hemisphere, and exceed natural background levels ($\sim$ 10 ppt) by several orders of magnitude in polluted urban air (up to 1 ppm) [Seinfeld and Pandis, 1997]. The ratio of NO and NO_2, called Leighton ratio, is linked with ozone and introduced below. The following sections give an overview of the most important chemical mechanisms involving nitrogen oxides and ozone chemistry.

3.2 The Leighton ratio

NO and NO_2 are rapidly converted into each other in the daytime atmosphere, therefore they are commonly summed up as NO_x (= NO + NO_2). All inorganic nitrogen species budget is given as NO_y. The Leighton ratio is formulated from the net balance of the

following reactions:

$$\mathrm{NO} + O_3 \rightarrow NO_2 + O_2 \tag{3.2.1}$$

$$\mathrm{NO_2} + \mathrm{h}\nu \rightarrow \mathrm{NO} + O(^3P) \qquad \lambda \leq 420nm \tag{3.2.2}$$

$$O + \mathrm{O_2} + \mathrm{M} \rightarrow O_3 + \mathrm{M} \tag{3.2.3}$$

where M is an inert molecule needed for the conservation of momentum. This partitioning is ozone controlled, which is expressed by the Leighton ratio L

$$\mathrm{L} = \frac{[NO]}{[NO_2]} = \frac{J.[NO_2]}{[O_3].k} \tag{3.2.4}$$

with k denoting the reaction rate constant, which is a measure for the speed of the specific reaction. The unit of k depends on the reaction order n: [k] $= molec^{-(n-1)}.cm^{(n-1)3}.s^{-1}$. J, the photolysis frequency in s^{-1}, is analogue to k for photochemical reactions.

The Leighton ratio depends on ozone concentration, the NO_2 photolysis rate and temperature. The percentage of NO_x present as NO_2 in equilibrium is defined as

$$\mathrm{f}_{NO_2} = \frac{[NO_2]}{[NO_x]} = \frac{1}{1+L} \tag{3.2.5}$$

In the boundary layer, most NO_x is usually present as NO_2 ($f_{NO_2} \approx 0:7, L \approx 0:4$). With increasing altitude, the Leighton ratio is shifted towards NO due to the temperature dependency of k and higher NO_2 photolysis frequencies; at 10 km altitude f_{NO_2} is about 0.4 (L = 1.5). In practice, however, NO_x and ozone chemistry is also controlled by other species like CO or volatile organic compounds. During night, all NO_x is shifted to NO_2, NO_3 and N_2O_5 (see Section 3.3), because no photolysis (reaction (3.2.2)) takes place.

Primarily most NO_x is emitted as NO and subsequently transformed to NO_2 by reaction (3.2.1). The dominating reactions leading to the formation of NO are described by the Zeldovich mechanism [Zeldovich and Raizer, 1967]. In connection with high temperatures ($> 2000°C$) that occur in burning processes (e.g., any kind of fossil fuel combustion or biomass burning) or lightning, air molecules (particularly O_2) dissociate:

$$\mathrm{O_2} + M \leftrightarrows O + O + M \tag{3.2.6}$$

NO is subsequently formed in the Zeldovich reactions:

$$\mathrm{O} + \mathrm{N}_2 \leftrightarrows NO + N \tag{3.2.7}$$

$$\mathrm{N} + \mathrm{O}_2 \leftrightarrows NO + O \tag{3.2.8}$$

The equilibria (reactions 3.2.7 and 3.2.8) strongly depend on temperature and are shifted to the right side for high temperatures. If the gas is exposed to a rapid cooling process (i.e. faster than the time the system needs to achieve equilibrium), NO is "freezing out". Further sources of nitrogen oxides are microbiological processes in soils [Yienger etal., 1995]. The transport of tropospheric NO_x to the stratosphere is only of minor importance, as the life time of NO_x is usually shorter than respective transport times.

3.3 Stratospheric nitrogen oxides

Nitrous oxide (N_2O) is the most important source of NO_x in the stratosphere. N_2O is emitted in the troposphere, where it is rather inert, in contrary to NO_x, with a lifetime of about 150 years. Tropospheric N_2O sources are both natural and anthropogenic. The major contributions come from oceans and tropical forests (soil), but also from chemical industry: N_2O is a widely used propellant and is found in artificial fertilizers. In consequence, the tropospheric N_2O level has risen with an average annual growth rate of$\sim$ 0.75 ppb [WMO, 2003] since preindustrial times. After it has been transported to the stratosphere, it is either photolyzed or oxidized to NO. 90% of N_2O in the stratosphere are removed by photolysis:

$$\mathrm{N}_2O + h\nu \rightarrow N_2 + O(^1D) \qquad \lambda \leqslant 298nm \tag{3.3.1}$$

The remaining N_2O can be oxidized to NO with electronically excited oxygen rad icals:

$$O(^1D) + N_2O \rightarrow 2NO \qquad (58\%) \tag{3.3.2}$$

$$\rightarrow N_2 + O_2 \qquad (42\%) \tag{3.3.3}$$

The photolysis of NO and the subsequent reactions of N with NO act as a sink for NO_x in the upper stratosphere with the net reaction:

$$\mathrm{NO} + \mathrm{N} \rightarrow N_2 + O \tag{3.3.4}$$

During the day NO and NO_2 are in a photochemical equilibrium as described by the Leighton ratio (see reaction(3.2.1)). With the beginning of night, NO is rapidly converted to NO_2 due to missing NO_2 photolysis. NO_2 is then oxidized to NO_3 by O_3:

$$\mathrm{NO_2} + O_3 \rightarrow NO_3 + O_2 \tag{3.3.5}$$

NO_3 does not exist during the day, because it photolyzes too rapidly. During night it reacts with NO_2 and forms N_2O_5. N_2O_5 is one of the dominant nighttime reservoirs for the active nitrogen species in the stratosphere. The catalytic destruction of ozone by NO and NO_2 is reduced by the formation of N_2O_5 [Mengistu et al., 2004].

$$\mathrm{NO_3} + NO_2 \rightarrow N_2O_5 \tag{3.3.6}$$

N_2O_5 reacts back to NO_2 and NO_3 by collisional decomposition or photolysis during day:

$$N_2O_5 + M \rightarrow NO_3 + NO_2 + M \tag{3.3.7}$$

$$N_2O_5 + h\nu \rightarrow NO_2 + NO + O_2 \qquad \lambda \leqslant 1252nm \tag{3.3.8}$$

Once sunlight is present, all NO_3 is destroyed very quickly. Therefore the photolysis of the remaining NO_2 and of N_2O_5 is initiated in the morning. Since the photolysis of

NO_2 proceeds some orders of magnitude faster than that of N_2O_5, the observed NO_2 concentration decreases in the morning until a photochemical steady state between NO and NO_2 via reactions (3.2.1 - 3.2.3) is established. Accordingly, the NO_2 concentration increases in the evening due to its reduced photolysis and the reaction of NO with O_3. The slow photolysis of N_2O_5 leads to an additional increase of the NO_2 concentration throughout the day. The result of these processes is a "tilted-u-shaped" diurnal variation of the NO_2 concentration. The only daytime sink for NO_x is the reaction of NO_2 with OH:

$$\mathrm{NO_2} + OH \rightarrow HNO_3 \tag{3.3.9}$$

while HNO_3 is usually removed from the atmosphere by precipitation. During long winter nights and especially during polar night, NO_2 is almost completely converted to its reservoir species N_2O_5 and HNO_3 by heterogeneous reactions, i.e. reactions in which the reactants are components of two or more phases (e.g. gaseous and solid or gaseous and liquid). N_2O_5 reacts with particles of Polar Stratospheric Clouds (PSCs) in the following reactions:

$$\mathrm{N_2}O_5 + HCl \quad \xrightarrow{hetrog.} \quad HNO_3 + ClONO_2 \tag{3.3.10}$$

$$N_2O_5 + H_2O \quad \xrightarrow{hetrog.} \quad 2HNO_3 \tag{3.3.11}$$

These processes lead to a pronounced seasonal variation of NO_x, with a strong concentration decrease during winter (denoxification). The strength of this seasonal cycle depends on temperature, duration of night time, as seasons themselves are latitude dependent. This can irreversibly remove inorganic nitrogen from the stratosphere (denitrification) and leads to stronger ozone depletion in polar spring (see section (3.4)). An important question of stratospheric nitrogen chemistry is the contribution of individual

species to the total NO_y abundance (all inorganic nitrogen species), referred to as NO_y partitioning. It is determined by the different life times of the NO_y species. Both the production and destruction of HNO_3, are slow processes so HNO_3 has only a small impact on the diurnal variation of NO_x. The denoxification during polar winter, however, renders HNO_3 by far dominant NO_y species in this time period, being also an important prerequisite for the formation of the ozone hole (see reaction (3.2.3)). As N_2O is the major source of stratospheric NO_y, the distribution of NO_y and N_2O are photochemically linked (reactions (3.3.2) and (3.3.1)). This correlation defines standard climatology of NO_y (= standard climatological NO_y) and any deviation is usually a sign of denitrication [Rinsland et al., 1996 ; Mengistu et al.,2005]. Below 30 km altitude, NO_y and N_2O are almost linearly anticorrelated. The slope of this lower stratospheric correlation is controlled by a combination of photochemistry and dynamics. Higher up (30 - 70 km) the correlation is dominated by the increasing destruction of NO_y by reaction (3.3.4)[Seinfeld ,J. H., Pandis, S. N, 2006].

3.4 Stratospheric ozone

More than 90% of the total atmospheric ozone is located in the stratosphere, where the ozone profile shows a distinct concentration maximum at 15-30 km altitude. This maximum is often referred to as the ozone layer (see Fig. 3.1), where most absorption of the harmful UV radiation takes place. Its height and intensity change with latitude, season, and meteorological conditions [Seinfeld ,J. H., Pandis, S. N,2006].

Ozone in the stratosphere is of great importance mainly because of the following main reasons. It forms a protective shield that reduces the intensity of UV radiation (with wavelengths between 230 and 320 nm) from the sun that reaches the Earths surface. Because of the absorption of UV radiation by O_3, it determines the vertical profile of temperature in the stratosphere. It also involved in many stratospheric chemical reaction.

In 1881 Hartley measured the UV radiation reaching the Earths surface and found a sharp cutoff at 300 nm; he correctly attributed this to absorption by O_3 in the stratosphere. Subsequent ground based UV measurements as a function of the suns elevation and the first measurements of the concentrations of stratospheric O_3 by balloons in the 1930s placed the maximum O_3 concentration in the lower part of the stratosphere.

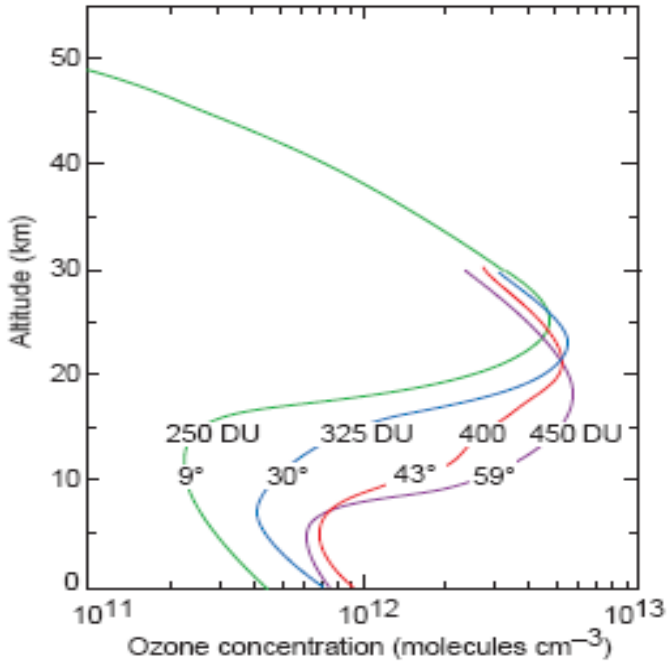

Figure 3.1: Mean vertical distribution of ozone concentrations based on measurements at different latitudes (given in degrees). Note the increase in the total ozone column abundance (given in DU) with increasing latitude. [Adapted from John M. Wallace and Peter V. Hobbs, Atmospheric science: an introductory servery, Elsevier, 2006].

In 1930 the first theory on the photochemical formation of ozone in the stratosphere was proposed by Chapman, predicting a maximum around 20 km altitude. Chapman describes the formation and destruction of ozone in the stratosphere by the so called odd-oxygen chemistry. The production of ozone is initiated by the photolysis of molecular oxygen:

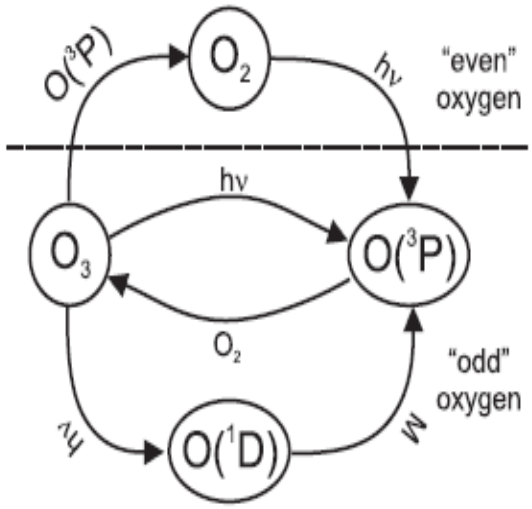

Figure 3.2: Schematic diagram of the Chapman Cycle.

$$\mathrm{O}_2 + h\,\nu \longrightarrow 2O(^3P) \qquad \lambda \leq 242nm \tag{3.4.1}$$

$$\mathrm{O}(^3P) + O_2 + M \longrightarrow O_3 + M \tag{3.4.2}$$

Ozone is formed via the reaction (3.4.2) from O and O_2 with a collision partner M. The ozone destruction proceeds via photolysis with UV radiation:

$$\mathrm{O}_3 + h\nu \longrightarrow O_2 + O(^1D) \qquad \lambda < 320nm \tag{3.4.3}$$

$$\mathrm{O}(^1D) + M \rightarrow O(^3P) + M \tag{3.4.4}$$

$$\mathrm{O}_3 + h\nu \rightarrow O_2 + O(^3P) \tag{3.4.5}$$

$$2\mathrm{O}(^3P) + M \rightarrow O_2 + M \tag{3.4.6}$$

$$\mathrm{O}(^3P) + O_3 \rightarrow 2O_2 \tag{3.4.7}$$

The photolysis of O_2 (reaction 3.4.1) and thus the O_3 production mainly takes place in the upper stratosphere where radiation at short wavelengths occurs with high intensity. Together with the O_3 photodissociation reactions (3.4.3) and (3.4.5) an equilibrium builds

up. Note that by O_3 photolysis atomic oxygen is produced which reacts back with O_3 in the order of seconds (3.4.2). Therefore the timescales on which these reactions occur need to be considered. This leads to the definition of the odd and even oxygen groups. Species can be transformed within their own group on short timescales while the lifetime of the whole group is rather long. A sketch of the Chapman cycle and its groups is shown in Fig. 3.2.

By observations it soon became clear that the Chapman cycle alone cannot explain the measured ozone profiles. Model calculations including only oxygen chemistry overestimated the stratospheric ozone abundance by a factor of two. Therefore additional ozone sinks must exist. In the following years the observed lower ozone levels were subsequently explained by stratospheric chemistry cycles involving species such as hydrogen and nitrogen as well as halogen compounds. These compounds all destroy ozone in catalytic reactions:

$$\mathrm{O}_3 + X \rightarrow O_2 + XO \tag{3.4.8}$$

$$\mathrm{O}(^3P) + XO \rightarrow O_2 + X \tag{3.4.9}$$

net: $O(^3P) + O_3 \rightarrow \mathrm{O}_2 + O_2$

where the radical groups HO_x, NO_x, ClO_x and BrO_x serve as X or as XO respectively, e.g. in the HO_x cycle X denotes OH and XO stands for HO_2. The HO_x cycle, denotes the first of numerous catalytic reaction cycles proposed for the destruction of ozone.

The HO_x cycle, a set of ozone destroying reaction cycles, involving hydrogen oxides, was first proposed by Bates and Nicolet [1950]:

$$\mathrm{O} + \mathrm{OH} \rightarrow O_2 + H \tag{3.4.10}$$

$$\mathrm{H} + \mathrm{O}_2 + M \rightarrow HO_2 + M \tag{3.4.11}$$

$$\mathrm{O} + \mathrm{HO}_2 \rightarrow O_2 + OH \tag{3.4.12}$$

net: $2O \rightarrow O_2$

$$\mathrm{O} + \mathrm{OH} \rightarrow O_2 + H \tag{3.4.13}$$

$$\mathrm{H} + \mathrm{O_3} + M \rightarrow OH + O_2 + M \tag{3.4.14}$$

net: $\mathrm{O} + \mathrm{O_3} \rightarrow 2O_2$

$$\mathrm{O_3} + OH \rightarrow O_2 + HO_2 \tag{3.4.15}$$

$$\mathrm{O} + \mathrm{HO_2} \rightarrow OH + O_2 \tag{3.4.16}$$

net:$O + O_3 \rightarrow 2O_2$

OH is produced in the stratosphere by the reaction of water vapor with $O(^1D)$. Since the cold tropopause prevents tropospheric water vapor from entering the stratosphere, water vapor is produced in the stratosphere by the oxidation of methane (CH_4):

$$\mathrm{CH_4} + O(^1D) \rightarrow OH + CH_3 \tag{3.4.17}$$

$$\mathrm{CH_4} + OH \rightarrow H_2O + CH_3 \tag{3.4.18}$$

$$\mathrm{O}(^1D) + H_2O \rightarrow 2OH \tag{3.4.19}$$

The compound responsible for the conversion of ozone to molecular oxygen is restored after one cycle and therefore remains available for the destruction of ozone unless it is removed by other sinks. This is why catalytic reactions have such a strong impact on the ozone budget even if their concentration is by far smaller than that of ozone. The HO_x cycle is particularly important for the ozone budget in the lower stratosphere (10 - 15) km altitude, where the catalytic cycles, reaction (3.4.10) to (3.4.19), are responsible for about 80 % of the total ozone loss processes.

The NO_xcycle involves nitrogen oxides via the following reactions [Crutzen 1970; Johnston 1971]:

$$\mathrm{O_3} + NO \rightarrow O_2 + NO_2 \tag{3.4.20}$$

$$\mathrm{O} + \mathrm{NO_2} \rightarrow NO + O_2 \tag{3.4.21}$$

net: $O + O_3 \rightarrow 2O_2$

$$O_3 + NO \rightarrow O_2 + NO_2 \tag{3.4.22}$$

$$NO_2 + O_3 + M \rightarrow NO_3 + O_2 \tag{3.4.23}$$

$$NO_3 + h\nu \rightarrow NO + O_2 \tag{3.4.24}$$

net: $2O_3 + h\nu \rightarrow 3O_2$

The NO_x cycles, reactions (3.4.20) and (3.4.24) are particularly important for the ozone budget in the middle stratosphere (30 - 40 km), where they are responsible for 60 - 70% of the odd oxygen loss. An anthropogenic influence on the stratospheric NO_x budget is given by the increasing abundance of the source gas N_2O, but also by direct emissions of nitrogen oxides in the stratosphere from supersonic aircrafts.

The ClO_x cycle was formulated following some observations. In the 1970s it was postulated by Molina and Rowland [1974] that the release of industrially produced halocarbons, in particular the chlorofluorocarbons (CFCs) $CFCl_3$ and CF_2Cl_2, could cause severe depletion of stratospheric ozone by reactions involving the photolytical products from CFC radicals Cl and ClO as catalysts. The following catalytic cycles involve also combined chlorine bromine chemistry:

$$\mathrm{Cl} + \mathrm{O_3} \rightarrow ClO + O_2 \tag{3.4.25}$$

$$\mathrm{ClO} + \mathrm{O} \rightarrow Cl + O_2 \tag{3.4.26}$$

$net : O + O_3 = 2O_2$

$$2\mathrm{Cl} + 2\mathrm{O}_3 \rightarrow 2ClO + 2O_2 \tag{3.4.27}$$

$$ClO + ClO + M \rightarrow Cl_2O_2 + M \tag{3.4.28}$$

$$Cl_2O_2 + h\nu \rightarrow Cl + ClO_2 \tag{3.4.29}$$

$$\mathrm{ClO}_2 + M \rightarrow Cl + O_2 + M \tag{3.4.30}$$

$net : 2O_3 \rightarrow 3O_2$

$$\mathrm{Cl} + \mathrm{O}_3 \rightarrow ClO + O_2 \tag{3.4.31}$$

$$\mathrm{Br} + \mathrm{O}_3 \rightarrow BrO + O_2 \tag{3.4.32}$$

$$BrO + ClO \rightarrow Br + ClO_2 \tag{3.4.33}$$

$$\mathrm{ClO}_2 + M \rightarrow Cl + O_2 + M \tag{3.4.34}$$

$net : 2O_3 \rightarrow 3O_2$

Under normal (non - ozone hole, see below) conditions, most of the chlorine in the stratosphere is usually bound in the reservoir species hydrogen chloride (HCl) and chlorine nitrate ($ClONO_2$) formed in the following reactions:

$$\mathrm{Cl} + \mathrm{CH}_4 \rightarrow HCl + CH_3 \tag{3.4.35}$$

$$\mathrm{ClO} + \mathrm{NO}_2 + M \rightarrow ClONO_2 + M \tag{3.4.36}$$

Remote sensing measurements of O_3 at Halley Bay (76^0 S) in the Antarctic for many years, reported a 30% decrease in springtime (october) total column O_3 since 1977 [John and Peter, 2006]. Mengistu et al. [2005] reported the chemistry of the observed reactive nitrogen species and ozone before and after the split of Antarctic polar vortex at lower and mid-latitude and isentropic levels during September/October 2002. Most of the available reactive nitrogen NO_y ($[NO_x] = [\mathrm{NO}] + [\mathrm{NO}_2]$) and NO_y (defined here as $[NO_y] = [\mathrm{HNO}_3]$

+ [ClONO_2] + [NO_x] + 2[N_2O_5]) and their partitioning in the polar vortex was in the form of HNO_3 and NO_x in the lower stratosphere except for the period 22-27 September when NO_y was mostly in the form of HNO_3 and $ClONO_2$ between the 400 K and 475 K levels. The dominant process throughout the lower stratosphere was enhanced photolysis of HNO_3 resulting in a steady increase of NO_x during the split of vortex. The enhanced photolysis was initiated following the displacement of the vortex to low and mid-latitudes. This observation was confirmed by the buildup of HNO_3 after this period in mid-October following the vortex repositioning on the pole. N_2O_5 inside the vortex increased above the 625 K level during the 22-27 September periods following the enhancement of NO_x from HNO_3 photolysis. On the 475 K level, the NO_y volume mixing ratio (VMR) inside the vortex is lower than the reference value derived from its proxy early winter exvortex relation by about 12.5 ppbv during the whole period.

Only about 10 % of the stratospheric inorganic chlorine is available in its activated forms Cl, ClO and Cl_x for the reaction cycles introduced in reaction(3.4.35) and (3.4.36). This situation changes significantly during polar winter and is closely related to NO_x. Reaction (3.4.36) shows that NO_x does not only lead to ozone depletion via the NO_x cycle, but that NO_x also plays a crucial role in slowing down ozone destruction by transforming other ozone depleting species into their reservoir gases. Besides reaction (3.4.36), NO_x is also involved in the HO_x cycle, transforming OH via NO_2 into HNO_3 (reaction (3.3.9)).

In polar winter, however, when NO_x is transformed into its reservoir species and when the denoxication process is very pronounced, a different chemistry starts to take place. Under the special conditions of the polar winter stratosphere (darkness, temperatures below 190 K and a stable polar vortex, heterogeneous reactions on the surface of polar stratospheric clouds (PSCs) can transform 30 - 60 % of chlorine into activated forms, e.g. into Cl_2 by:

$$\mathrm{ClONO_2} + HCl \quad \xrightarrow{hetrog.} \quad Cl_2 + HNO_3 \tag{3.4.37}$$

As a result, molecular chlorine can accumulate inside the polar vortex during polar

winter, while at the same time sedimentation of HNO_3-containing PSCs takes place and the reservoirs of nitrogen oxides are effectively removed from the polar vortex (denitrification). As soon as sunlight is present during polar spring the photolysis of Cl_2

$$Cl_2 + h\nu \rightarrow Cl + Cl \tag{3.4.38}$$

produces chlorine atoms which can effectively destroy ozone in the catalytic cycles, reactions (3.4.25)-(3.4.26), (3.4.27)-(3.4.30) and - if bromine is present reactions (3.4.32)-(3.4.33). During polar spring these processes lead to the stratospheric ozone hole, where, over Antarctica, typically all ozone at about 15 - 20 km altitude is destroyed. These reactions are particularly efficient, because the formation of $ClONO_2$ by reaction (3.4.36) cannot take place due to missing NO_x. The ozone depletion continues until the polar vortex breaks up and NO_x is restored by inflow from mid-latitudes. In summary, the consideration of all catalytic cycles described above leads to an ozone budget in the stratosphere which is consistent with the observations [Molina and Rowland 1974; Molina and Molina 1987; McElroy et al. 1986].

3.5 Tropospheric nitrogen oxides and ozone

In the troposphere, NO_x and ozone chemistry is generally different from the stratosphere. Reactions (3.4.20) and (3.4.21) of the NO_x cycle are negligible due to low concentrations of atomic oxygen, and ozone production via reactions (3.4.1)and (3.4.2) of the Chapman cycle needs UV light below 242 nm, which is - thanks to stratospheric ozone - not available in the troposphere. While NO_x sources are tropospheric already, it was commonly assumed until the late 1970s that tropospheric ozone has its origin in the stratosphere (e.g. [Junge, 1963]). Stratospheric ozone was assumed to mix through the tropopause region, exhibiting a gradient towards the earth's surface, which was also thought to be the dominant sink. Today it is believed that only about 10 % of the tropospheric ozone has

its origin in the stratosphere. Tropospheric sources of ozone are given by NO_x chemistry and reactions involving methane and other reactive hydrocarbons [Fishman and Crutzen 1978], as well as reactions with CO and Volatile Organic Compounds (VOCs). The oxidation of these species in the presence of NO_x in most cases results in ozone production. For very high levels of NO_x, however, a further increase of NO_x does not lead to higher ozone production anymore; this phenomenon is called the VOC- limited regime and is described below.

A key sequence for the formation and destruction of tropospheric ozone are reactions (3.2.1)-(3.2.3) involving NO_x. In areas with elevated NO_x (10 - 30 ppt), nitrogen and hydrogen oxides are able to produce ozone by reactions with CO, methane (CH_4) or higher hydrocarbons and VOCs. The ozone production, e.g. by oxidation of CO is initiated by a reaction with OH:

$$\mathrm{CO} + \mathrm{OH} \rightarrow CO_2 + H \tag{3.5.1}$$

$$\mathrm{H} + \mathrm{O_2} + M \rightarrow HO_2 + M \tag{3.5.2}$$

$$\mathrm{HO_2} + NO \rightarrow OH + NO_2 \tag{3.5.3}$$

$$\mathrm{NO_2} + h\nu \rightarrow NO + O \tag{3.5.4}$$

$$\mathrm{O_2} + O + M \rightarrow O_3 + M \tag{3.5.5}$$

$net : CO + 2O_2 \rightarrow CO_2 + O_3$

In the presence of NO the following reaction

$$\mathrm{NO} + \mathrm{HO_2} \rightarrow NO_2 + OH \tag{3.5.6}$$

competes with the ozone destructive reaction of NO with O_3 to form NO_2 (reaction (3.2.1)). With NO sources being primarily in urban areas, the freshly emitted NO reacts via (3.2.1) with already present ozone. So NO_x can also cause ozone loss. In fact, during ozone smog periods ozone concentrations in cities can be lower than in the rural areas

around, where neither NO sources nor primarily higher ozone values are found. The plumes of NO_x-rich air are then transported by wind to the countryside. Since sunlight is needed to produce new NO from NO_2 (reaction (3.2.2), ozone smog is a typical problem of long and sunny summer days.

The oxidation of CH_4 and VOCs leading to ozone production is more complex, as several branchings of reaction paths occur. In general, peroxy radicals (RO_2) are produced that can oxidize NO to NO_2 in analogy to reaction (3.5.6):

$$\mathrm{NO} + \mathrm{RO_2} \rightarrow NO_2 + RO \tag{3.5.7}$$

The peroxy radical family consists of HO_2 and RO_2 with R representing the unreactive organic part of the molecule. Thus the oxidation of CO and VOCs leads to ozone production via (3.2.2) and (3.2.2), if NO_x levels are high enough to compensate the ozone losses of the HO_x loss cycle (see reaction (3.4.12 or 3.4.16)). This holds true for NO_x concentrations above a 10 - 30 ppt threshold. This threshold typically separates rural areas with a background NO_x concentration of about 10 ppt from urban areas, that exhibit higher concentrations. Below this threshold, CO and hydrocarbons instead lead to destruction of ozone:

$$CO + OH \rightarrow CO_2 + H \tag{3.5.8}$$

$$H + O_2 + M \rightarrow HO_2 + M \tag{3.5.9}$$

$$HO_2 + O_3 \rightarrow OH + 2O_2 \tag{3.5.10}$$

net: $CO + O_3 \rightarrow CO_2 + O_2$

For very high NO_x concentrations, however, up to several 100 ppb in heavily polluted urban air, reaction (3.3.9) removes NO_x from the system and competes with reactions of OH with CO reaction (3.5.1) and VOCs. In this case, increasing NO_x emissions can

reduce ozone concentrations if not enough VOCs are present for the formation of HO_2 and RO_2. This situation is called the VOC limited regime, in contrast to the NO_x limited regime, where ozone increases with increasing NO_x emissions. For a successful strategy against ozone pollution in cities, it is therefore crucial to distinguish between VOC limited and NO_x limited regimes and to focus on the reduction of the limiting pollutants. Besides the removal of NO_2 by OH producing HNO_3 (reaction (3.3.9)), night time reactions via NO_3 and N_2O_5 and the heterogeneous reactions of N_2O_5 with aerosols, are further NO_x sinks. The produced HNO_3 is finally removed from the atmosphere by precipitation, which is apart from H_2SO_4 the important constituent of acid rain, causing severe damage to ecosystems. Summary of ozone chemistry is given in Appendix A.2.

Chapter 4

Data and Methodology

In this chapter, the data and methodologies used are presented. The first section of this chapter is devoted to description of instruments used to measure ozone. It is followed by the description of MOZAIC, TOMS, ECMWF ERA-Interim data. In the second section, the methodologies used to carry out the analysis of the data are presented in greater detail.

4.1 Data sources

4.1.1 MOZAIC

The MOZAIC programme was initiated in 1993 by European scientists, aircraft manufacturers and airlines (Airbus, Lufthansa, Air France, Sabena, and Austrian Airlines) to collect automatic and regular measurements of O_3, H_2O, CO and NO_y by five long range passenger airliners flying all over the world. The programme is funded by the European Commission and national agencies. Three phases have followed one another since 1994 [Marenco et al., 1998]. The first phase, MOZAIC I, extends from January 1993 to September 1996 and consisted of development/installation of the instrumentation and making/interpreting O_3 and H_2O in-flight measurements, a second three year phase, MOZAIC II started in October 1996 with the aim of continuing measurement of O_3 and

H_2O and their interpretation, and carry out a feasibility study of new airborne instruments to measure NO_y and CO. At third phase, MOZAIC III, installed new devices to fly for several years the whole set of instruments (O_3, H_2O, NO_y, CO).

MOZAIC's general goals are to contribute to the assessment of climate change and the impact of aircraft on the atmosphere. Ozone and water vapour in the Upper Troposphere and Lower Stratosphere have a large natural spatial and temporal variability and have key roles with regards to climate. Comprehensive, detailed and continuous observations are highly needed with respect to this task [IPCC, 2001]. Passenger aircraft are a very powerful observing platform for this purpose. The main contributions of the MOZAIC programme deals with more specific goals of MOZAIC that are to perform long term observations of the atmosphere, to investigate the impact of transport and chemical processes to establish the tropospheric budget of ozone and water vapor, to investigate upper-tropospheric relative humidity distribution, climatology of ozone in the upper troposphere and lower stratosphere, tropospheric ozone budget, stratosphere-troposphere exchanges and process studies, tropospheric ozone precursors chemistry, transport models validation, sensitivity experiments, assessment of the impact of aircraft emissions.

The measurement uses the aircraft's power supply and is driven by a computer which controls the instruments. It receives the aircraft flight positions (latitude, longitude, level, i.e atmospheric pressure and altitude). These data values are stored on the removable high capacity disks. The system works automatically, without involving the flight crew. It automatically detects the different phases of the flight (to control instruments and data recording) and provides maintenance information (fault lamp, error messages) on the ground. The airline's routine maintenance consists only in the replacement of data disk and water vapor sensor during each check of the aircraft after 500 hours of flight.

Ozone analyzer

A. Sensors

The ozone analyzer is a dual beam UV absorption instrument (Thermo-Electronic, Model 49-103). A teflon KNF Neuberger pump is used for pumping air through the analyzer, from the external pressure of 150-250 hPa at cruise altitude. The instrument has the detection limit of 2 ppbv, overall precision $\pm[2ppbv + 2\%]$. The schematic diagram of dual beam UV spectrometer is depicted in Fig. 4.1.

B. Mounting

The MOZAIC instrumentation has been developed for automatic measurements during in service flights of the aircraft. It consists of a specially designed rack, installed in the right side of the avionic component (below the cockpit), and of a probe plate located on the fuselage seven meters back from the nose of aircraft (Fig. 4.2). The plate holds the pitot tube (ozone) and Rosemount housing (humidity , temperature) such that the inlets (seven and ten cm high above the plate) are well outside the aircraft boundary layer. The procedure of sampling the external air for ozone measurement only after take off and before landing is used to prevent contamination of the input line by deposition of organic compounds and dust while the aircraft is on the ground and subject to local pollution.

C. Operation

The system uses the aircraft power supply and is computer controlled, with an auto-start mode. Through software held on the storage disk, an electronic interface controls the axillary devices (pumps, teflon electro valves, mass flow meters, error detection system, water vapor and temperature electronic transmitter units). Measurements are taken every 4 s, starting after takeoff and continuing up to landing. Data (O_3, H_2O, T, and status of control parameters) and aircraft parameters from the Air Data computer (time, latitude,

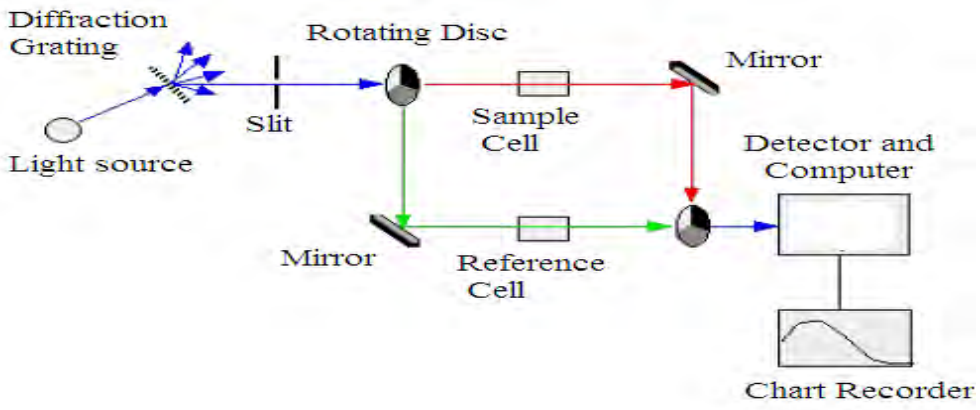

Figure 4.1: Schematic diagram of a simple double beam spectrometer.

Figure 4.2: View of the removable plate with probes: Pitot tube (O_3) sampling and Rosemount housing (H_2O and temprature sensors), installed on a MOZAIC A340 airbus.

longitude, altitude, pressure, aircraft seed, wind direction and velocity) are stored on the removable high capacity disk [Marenco et al., 1998].

4.1.2 Nimbus-7 TOMS instrument and satellite information

The series of American Nimbus satellites were designed to demonstrate the utility of weather satellites for forecasting the weather. The first satellite was launched in 1964 and the seventh, which was the first in a series of four satellites to have the TOMS instrument

on board, in 1978. The objective of Nimbus 7 was the physical characterization of the global atmosphere, the oceans, the interface between ocean and atmosphere and the heat balance of the earth. Along with the TOMS instrument, NIMBUS-7 also had sensors on board to measure other atmospheric gases and aerosols, as well as a forerunner of the SeaWifs sensor for measuring oceanic parameters. The TOMS instrument calculates the total content of O_3 on the basis of diffused UV radiation and direct irradiance. The TOMS program began with the launch of TOMS Flight Model 1 on the Nimbus-7 spacecraft on October 24, 1978. Valid measurements started in November of that same year and the instrument continued to return data long after all other on-board experiments had failed. The TOMS instrument fell silent in May 1993. The software to derive useful information from the data returned by Nimbus-7 TOMS is the basis for the algorithm used to analyze all TOMS data and has gone through a lengthly evolutionary process bring it to the current version. The Version-7 processed data include a revised instrument calibration based on analysis of the entire 14.5 year data record (including a correction for a 0.2 nm wavelength error which caused a 3% absolute offset relative to Dobson) as well as an improved algorithm. Algorithmic improvements include:

- use of wavelength "triplets" that correct for errors linear in wavelength;
- improved International Satellite Cloud Climatology Project (ISCCP) cloud height climatology, higher resolution terrain height maps;
- use of improved profile shape selection to improve total ozone at very large solar zenith angles;
- use of a more accurate model for partially-clouded scenes;
- improved radiative transfer calculations for table generation.

Nimbus-7 satellite provided daily global coverage of the Earth's total ozone by measuring backscattered ultraviolet sunlight. TOMS instruments map total ozone by scanning

through the subsatellite point in a direction perpendicular to the orbital plane (Nadir)

The Nimbus-7 TOMS instrument had a single, fixed monochromator and a scanning mirror to sample the backscattered solar ultraviolet radiation. The slit functions were triangular with a nominal 1-nm bandwidth. The order of individual measurements was determined by a chopper wheel. As it rotated, openings at different distances from the center of the wheel would pass over the exit slits, allowing measurements at the different wavelengths. The order was not one of monotonically increasing or decreasing wavelength; instead, the wavelengths were interleaved to minimize the effect of scene changes on the ozone retrieval. The instrument IFOV was 3×3 degrees. A mirror scanned perpendicular to the orbital plane in 3-degree steps from 51 degrees on the right side of spacecraft nadir to 51 degrees on the left (relative to direction of flight), for a total of 35 samples. At the end of the scan, the mirror would quickly return to the first position, not making measurements on the retrace. Eight seconds after the start of the previous scan, another would begin. Consecutive cross-scans overlapped, creating a contiguous mapping of ozone. A ground aluminum diffuser plate was deployed to reflect sunlight into the instrument to measure the solar irradiance. This diffuser plate was shared with the Solar Backscatter Ultraviolet (SBUV) experiment. It was normally deployed once a week for TOMS solar irradiance measurements, in addition to the SBUV deployments. The TOMS scanner had four operating modes determining data processing sequences and data formats:Normal scan mode, single step mode, view diffuser mode, stowed mode.

The primary operating mode of the TOMS was normal scan mode. It was in this mode that the scanning mirror sampled the 35 scenes corresponding to the scanner view angles, measuring the backscattered Earth radiances used for deriving column ozone. In the single step mode, the scanner was controlled by ground commands. Solar irradiance measurements were made in the view diffuser mode. The scanner would move to the view diffuser position and stop. In-orbit wavelength calibration occurred in the stowed mode. The scanner slowed to the stowed position and stopped, the mercury-argon lamp

was turned on and the diffuser plate was deployed to reflect light from the lamp into the instrument.

The TOMS instruments use six discrete wavelength in the UV/visible part of the spectrum to derive total ozone, an aerosol index, and SO_2 selected by a chopper wheel in the light path behind the monochromator grating. The solar irradiance is measured using a diffuser plate to reflect sunlight into the instrument. Actually, three diffuser plates are installed, which are used at different frequency. Comparisons of the signals of these diffusers allow the determination of degradation rates of the diffusers. The measurements used for ozone retrieval are made during the sunlit portions of the orbit. For a detailed discussion of TOMS instrument and ozone retrieval is well elaborated by Richard et al.[1996].

4.2 Data description

4.2.1 MOZAIC data

In the MOZAIC programme data are taken every four seconds recorded from aircraft take-off to landing, providing vertical profiles and cruise data between 8 and 12.5 km altitude. Vertical profiles are from surface to 10 km (250 hPa), while along track measurements are of cruising altitude of 12 km (200 hpa). The vertical take-off speed of the aircraft is around 5-7ms^{-1}, leading to a vertical resolution of the data of about 20-28 m [Thouret et al., 1998 b]. In this study only cruise data between the flying altitude 200-250 hpa over the equatorial and north Africa regions are considered.

Each data line contains 4 second resolution of pressure, temperature, relative humidity (unit %) with respect to liquid water, a validity tag and the relative uncertainty of the humidity measurement, the computed water vapor mixing ratio (mass mixing ratio, units g/kg), volume mixing ratio (ppbv) . Data not collected by MOZAIC are assigned different codes, missing ozone values are represented by -9999. The data lines contain furthermore

the current flight position (longitude, latitude, altitude) and date and time (hr, min and sec).

4.2.2 ECMWF-ERA interim reanalysis data sets

ERA-Interim is the latest global atmospheric reanalysis produced by the European Center for Medium-range Weather Forecast (ECMWF). ERA-Interim covers the period from 1 January 1989 onwards, and continues to be extended forward in near-real time. An extension from 1979 to 1989 is currently in preparation. Gridded data products include a large variety of 3-hourly surface parameters, describing weather as well as ocean-wave and land-surface conditions, and 6-hourly upper-air parameters covering the troposphere and stratosphere. Vertical integrals of atmospheric fluxes, monthly averages for many of the parameters, and other derived fields have also been produced. Information about the current status of ERA-Interim production, availability of data online, and near-real-time updates of various climate indicators derived from ERA-Interim data, can be found at http://www.ecmwf.int/research/era.

Reanalysis data provide a multivariate, spatially complete, and coherent record of the global atmospheric circulation. A multivariate reanalysis is physical coherence, meaning that estimated parameters must be consistent with the laws of physics as well as with observations. This is a defining property of reanalysis, which differentiates it from other methods for estimating geophysical parameters from observations. A sufficiently realistic model is able to extrapolate information from locally observed parameters to unobserved parameters at nearby locations, and it can also propagate this information forward in time. The skill of the reforecasts depends on the accuracy, completeness, and physical coherence of the reanalysed fields, as well as on the quality of the model used

Data assimilation

The ERA-Interim reanalysis is produced with a sequential data assimilation scheme,

advancing forward in time using 12-hourly analysis cycles. In each cycle, available observations are combined with prior information from a forecast model to estimate the evolving state of the global atmosphere and its underlying surface. This involves computing a variational analysis of the basic upper-air atmospheric fields (temperature, wind, humidity, ozone, surface pressure), followed by separate analyses of near surface parameters (2m temperature and 2m humidity), soil moisture and soil temperature, snow, and ocean waves. The analyses are then used to initialise a short-range model forecast, which provides the prior state estimates needed for the next analysis cycle. The forecast model has a crucial role in the data assimilation process. Use of the model equations makes it possible to extrapolate information from locally observed parameters to unobserved parameters in a physically meaningful way, and also to carry this information forward in time.

The skill and accuracy of the forecast model determines how well the assimilated information can be retained; better forecasts mean that smaller adjustments are needed to maintain consistency with observations as time evolves. Additionally, while producing a forecast, the model estimates a wide variety of physical parameters such as precipitation, turbulent fluxes, radiation fields, cloud properties, soil moisture, etc. Even if not directly observed, these are constrained by the observations used to initialize the forecast. The accuracy of these model-generated estimates naturally depends on the quality of the model physics as well as that of the analysis. The data assimilation thus produces a coherent record of the global atmospheric evolution constrained by the observations available during the period of reanalysis.

The ERA-Interim archive currently contains 6-hourly gridded estimates of three-dimensional (3D) meteorological variables, and 3-hourly estimates of a large number of surface parameters and other two-dimensional (2D) fields, for all dates from 1 January 1989. The core component of the ERA-Interim data assimilation system is the 12-hourly 4D-Var of the upper-air atmospheric state. The defining feature of 4D-Var is that it uses

the forecast model to constrain the state evolution within each analysis window. The version of 4D-Var used for ERAInterim also updates a set of parameter estimates that define bias corrections needed for the majority of satellite-based radiance observations. For furter details of reanalysis and model performance see [eg. Dee, April 2011]

In this thesis we have used potential vorticity, ozone, cloud liquid water content, vertical, zonal and meridional wind fields derived from ECMWF ERA-interim. The ERA-Interim archive is more extensive than its predecessor ERA-40, e.g. the number of pressure levels increased from ERA-40's 23 to 37 levels, the resolution from 2.50 to 1.50 and several products are included that were not available for ERA-40. Based on internal evaluations and comparisons with other reanalysis, the quality of ERA-Interim products is generally good and its long-term homogeneity has improved considerably over that of ERA-40. Internal validation of the ocean wave height analysis produced with ERA-Interim also indicates a higher degree of homogeneity. Verification against independent body of measurements shows rms errors that are stable and much smaller than ERA-40. Also there is reduced 10- meter wind speed bias over extra tropical ocean areas in the northern hemisphere. The data on both pressure and potential temperature levels are $1.5^0 \times 1.5^0$ resolution. ERA-Interim make use of data from the increasing number of new instruments on satellites from 2003 onwards as discussed by Graeme Kelly and Jean-Nol Thpaut [ECMWF Newsletter No. 113, 2007]. In particular 4D-Var improve the extraction of information from data provided by high-resolution instruments. Nevertheless, especially designed observing system experiments may be needed to help interpret climate signals in the ERA-Interim time series. The ERA-Interim data assimilation has T255 horizontal resolution, better formulation of background error constraint, reprocessed ozone profiles from GOME data from the Rutherford Appleton Laboratory from 1995 onwards and CHAMP GPS radio occultation measurements, reprocessed by university corporation for tmospheric research (UCAR) since February 11, 2001 [Wickert et al., 2005]. ERA-Interim uses mostly the sets of observations acquired for ERA-40, supplemented by data for later

years from ECMWF's operational archive. EUMETSAT provided reprocessed winds and clear-sky radiances from Meteosat-2 (1982-1988) for ERA-40 and has reprocessed later Meteosat data for ERA-Interim [ECMWF, 2008]. The data sets from ECMWF ERA-interim with variable vertical resolution in pressure level with a 6-hourly analysis frequency i.e. 0, 06, 12 and 18 UTC. The vertical levels used for this analysis are partitioned in such a way that there are 6 levels within 900-775 hPa layer at an interval of 25 hPa, 11 levels within 750-250 hPa layer at an interval of 50 hPa, 7 levels within 250-100 hPa layer at interval of 25 hPa, 2 levels at 70 and 50 hPa each.

4.2.3 TOMS' data

Nimbus-7 monthly mean TOC data is gridded ozone values stored as 3-digit integers in units of Dobson (DU). They are ordered from south to north with the first zone centered at 89.5^0S. Within each latitude zone, values are given for each of 288 longitude zones from 180 W through 0 (Greenwich) to 180 E. The first longitude zone is centered at 179.375^0 S. Data for each day are gridded into 1^0 latitude 1.25^0 longitude zones, where latitude and longitude ranges run from 89.5^0 N to 89.5^0 S and 179.375^0 W to 179.375^0 E respectively. Zeroes denote missing data; that is data that could not be collected due to lack of sunlight or other problems. In this study monthly mean TOC data for the years January 1979-January 1992 (fourteen years) are analyzed. Geographical region 37.5^0 N - 37.5^0 S and 20^0 W - 55^0 E are considered.

4.2.4 Miscellaneous data sets

The latent heat data set was obtained from Mirador, Goddard earth sciences data and information center. Mirador contains a series of land surface parameters simulated from the Common Land Model (CLM) V2.0 model in the Global Land Data Assimilation System (GLDAS). The data are in 1.0 degree resolution and range from 1979 to the present. The temporal resolution is 3-hour [http://mirador.gsfc.nasa.gov]. Outgoing

Long-wave Radiation (OLR) is used to investigate the convective phenomena. NOAA daily mean OLR data from NCAR archives, with gaps filled with temporal and spatial interpolation 2.5 degree latitude x 2.5 degree longitude global grid (144x73)[*http* : *//www.esrl.noaa.gov/psd/data/gridded/data*]. The pressure and temperature profiles used to identify tropopause level are obtained from NASA Goddard Space Flight Center's Laboratory for Atmospheres data can be automatically downloaded using e-mail address (scimanager@hyperion.gsfc.nasa.gov).

4.3 Methodology

The methods used to study ozone dynamics during STE, high latitude equatorial interaction, and seasonal and spatial variability of ozone over Africa are presented. First we will see methodologies employed to study ozone dynamics during stratosphere-troposphere exchange events over equatorial and North Africa. Ozone seasonal and spatial variability over Africa are followed.

4.3.1 Ozone dynamics over Equatorial and North Africa.

As outlined above, we are interested in cases of cruise enhanced ozone sampled by MOZAIC at upper troposphere for both equatorial and North Africa. Thus the data used in this study is limited to a cruise flying altitude of 8-12.5 km. For diagnostic purpose different data sets mentioned in the data description part are used to investigate the observed events.

Diagnostic tools

There is distinct variation in the IPV/PV and water vapor content of the stratosphere and troposphere [Danielsen et al., 1980, 1987; Zbinden et al., 2006]. We have used potential vorticity (PV) on isobaric coordinate and isentropic potential vorticity (IPV) in conjunction with relative humidity record, to identify from where enhanced ozone

have originated. Stratosphere air has very high ozone concentration but it is day and therefore have low relative humidity content. Thus we have used relative humidity as a proxy to trace the region of ozone rich air mass transport. We have produced meridional cross-section of potential vorticity at equator and North Africa. Isentropic surfaces in the range of 330-475 K are overlayed on the PV plot to distinguish whether there exists across isentropic surface air mass transport. IPV are also used to identify horizontal transport mechanisms. Wind streamlines calculated from zonal (U) and meridional (V) wind fields overlayed on 350 K IPV isentropic surfaces are used to investigate the impact of wind fields on IPV and ozone distribution.

We further calculated equivalent latitude to study ozone transport. Equivalent latitude is a Lagrangian coordinate used in atmospheric science, particularly in the study of stratospheric dynamics. Each isoline in a map of equivalent latitude follows that of an atmospheric tracer and encloses the same area as the latitude line of equivalent value, hence "equivalent latitude". Equivalent latitude (PVEL) is calculated from potential vorticity, from passive tracer simulations and from actual measurements of atmospheric tracers such as ozone. The equivalent latitude from the area is given as:

$$\phi_q = sin^{-1}(\frac{A}{2\pi R^2} - 1) \tag{4.3.1}$$

where A = A (q, θ, t) is the area in which PV is less than q on a particular isentropic surface with potential temperature θ at time t, and R is the radius of the earth. This would be the limiting latitude if A were reshaped into a pole-centered circle. To the extent that isentropic winds are divergence free and that PV is materially conserved, ϕ_q is also conserved. Since ϕ_q itself is moving with the air, effects of adiabatic transport can be removed when a quantity is measured in the (ϕ_q, θ) coordinate.

Calculation of PVEL involves creating a monotonic mapping between the values of equivalent latitude and the tracer it is based upon: higher values of the tracer map to higher values of PVEQ. A precise method is to assign a representative area to each of the

tracer measurements, filling the entire globe. Thus, for a tracer field regularly gridded in longitude and latitude, grid points closer to the pole will take up a smaller area, in proportion to the cosine of the latitude. Now, rank all the tracer values then form the cumulative sum [Douglas, 2003 ; Neal, 1986].

Irreversible deformation IPV indicate Rossby waves. As Rossby waves appears, zonal wind blow from the stratosphere down into troposphere [Kodera et al., 1990]. We have produced meridional cross section of zonal wind in the region of IPV deformation to demonstrate Rosbby waves.

The presence of convection described using proxy parameters such as latent heat, OLR, cloud cover and cloud water content and vertical wind (ω). These parameters are good proxies for the location and intensity of tropical convection. The possible ozone distribution in the troposphere is investigated using ozone VMR from ECMWF. Meridional cross section of ozone VMR is used at the two coupled events, intrusion and convection, mainly over equatorial Africa and intrusion over north Africa.

Defining tropopause level

I. At tropical latitude

The numerical method of objectively determining approximate tropopause pressure and temperature values using only mandatory height and temperature data is described. This method is a revised version of the method that is briefly outlined in an article that was presented by Hughes [1981] before the International Civil Aviation Organization (ICAO) Area Forecast Panel in Montreal, Canada. The major premise upon which this proposed numerical method rests is the WMO operational definition for the tropopause. That definition states that the conventional tropopause is the lowest level at which the lapse-rate decreases to 0.002 ^{0}C/m or less, and the average lapse-rate from this level to any level within the next higher 2000 m does not exceed 0.002 ^{0}C/m [McCalla, 1981].

Using only the mandatory height and temperature data (i.e. 500 - 50 mb), simple lapse-rates (i.e. $\gamma = \Delta T/\Delta z$) are computed for each layer. The lapse rates are assumed to vary linearly with pressure and, for modelling purposes, are taken to be valid at the central pressure of each layer [Hughes, 1981]. Mandatory data below 500 mb are not used in order to avoid the possibility of misinterpreting a low-level inversion for the level of the tropopause.

After each layer lapse-rate for a radiosonde or grid point sounding has been computed, the sounding is scanned in the direction of decreasing pressure until a layer is encountered wherein the lapse-rate is less than 0.002 ^{0}C/m. Whenever this occurs, the central pressure of that layer (i.e. Layer I) is assumed to be above the tropopause and the central pressure of the previous or lower layer (i.e. Layer I-l) is assumed to be below the tropopause (See Fig. 4.4). If, however, the tropopause cannot be bounded in this fashion, or if the computed tropopause pressure is less than 85 mb, then the tropopause pressure is set equal to 85 mb and the temperature at that level is determined by interpolation. Once Layer I and Layer I-1 have been determined, the tropopause pressure (PTROPE) may be computed by linear or log-linear interpolation between the central pressures of these two

layers to the level at which the lapse-rate is equal to 0.002 ^{0}C/m.

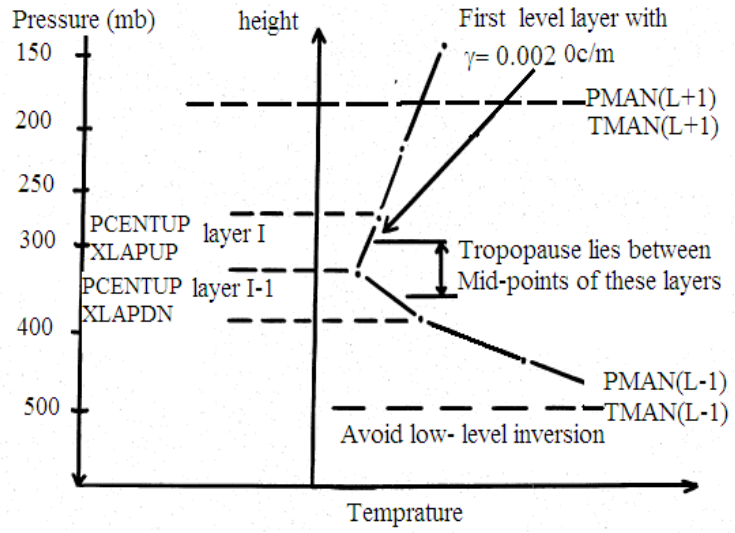

Figure 4.3: Basic model description of tropopause [McCalla, 1981].

The variable names are

- PMAN(L-1) - The pressure of the higher pressure mandatory level of Layer I-1;
- PMAN(L) - Simultaneously, the pressure of the lower pressure mandatory level of Layer I-1 and the pressure of the higher pressure mandatory level of Layer I;
- PMAN(L+1) - The pressure of the lower pressure mandatory level of Layer I.
- TMAN(L-1) - The mandatory temperature at the higher pressure mandatory level of Layer I-1;

Because the lapse-rates are assumed to be valid at the central pressure of each layer, a tropopause found to be below the midpoint of the lowest layer tested would have its pressure set equal to 450 mb and the tropopause temperature at 450 mb would be determined by interpolation between the 500 and the 400 mb levels;

- TMAN(L) - Simultaneously, the mandatory temperature at the lower pressure mandatory level of Layer I-1 and at the higher pressure mandatory level of Layer I;

- TMAN(L+1) - The mandatory temperature at the lower pressure mandatory level of Layer I.
- PCNTDN - The central pressure of Layer I-1;
- PCNTUP - The central pressure of Layer I;
- XLAPDN - The lapse-rate valid at the central pressure of Layer I-1;
- XLAPUP - The lapse-rate valid at the central pressure of Layer I;

If it is assumed, as in the Hughes article, that the lapse-rate varies linearly with pressure, then PTROPE may be determined as follows,

$$PTROPE = \frac{PCNTUP+(0.002-XLAPUP)(PCNTDN-PCNTUP)}{(XLAPDN-XLAPUP)} \tag{4.3.2}$$

If PTROPE is equal to PMAN(L),then the tropopause temperature (TTROPE) is equal to TMAN(L). If, however, PTROPE is not equal to PMAN(L), then the tropopause temperature must be determined by the method of linear interpolation ;

$$TTROPE = \frac{TMAN(L+1)+(lnPTROPE-InPMAN(L+I))(TMAN(L)-TMAN(L+1))}{lnPMAN(L)-InPMAN(L+1))} \tag{4.3.3}$$

for PTROPE $<$ PMAN(L) and,

$$TTROPE = \frac{TMAN(L)+(inPTROPE-InPMAN(L))(TMAN(L+1)-TMAN(l))}{(lnPMAN(L-1)-lnPMAN(L))} \tag{4.3.4}$$

for PTROPE $>$ PMAN(L).

II. At extratropical latitude

PV does not provide a well defined dynamical tropopause for the tropics and is only used in the extratropics [see, e.g.,Holton et al., 1995]. There is no universally used PV threshold for the dynamical tropopause, but the most common choice is the 2 PVU surface (1 PVU = $10^{-6}Km^2kg^{-1}s^{-1}$, standard potential vorticity unit) [e.g., Holton et al., 1995].

The original concept of the dynamical tropopause was based on the isentropic gradient of potential vorticity (PV) [Reed, 1955], but it has been most often represented by a particular PV surface to simplify matters [e.g., Hoskins et al., 1985; Holton et al., 1995]. In the study of STE over North Africa, we have defined tropopause level at 2 PVU over the region of our consideration $(20 - 60^0)$N.

4.3.2 Seasonal variability of ozone over Africa

The latitude regions of both north and south of Africa is divided into seven sub-regions of 5^0 latitude band each. 61 data points along the longitude and 5 data points in each latitude interval averaged to get one data point in each grid. Fourteen years monthly ozone concentration mean within 0 to 34.5^0 is calculated for both north and south latitude of the equator. Each data point is calculated using the following equation:

$$S_{i,j} = \frac{\sum_{i=1}^{n}(\sum_{j=1}^{m} a_{i,j})}{k} \quad , \tag{4.3.5}$$

where $a_{i,j}$ represents each data point and $S_{i,j}$ is a an average of k $= n \times m$ data points.

In addition, to study latitudinal spatial and seasonal variability of monthly ozone three arbitrarily years 1980, 1985, 1990 selected. The mean of 61 data points calculated in the longitude interval 20^0 W - 55^0 E to get one data point in each latitude band:

$$S_{i,j} = \sum_{i=1}^{z} \frac{(\sum_{j=1}^{m} a_{i,j})}{j} \tag{4.3.6}$$

where m and z represent number of data points with in 20^0 W - 55^0 E and 34.5^0 N- 34.5^0 S respectively.

Chapter 5

Results and Discussion

In this chapter, we present the results of analysis using the data sets and methodologies discussed in Chapter 4. The results are placed in two sections. The first part discusses enhanced ozone transport from stratosphere and/or high latitude to troposphere over equatorial and north Africa. At equatorial Africa, we attempt to explain the distribution of ozone in the troposphere due to dynamical events. Over north Africa, the modes of ozone transport observed during both stratospheric intrusion and isentropic transport from high latitude are presented. The second section discusses seasonal variability of ozone over Africa.

5.1 Ozone dynamics over Equatorial Africa.

Tropospheric ozone is a trace gas with a large natural variability in space and time and a mixing ratio in the range of about 10-100 ppbv [Zbinden et al., 2006]. In very few MOZAIC flights from Johannesburg to Vienna over equatorial Africa shown in Fig.5.1 (black rectangular box), spiky ozone enhancements, exceeding 100 ppbv VMR were observed during 1995-97 within 250-200 hPa baro-altitude range. Four of the spiky ozone and relative humidity enhancements listed in Table 5.1 are depicted in Fig. 5.2. There are only two possibilities for the observed ozone enhancements: in-situ production or transport from stratosphere during intrusion. In-situ chemical production in the troposphere

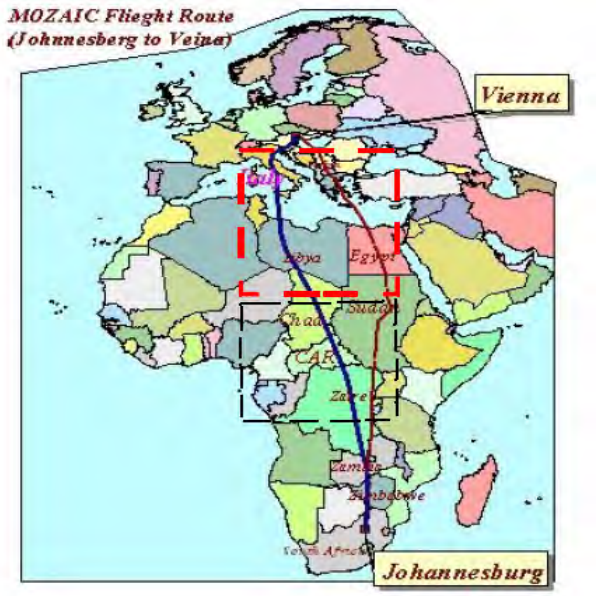

Figure 5.1: Most frequent MOZAIC flight routes from Johannesburg to Vienna. The dotted black and red rectangular boxes denotes regions of ozone enhancements at a flying altitude of 250-200 hPa

cannot lead to O_3 VMRs of 150-300 ppbv. This path way is disregarded right from the outset of the analysis. The other possible source of O_3 rich air masses are stratospheric intrusion. High relative humidity (RH >100 %) also observed at this cruise level over the region of elevated O_3 VMR. The release of latent heat affects the lapse rate, which is the rate at which atmospheric temperature declines with height. An ascending parcel of air cools as it expands. Parcels increase their RH rapidly as they ascend, for instance Dessler and Sherwood [2000], in their work on upper tropospheric humidity, reported RH of 20% at 300 hPa will saturate to RH of 100 % at about 215 hPa. Since the relative humidity content of the stratosphere is very low, less than 50 % [Zbinden et al., 2006], in addition to stratospheric intrusion there has to be other physical process happening in the troposphere. Thunderstorm activity would be one of the most likely events that could produce high latent heat and hence relative humidity record in the order of 100% in the vicinity of high ozone observation (see Fig. 5.2). Table 5.1 summarizes the mean enhanced ozone

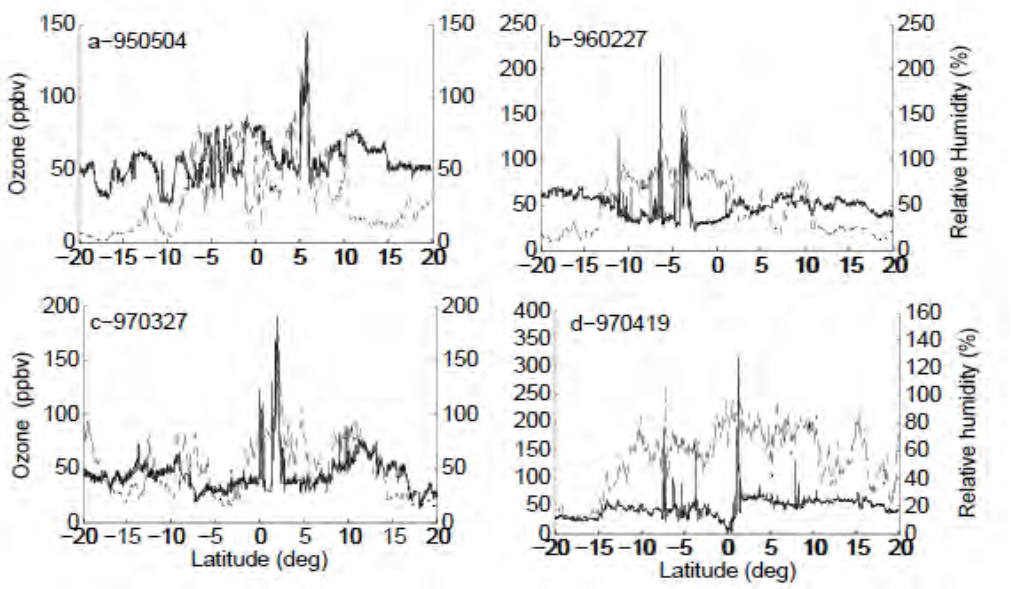

Figure 5.2: MOZAIC cruise ozone (solid line) and relative humidity (dash line) spikes observed on May 4, 1995, Feb.27, 1996, March 27 and April 19, 1997 at the flying altitude of 250-200 hPa

and relative humidity observations. We have investigated the presence of the coupled events, intrusion and convection. First we look at existence of ozone transport across the tropopause during intrusion. Potential vorticity is used to investigate stratospheric intrusion which induces very high ozone VMR to the troposphere along the PV tongue. Vertical velocity, OLR, cloud liquid water content and latent heat flux data sets of the same day are also used to see convective activity that could lead to the transport of cloud liquid water content to the upper troposphere where the airplane measure high relative humidity.

First we investigated the existence of stratospheric intrusion at the area of the flight prior to the plane traversing the route. The selected four events occurred before mid night on May 4, 1995 at 211558-221959 UTC, at 213832-214716 UTC on February 27, 1996, at 211631-211239 UTC on March 27, 1997 and after mid night 040258-040702 UTC on April 19, 1997. Therefore we have used potential vorticity ahead of the events at 18 UTC.

Table 5.1: Enhanced ozone and relative humidity spikes observed at equatorial Africa at a flying altitude of 250-200 hPa

Dates	Time (UTC)	Observation site		Mean (O_3)	Mean (RH)
		Lat(deg)	Long(deg)		
950504	211558-221959	5.34-6.02	29.71-29.75	109.98	114.65
960221	211631-211239	-6.67-7.16	26.90-27.03	124.8	180.08
960227	221059-221559	5.34-6.02	29.71-28.75	99.66	126.95
960406	221059-221559	5.02-6.50	28.71-29.75	103.45	no record
970118	013304-0149034	1.17-1.62	29.00-29.36	109.61	87.80
970327	222030-222454	1.69-2.26	25.80-25.87	135.10	134.95
970419	040258-040702	1.21-1.46	24.34-24.78	154.56	103.44
970424	032551-032903	4.91-5.66	23.82-24.04	182.89	153.26

Fig. 5.3 shows ozone VMR overlaid by wind fields (upper panels) at 100 hPa and daily mean OLR (lower panels). There is a clear relationship between OLR ($< 220\ W/m^2$) and convection as revealed by the overlaid wind fields in the upper panels of Fig. 5.3. In particular, the relationship is more apparent over regions bounded by 5 S, 20 E on May 4, 1995, 10 S, 40 E and 10 N, 25 E on February 27, 1996; as well as by $20-30$ E, $10-20$ S as well as $0-10$ N, 20 W on April 18, 1997.

Very high ozone VMR is observed in the regions characterized by low OLR and the overlaid stream lines showed anticyclonic flow in all cases over ozone rich region with the exception of panel c of Fig. 5.3 indicating there were upper-level out flows. However, in panel c of Fig. 5.3, there is cyclonic flow south of peak ozone axis and anticyclonic curvature on its northern side which likely indicates descending motion on its southern side and ascending motion over the northern side of peak ozone axis.

There is low OLR record in the region of cloud cover, this is illustrated with the cloud cover overlayed by streamlines at 200 hPa level shown in Fig. 5.4 for March 27, 1997 at 21 UTC (left panel). Strong cloud cover is observed with in 10 S - 10 N, 15-40 E and also anticyclone circulation centered at 20 E, 10-20 S (high pressure area). These are regions of low OLR as can be seen in Fig. 5.3 c. Similar case is shown 6 hours later for March 28, 1997 at 00 UTC (right panel). In both cases an easterly propagating trough observed

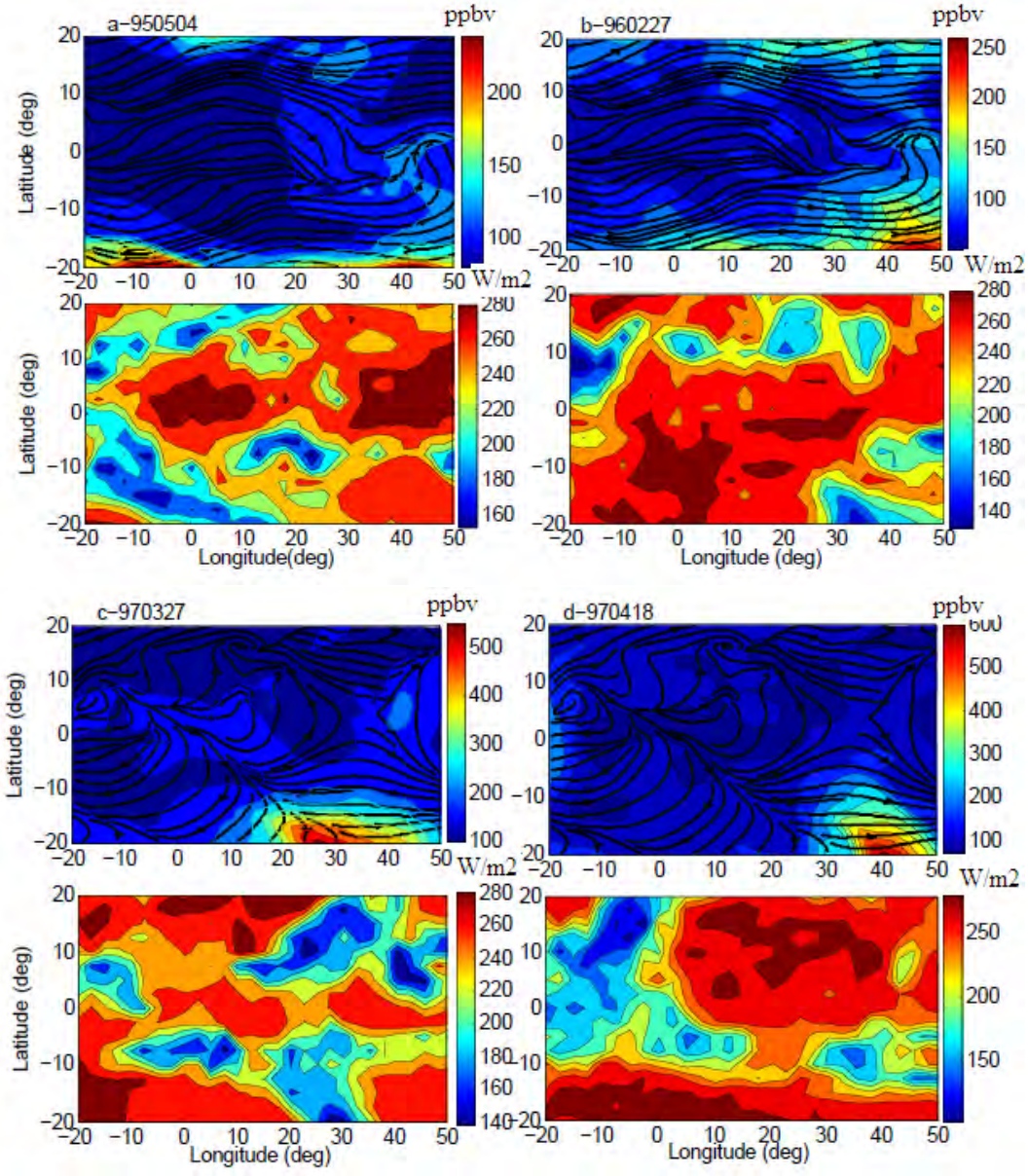

Figure 5.3: Ozone distributions at 100 hPa level (upper panels) and OLR (lower panels) for May 4, 1995(a), Feb. 27, 1996 (b), March 27, 1997 (c) , and April 18, 1997 (d) at 18 UTC. The black lines overlaid on the ozone plots are wind fields

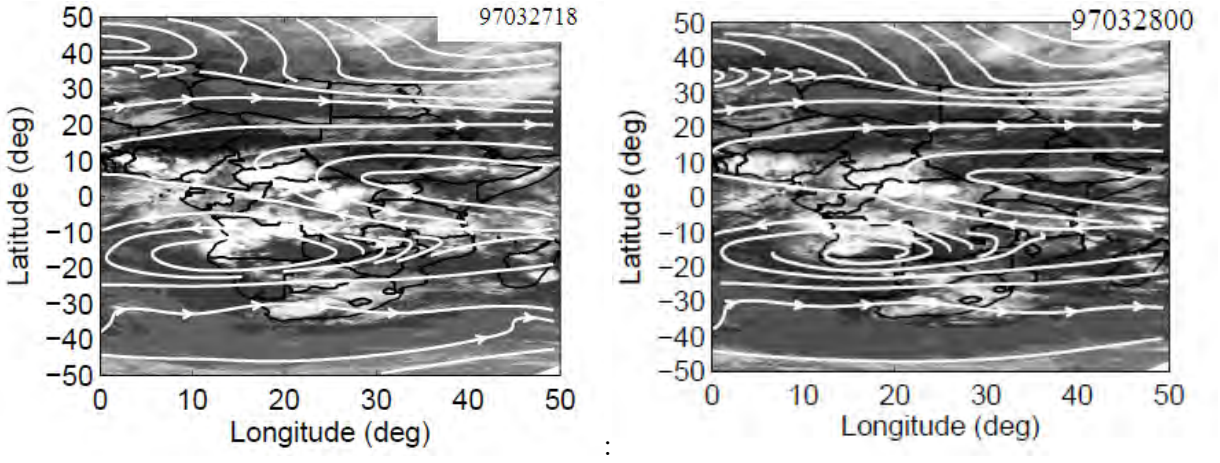

Figure 5.4: Meteosat-5 satellite image at 21 UTC overlayed by streamline of 18 UTC at 200 hPa of March 27, 1997 and Meteosat-5 image of March 28, 1997 at 00 UTC overlayed by streamline of the same time at 200 hPa.

along 10 E, which is a low pressure area which indicates the presence of ascending airmass. We further have investigated the presence of intrusion over these regions using vertical cross section of potential vorticity.

The latitudinal cross-sections of potential vorticity for the four days at 18 UTC are depicted in Fig. 5.5. The cross sections are made at the region of high ozone VMR observations at 25.5 E and 37.5 E for March 27, and April 18, 1997 respectively. For May 4, 1995 and February 27, 1996 the longitudinal cross section was made at 15 E and 25.5 E across strong convective events. High potential vorticity value greater than 2 PVU is well below tropopause level (marked by black crosses) determined using numerical model based on WMO operational definition of tropopause [McCalla, 1981]. In addition, PV tongues cross the isentropic surfaces indicated by white dotted lines overlaid on the PV plots. These cases demonstrate the existence of stratospheric intrusion. Stratospheric intrusions are capable of inducing high concentration ozone of stratospheric origin to the troposphere. Comparing the high ozone VMR in $10-20$ S shown in Fig. 5.3 c and d and PV depicted in Fig. 5.5 c and d illustrate the relationship between ozone and potential vorticity.

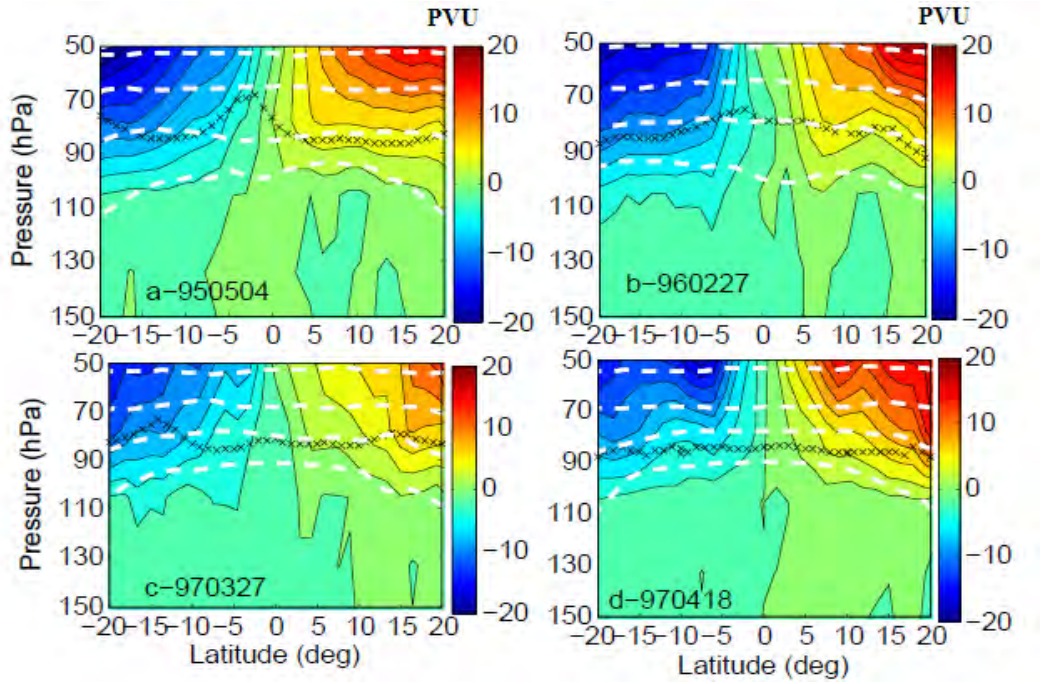

Figure 5.5: Potential vorticity vertical cross section at 25.5 E for May 4, 1995 (a), at 15 E for Feb.27, 1996 (b), at 25.5 E for March 27, 1997(c), at 37.5 E for April 18,1997 (d) at 18 UTC. Black cross lines show the tropopause levels and the white dashed lines represent isentropic levels at 370, 395, 430 and 475 K.

There would be high ozone VMR transport following the intrusion. Thus, we produce meridional cross-section of ozone VMR as shown in Fig. 5.6 (for clarity the altitude is restricted to 1000-100 hPa layer). Enhanced ozone VMRs of about 160 ppbv (upper panels) and 140 ppbv (lower panels) are observed. Ozone descends down with a decreasing concentration all the way down towards the boundary layer as clearly seen in the lower panels. At the boundary layer 0-2 km (approximately from surface to 780 hPa), where ozone is considered as a pollutant, enhanced ozone is observed. The upper panels for May 4, 1995 and for Feb. 27, 1996 are cross-sectioned across the convective regions. Both figures illustrate how intrusion and convective events are strongly affecting the vertical ozone distribution. Convection is likely to deplete the ozone distribution around 5^0 E over altitude range of 900-600 hPa on Feb 27, 1996 and around 10^0 E on April 18, 1997. The

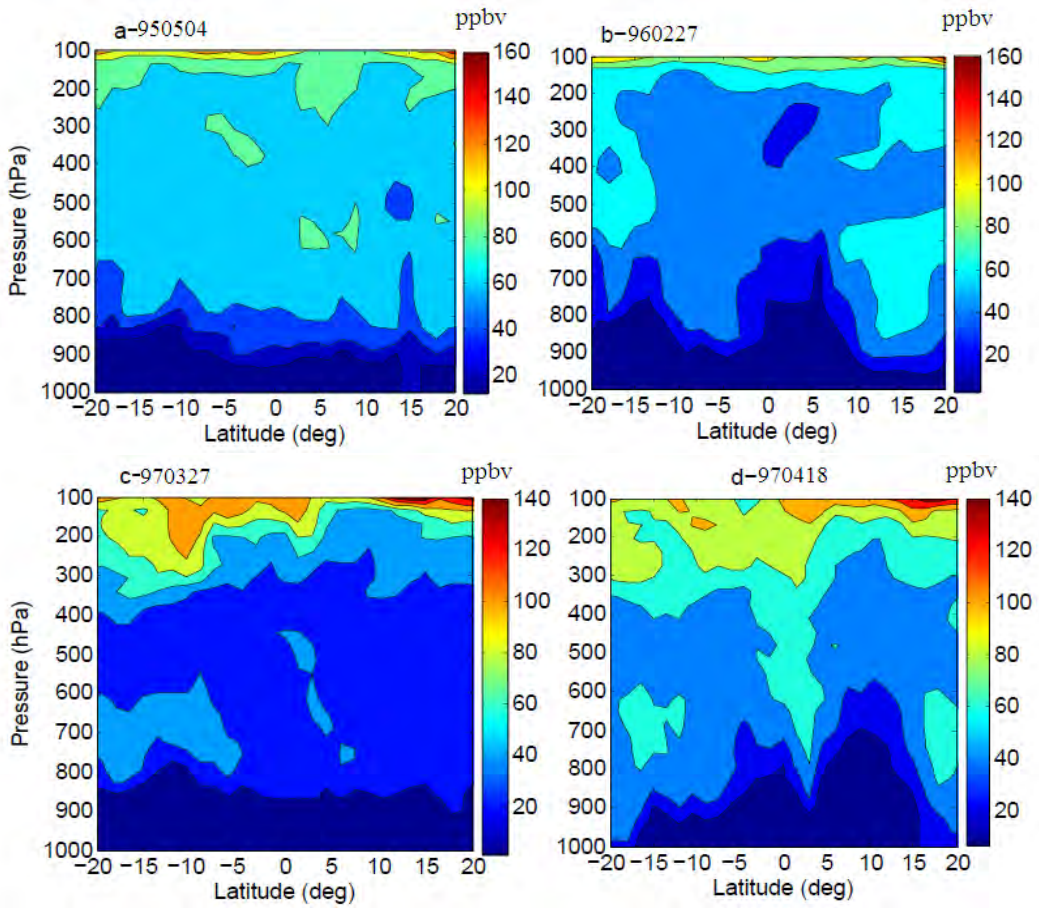

Figure 5.6: Ozone VMR vertical cross section at 25.5^0 E for May 4, 1995 (a), at 15^0 E for Feb. 27, 1996 (b), at 25.5^0 E for March 27, 1997 (c), and at 37.5^0 E for April 18, 1997 (d) at 18 UTC.

lower panels of Fig. 5.6 for March 27, 1997 and April 18, 1997 cross-sectioned across the highest ozone VMR, i.e in the regions of highest PV intrusion. The strong PV intrusion is able to transport very high ozone up to 100-400 hpa pressure level. Atmospheric upwelling and downwelling action during coupled events, i.e intrusion and convection, further transport ozone VMR of 40 ppbv and 60 ppbv on March 27, 1997 and April 18, 1997 respectively to the boundary layer. Ozone VMR of 60 ppbv and above could produce ozone pollution.

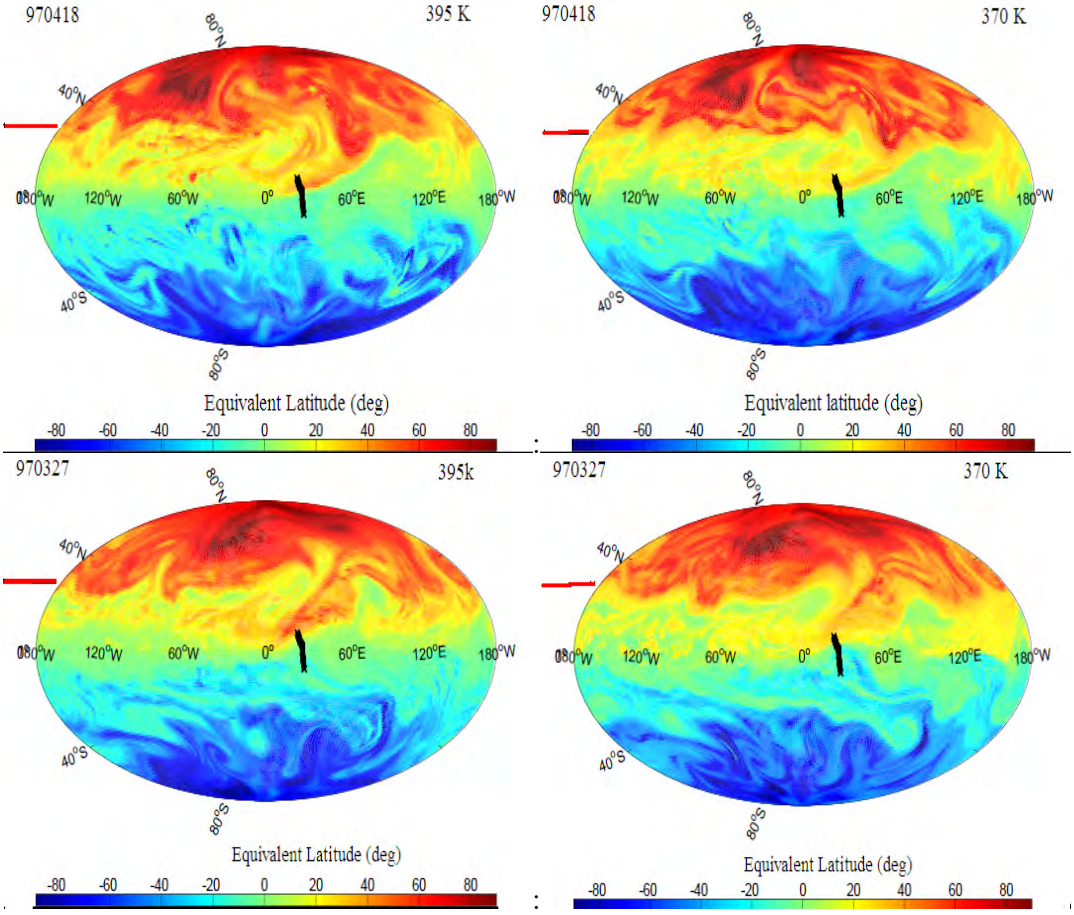

Figure 5.7: Equivalent Latitude on 395 k and 370 k isentropic surface for April 18, 1997 (upper left and right panels) and for March 27, 1997(lower left and right panels)at 18 UTC.

Convective and high latitude interaction also modifies the distribution within the troposphere. However, we did not show the possible location within the high latitude where it is originated. Fig. 5.7 shows the equivalent latitude at 370 k and 395 K for April 18, 1997 (upper panel) and March 27,1997 (lower panel). Fig. 5.8 depicts ozone distribution along the equivalent latitude . In both lower and upper panels elongated trough of equivalent latitude are observed between $0 - 60^0 E$ longitude with higher latitude airmass on the 395 K isentropic surface. There is also zonal equivalent latitude undulations along the line marked with red on the left side of each panels. The cause of these undulations could be Rossby waves propagations. Rossby waves produce irreversible PV deformations

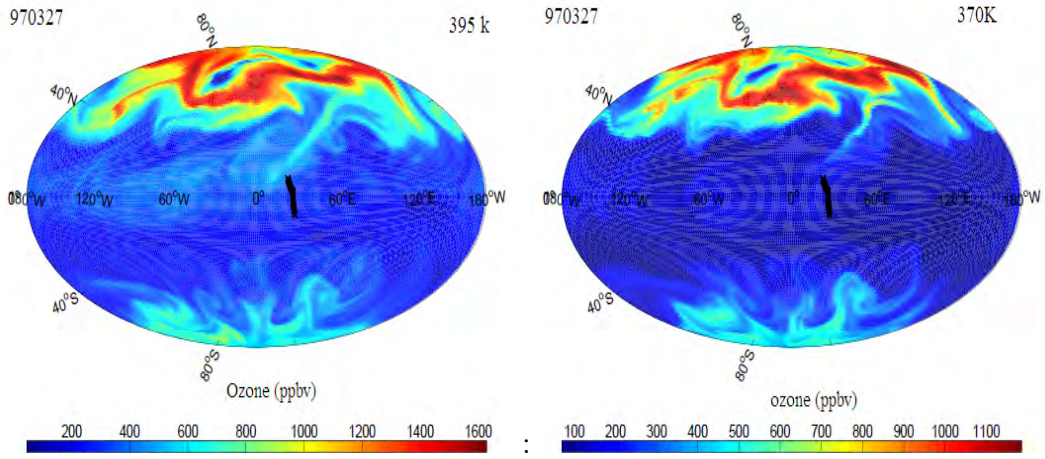

Figure 5.8: Ozone VMR on 395K (left) and 370 K (right panel) isentropic surface for March 27, 1997 at 18 UTC.

[Holton,1995] therby allowing mixing of different air masses. Rossby wave breaking at the subtropical tropopause in the vicinity of the subtropical jet stream can transport stratospheric air into the tropical upper and middle troposphere [Zachariasse et al., 2001]. The black line marked between $0 - 60^0E$ shown over the equator is the MOZAIC flight route where the plane record enhanced ozone spikes.

In addition to OLR and wind fields discussed in Fig. 5.3 the existence of convective air movement was confirmed using vertical wind (ω) and latent heat. Large amount of latent heat is released during thunderstorm. Latent heat released in deep convection in tropics is a very important source of energy for the general circulation of the atmosphere [Kiladis, 1998]. According to Kiladis [1998], the upper-level PV initiates and supports convection by destabilizing the lower troposphere and causing upward motion ahead of the tongues. The existing hypothesis for connection between PV intrusions and convection proposes that convection occurs as a result of decreased static stability and enhanced upward motion in the area of positive vorticity advection ahead of the intrusion [Waugh, 2005]. The intrusions transport high-ozone, low-water vapor stratospheric air into the subtropical middle-upper troposphere while the convection ahead of the intrusion transport low-ozone,

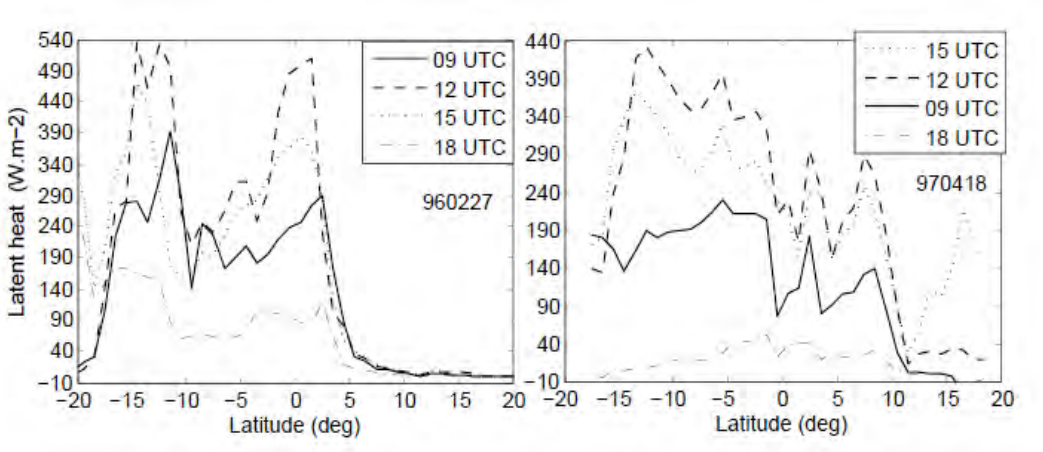

Figure 5.9: Latent heat at 25.5^0 E for March 27, 1997 (left panel) and 37.5^0 E for April 18, 1997 (right panel).

high-water vapor air into the upper troposphere [Waugh, 2005]. There is strong vertical air mass transport in the regions of low OLR (threshold 205 Wm^2, e.g., [Gettelman and Forster, 2002]).

In addition to Meteosat-5 and 6 images (Fig. 5.6), we have used additional proxy parameters such as cloud liquid water content and latent heat data which are indicators of the existence of thunderstorm activity. Thunderstorm is associated with release of very high latent heat. On Feb. 27, 1996, very strong latent heat in the region of cloud cover was observed. For instance, at 15.5 S, the latent heat records at 09, 12, 15 and 18 UTC were 281, 534, 469, 164.5 W/m^2 respectively (see Fig. 5.9, left panel). Again for the April 18, 1997, the latent heat flux at 09, 12, 15 and 18 UTC at 12.5 S are 188, 431, 188, 6.9 W/m^2. From these records it is apparent that thunderstorm dissipation likely to occur between 12 and 15 UTC because the heat flux grew from 09 to 12 UTC and then decreased in between 12 and 15 UTC. These observations are in agrement with the frequent thunderstorm observations at 14.00 UTC at equatorial Africa [Price and Asfur, 2006]. In addition, cloud liquid water transport is another indicator of thunderstorm activity. Comparison of cloud liquid water content between 12 and 18 UTC of each day

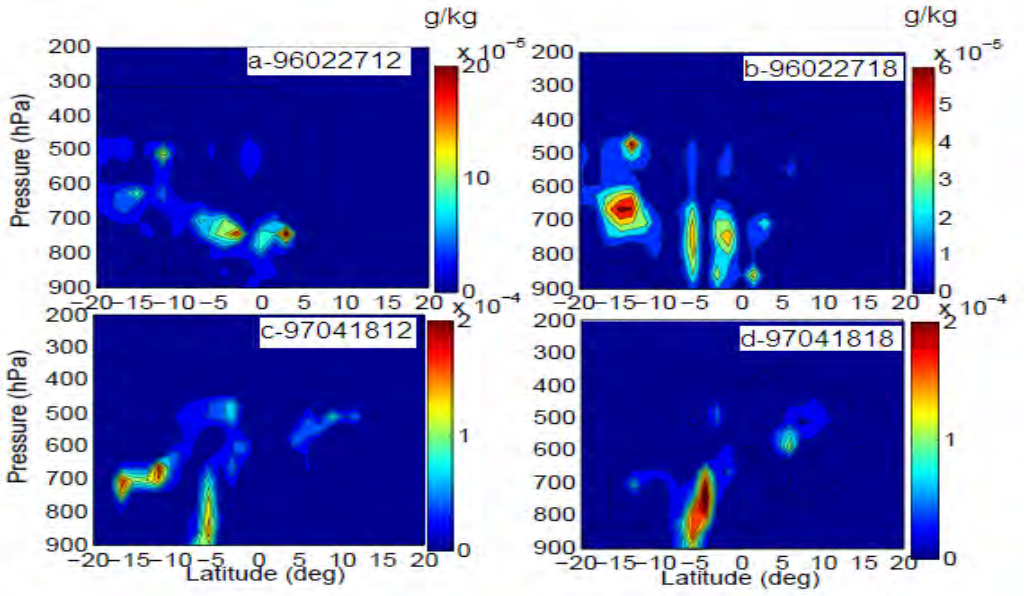

Figure 5.10: Meridional cross-section of liquid water content transport between 12 and 18 UTC at 15^0 E for Feb. 27, 1996 (upper panel) and at 37.5^0 E for April 18, 1997 (lower panel)

(Fig. 5.10 a and b for Feb. 27, 1996, Fig. 5.10 c and d for April 27, 1997) shows a spatial variability with time. This observation reveals a clear transport of liquid water content which is the main manifestation of the existence of thunderstorm in the vicinity of peak latent heat observations. The liquid water content may be transported further upward to upper troposphere where the air plane records high relative humidity between 21-04 UTC. Negative values of vertical wind (ω) at 1000-600 hPa and 200-400 hPa further demonstrate the existence of convective activity at 5-10^0 N, 5^0 S-5^0 N and 15^0 S on Feb. 27, 1996 (see Fig. 5.11 a left panel). In the localities indicated, ozone VMR is depleted due to convective erosion (see Fig. 5.6 b). Similar case is shown in Fig. 5.6 d where there is convection at 1000-700 hPa around 0^0 latitude, 900-500 hPa at about 5-15^0 N, downward air movement from 900-450 hPa mainly between 0-5^0 N for the 18 April 1997. These two cases clearly show how ozone distribution affected by vertical wind field.

The above discussions show how ozone of stratospheric origin transported during PV

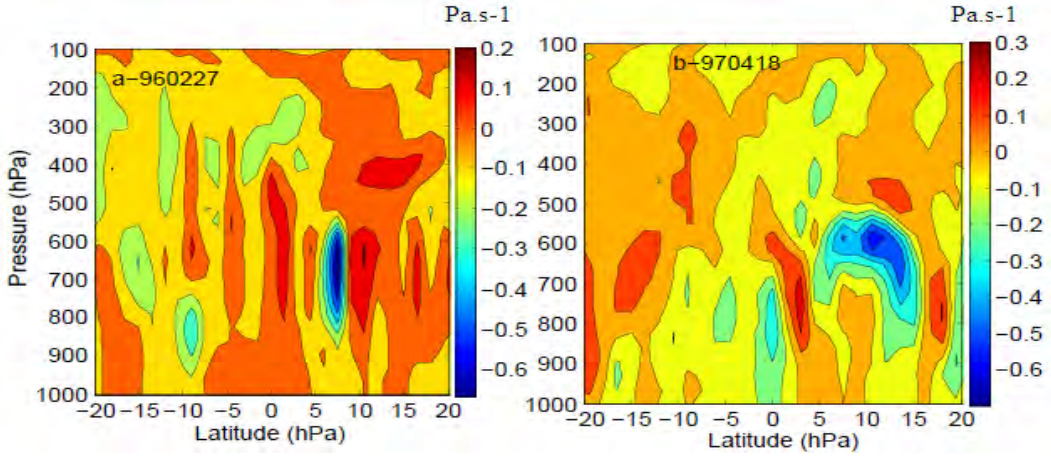

Figure 5.11: Meridional cross-section of vertical wind field (ω) at 15^0 S for Feb. 27, 1996 (left panel) and 37.5^0 E for April 18, 1997 (right panel)

intrusion and the effect of convection on the distribution of ozone. The two main factors that deplete the ozone concentration are thunderstorm and convective erosion. During thunderstorm the high voltage causes dissociation in the oxygen molecules to atomic oxygen then further reaction of oxygen atom with oxygen molecule produces ozone. Ozone produced by this mechanism is very low. The lightning event also favors high nitrogen oxide (NO) production. NO reacts with ozone which leads to the production of nitrogen dioxide (NO_2) which is manifested in a decrease of O_3 concentration. The net result is reduction of ozone or scavenging within the thunderstorm cloud. According to Hill et al [1988] and Franzblau [1991], NO_x (NO $+NO_2$) is produced mainly by hot lightning strokes, in contrast ozone may be destroyed in hot flash channel [Noxon, 1978]. Vertical wind field triggered by latent heat and PV intrusion reduces ozone concentration. These events produce convective erosion.

5.2 Ozone dynamics over North Africa

In Fig. 5.1, the red dotted rectangular box is a region of MOZAIC ozone enhancements. Along the routes, high ozone peaks over North Africa (20-35^0 N) and mid latitude (35-48^0 N) regions are observed at a flying altitude of about 250-200 hPa. On a cruise flying altitude there are quite a number of enhanced ozone records at mid-latitude and in few occasions over North Africa. Here we discuss only the dynamics associated with the observed ozone enhancements over North Africa.

The number of MOZAIC flights in the year 1996-1997 are shown in Table 5.2. This period has one of the most frequent MOZAIC flight records from Europe to Africa. Table 5.3 shows the chosen six ozone enhancements and we discuss the main dynamical events associated with them.

Table 5.2: MOZAIC flight statistics between Johannesburg to Vienna.

year	Jan	Feb	Mar	Apr	May	Jun	Jul	Aug	Sep	Oct	Nov	Dec	Total
1996	10	8	10	8	5	8	9	9	8	6		7	88
1997	10	8	4	8	6	4	2	5		4	4	6	61

Table 5.3: Dates and positions of ozone enhancements over North Africa for six flights chosen for case study. 1 and 2 represent segments of a single flight

Dates	Time (sec)	Latitude band (deg)	Flight altitude (hPa)
96.02.28	021635-024537	30.39-34.31	238
96.04.24[1]	234814-233517	33.03-34.67	250
96.04.25[1]	005222-012042	21.56-24.92	250
96.04.25[1]	005222-012042	26.59-29.35	250
96.06.07[2]	235006-235650	33.17-34.14	262
96.06.08[2]	000106-010804	23.02-32.55	240
97.02.08	004147-013000	30.36-36.83	261
97.06.15	000013-002500	22.19-25.16	238
97.07.27	005744-010936	28.39-29.90	238

Fig.5.12 depicts MOZAIC ozone (black solid lines) records shown in Table 5.3. The red

dashed lines show potential temperature along the flight routes calculated from MOZAIC temperature and pressure records. Low potential temperature (high gradient at the enhancements) observed in five of the events shown in Fig.5.12 a, b, c, d and e. The second different case, Fig.5.12 f, show an elevated potential temperature over the regions of ozone enhancements. Since the aircraft is not θ following, change in θ (i.e large θ gradient) across the enhanced O_3 latitude region implies at most the air mass is originated from a different area. Additional data sets also used to identify the source regions of ozone rich air mass.

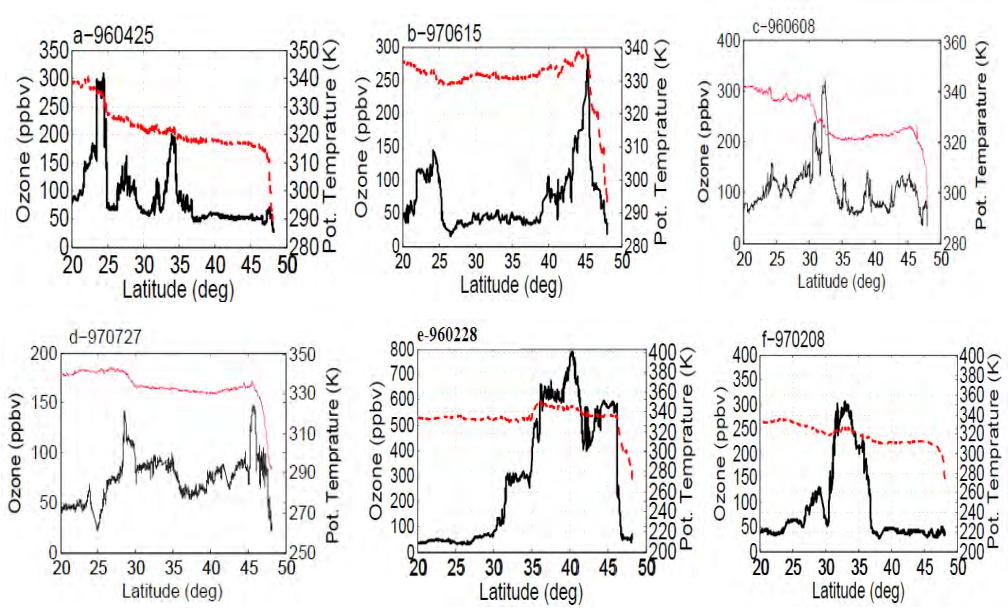

Figure 5.12: MOZAIC enhanced ozone (solid line) observations at north Africa for April 25, 1996 (a) and June 15, 1997 (b) 08 June, 1996 (c) 27 July, 1997 (d) 28 Feb. 1996(e) and 08 Feb. 1997 (f) respectively . The dotted red line indicates potential temperature along the flight route.

Fig. 5.13 depicts MOZAIC relative humidity record measured simultaneously with ozone. Very low relative humidity is observed over the regions of MOZAIC ozone enhancements. This can be shown in Fig. 5.13 a, at $20-25^0$, 27^0 and 33^0 N, in Fig. 5.13 b, at $20-25^0$ N, in Fig 5.13 c at $20-33^0$ N in Fig. 5.13 c, at $30-35^0$ N and in Fig. 5.13 d, at $25-30^0$ N, in Fig. 5.13 e, at $30-45^0$ N, and in Fig. 5.13 f, at $25-29^0$ N and $31-36^0$ N. In all the cases shown, higher ozone concentration coincide with lower

relative humidity records. Since stratospheric air is very dry it has low relative humidity. Therefore relative humidity can be used as a proxy to indicate ozone source regions. These analysis indicate that stratosphere could be the source region [Danielsen, 1982; Danielsen et al., 1987, Zbinden et al., 2006]. However, this has to be further complemented by other diagnostic tools such as potential vorticity.

Meridional cross-sections of potential vorticity are shown in Fig. 5.14. Troposphere and stratosphere are well separated by a 2 PVU contour line. The red dotted lines show the flight routes of the plane. Isentropic surfaces are indicated by a black dotted lines. In all cases shown, there are PV intrusions in the regions between $25-35^0$ N across isentropic surfaces. The tropopause level strongly vary from 250 hPa in April 25, 1996 to 440 hPa in February 08, 1997 as shown in the figure. These cases show strong variability in the tropopause level with time.

The regions of MOZAIC ozone enhancements (Fig. 5.12) can be identified using PV plots along with the flight routes. The three ozone enhancements shown Fig.5.12 a are measured between April 24, 1996 at 233517 UTC to April 25, 1996 at 012043 UTC (Table 5.3). Therefore we have used PV closer to the flight time at 00 UTC of April 25, 1996. Two of the observed ozone peaks are fall with in the stratosphere (see Fig. 5.14 a). However the third enhancement observed during 005222-012042 UTC between $21.56 - 24.92^0$ N is within troposphere. Fig.5.14 b is the potential vorticity for June 15, 1997. The airplane was flying above the 2 PVU contour and therefore ozone enhancement shown in Fig. 5.12 b is within stratosphere. In all the remaining four cases the airplane was flying with in the stratosphere and ozone enhancements shown in Fig. 5.12 c, d, e and f are all fall within the stratosphere. Except one of the enhancements shown during April 25, 1996 all the rest observations are within stratosphere. These observations prove that the ozone enhancements records by MOZAIC are the result of airplane flying within the lower stratosphere. These enhancements are mainly the result of change in the tropopause level which is quite extraordinary.

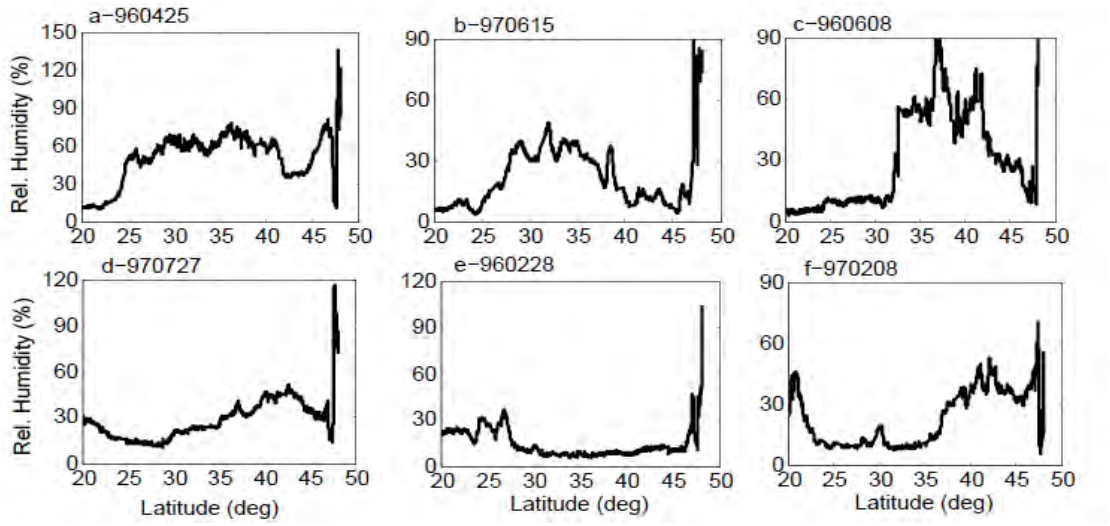

Figure 5.13: MOZAIC relative humidity observations April 25, 1996 (a) and June 15, 1997 (b) 08 June, 1996 (c) 27 July, 1997 (d) 28 Feb. 1996(e) and 08 Feb. 1997 (f) respectively.

To distinguish the presence of cross tropopause stratospheric ozone transport to upper troposphere, we have produced the vertical cross-sections of ERA-interim ozone in the regions of PV plots as shown in Fig. 5.15. Tropopause level at 2 PVU is indicted by white solid line. The white dotted lines show flight route. Fig. 5.15 a indicates meridional cross-section of ozone for April 25, 1996. A region below 250 hPa in the latitude band of $20-45^0$ N is within the troposphere. Ozone VMR of above 200 ppbv is clearly observed in the region. The protruding tongue of ozone between $21.56 - 24.92^0$ N is likely measured by MOZAIC.

MOZAIC captured well the ozone VMR revealed by ERA-interim for June 15, 1997 shown in Fig. 5.15 b within $22.19 - 25.16^0$ N latitude band. This ozone tongue also observed below the tropopause. Two more similar cases of enhanced ozone transport across tropopause are shown Fig.5.15 c and d for June 08, 1996 and July 27, 1997. These cases demonstrate the transport of enhanced ozone to upper troposphere North Africa. The last two events shown in Fig. 5.15 e and f represent meridional cross-section of ozone VMR for Feb. 28, 1996 and Feb. 08, 1997. Unlike the four cases discussed above, in

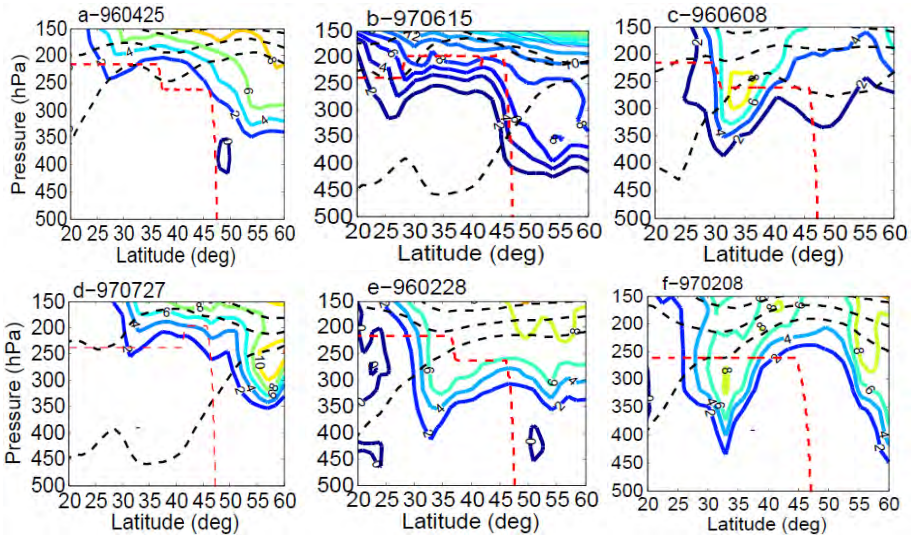

Figure 5.14: Meridional cross-section on potential vorticity at 31.5 E on 25 April 1996 (a) at 16.5 E on 15 June1997(b) at 12 E 08 June 1996 (c) at 13.5 E for 27 July. 1997 (d) at 13.5 E for 08 Feb 1997(e) at 00 UTC. The black dashed lines are isentropic lines at 330, 350 and 370 levels. The red dotted lines are the flight routes

these two cases there is little or no enhanced ozone transport across the tropopause. This may be due to strong downward at the pole but weak equatorward transport. The other possible case could be the displacement of the tropopause level up to 440 hPa.

So far we have seen that there were massive shift in the tropopause level and as a result MOZAIC has encountered stratospheric airmass within the stratosphere. Analysis of ERA-interim ozone shows that enhanced ozone was also observed within the troposphere in the region where the tropopause level are lowered. To illustrate the mechanism of ozone transport we have analyzed IPV at different isentropic surfaces.

The IPV plots are with five different levels in the vicinity of the MOZAIC flight level and above. These plots would be helpful to see the vertical and horizontal air mass transport within the stratosphere that led to the observed MOZAIC ozone enhancements. The IPV at 475, 395, 370, 350, and 330 K are shown in Fig. 5.16. The first and second column show strong airmass subsidence at mid latitude as revealed by IPV of April 25, 1996 and June 08, 1996 respectively. Similar cases were also observed for July 27, 1997

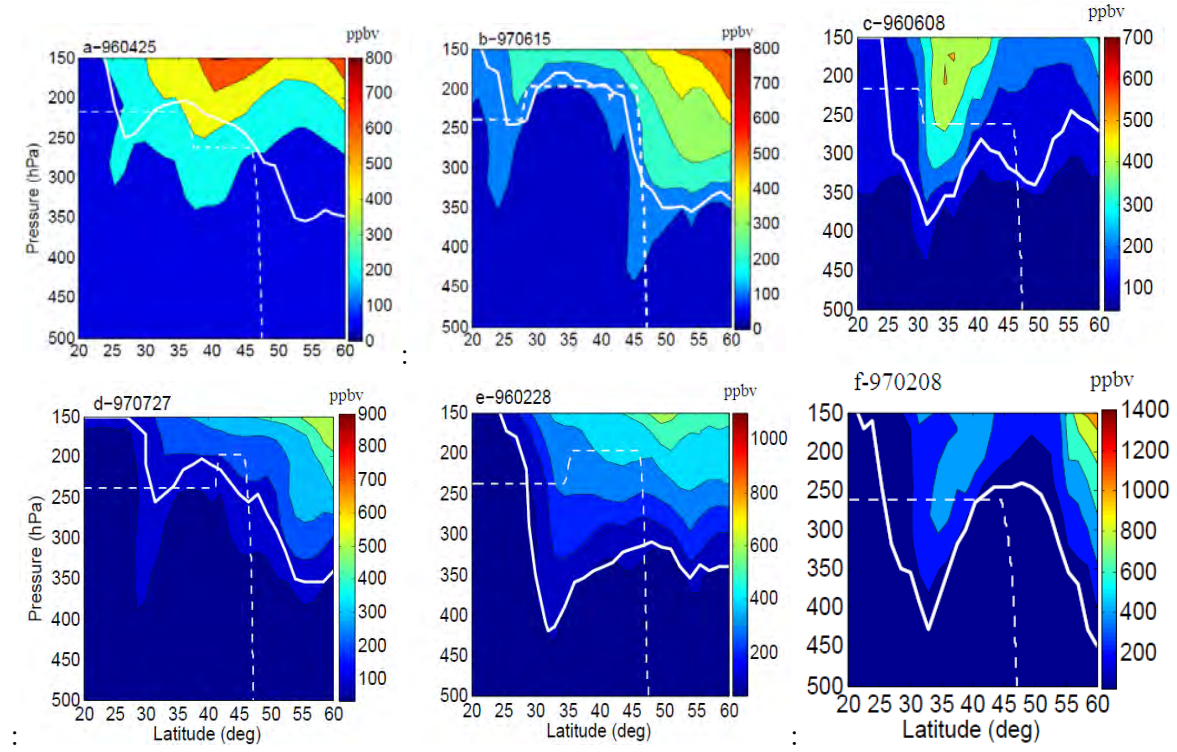

Figure 5.15: Meridional cross-section ozone mass mixing ratio at 31.5 E on 25 April 1996 (a) at 16.5 E on 15 June 1997(b) at 12 E 08 June 1996 (c) at 13.5 E for 27 July. 1997 (d) at 13.5 E for 08 Feb 1997(e) at 00 UTC. The white solid line is tropopause level at 2-PVU. The whte dotted lines are the flight routes

and June 08, 1996 (not shown). The first column, for April 25, 1996, at 475 and 395 K surfaces show PV centers between $40 - 65^0$ N. The next two surfaces 370 350 and 330 K, IPV do not show clearly defined orientations. This could be due the modification of IPV by wind fields. The second column shows high PV at 475 and 370 K surface between $40 - 65^0$ N, however in the next three levels from 370 to 330K IPV is strongly modified which might be due to wind fields.

Third and fourth columns depict the IPV for Feb. 28, 1996 and Feb. 08, 1997. At 475 K, high IPV value about 55 and 45 PVU respectively are observed between $60 - 90^0$N. Similar cases are shown for the two days at 395 and 370 K with a decrease in IPV values. However, in the next two levels, at 350 and 330 K, IPV do not show clearly

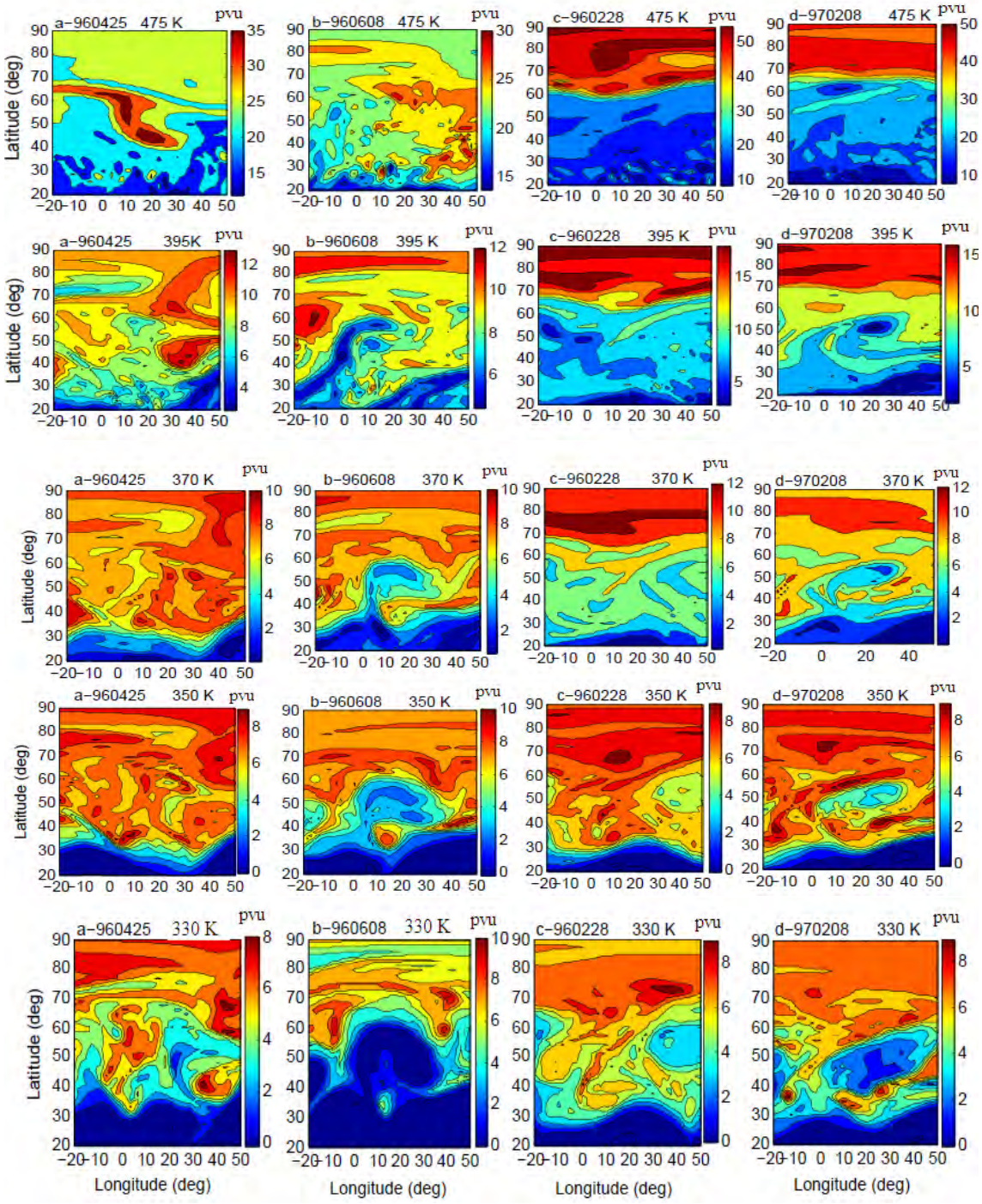

Figure 5.16: Potential vorticity on 475, 395, 370, 350, 330 K isentropic surfaces for April 25, 1996 and June 08, 1996 (first and second column) and for and February 28, 1996 and February 08, 1997(third and fourth column) respectively.

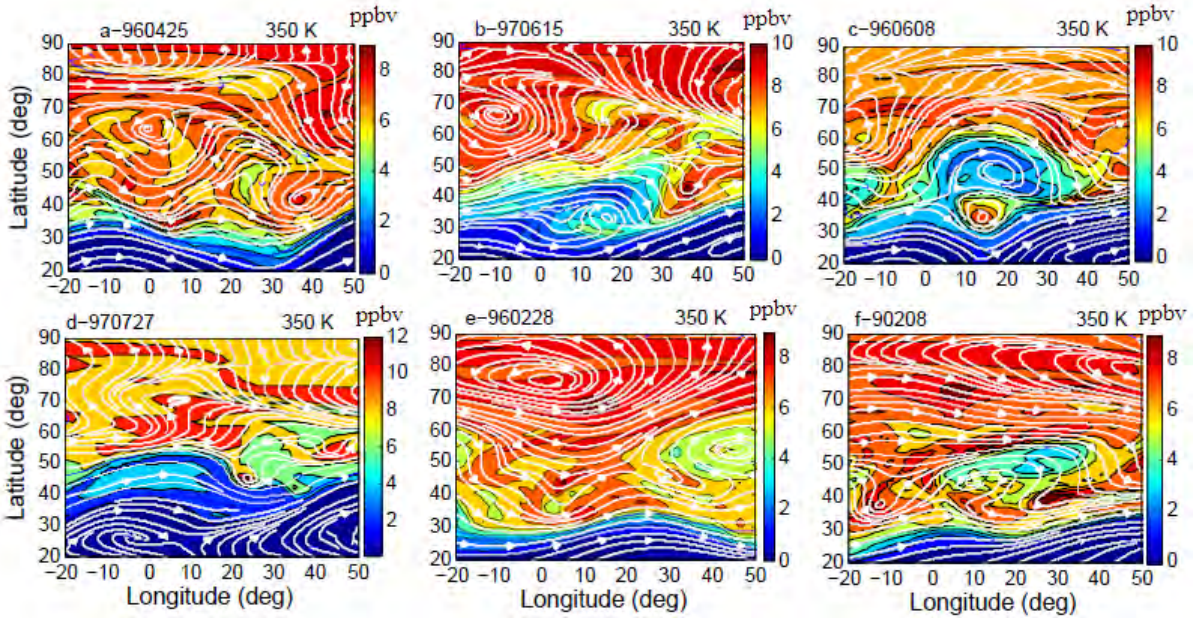

Figure 5.17: Wind fields (white solid lines) and potential vorticity (colored contour) at 350 K isentropic surface for April 25, 1996 (a) June 15, 1997 (b) June 08, 1996 (c) July 27,1997(d) February 28, 1996 (e) February 08, 1997 (f) at 0.00 UTC.

defined orientation. Moreover they extends extends well belw 30^0 N with a decreasing magnitude. In contrast to the observed two cases, for April 25, 1996 and June 08, 1996 whose strong IPV are confined within $40 - 65^0$ N the IPV for Feb., 28 1996 and Feb., 08 1997 extends from polar region well below 30^0N. These two cases demonstrate strong air mass subsidence at the pole and subsequent airmass transport towards north Africa.

The possible impact of wind fields on IPV are examined by wind streamlines and zonal wind fields. First we will investigate the IPV modifications brought about by wind fields. In each 330 and 350 K surfaces shown in Fig. 5.16, IPV has a non-clearly defined orientation. Therefore wind streamlines are overlayed on each 350 K IPV surfaces. High PV are observed at circulating wind fields 35^0 N, 40^0 E for April 25, 1996 and at 30^0 N, 15^0 E for June 08, 1996. On the other hand very low IPV are observed at 40-60^0 N, 5-35^0 E for June 08, 1996. Similarly low IPV is also observed at 40-60^0 N, 32 -50^0 E for Feb. 28, 1996. Very low PV also observed along 20-30^0 N for all the days. The above cases

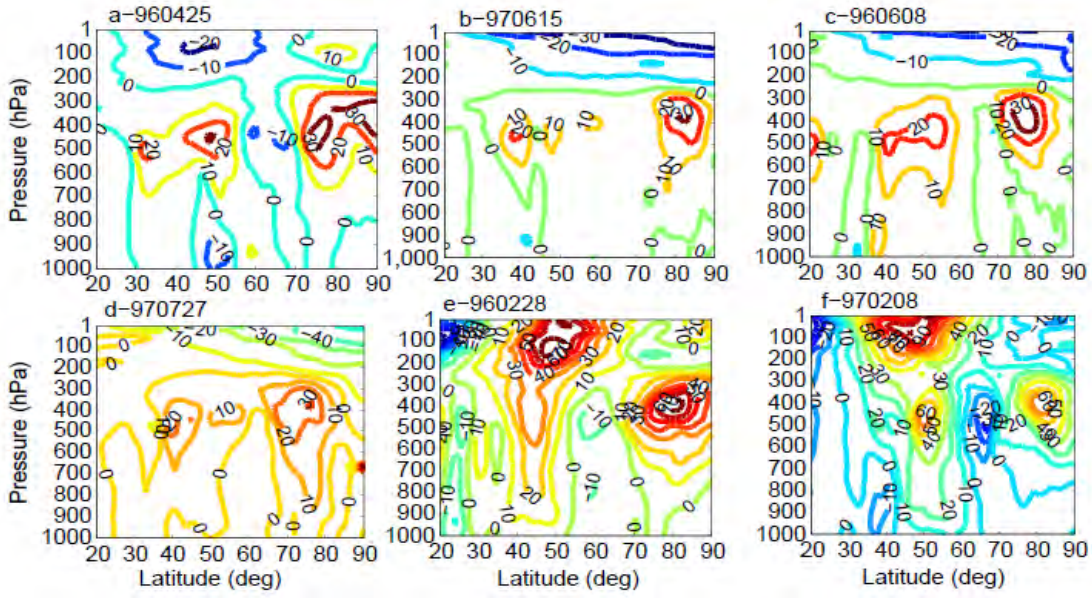

Figure 5.18: Vertically propagating zonal wind fields cross-sectioned at 30^0 E for for April 25, 1996 (a) June 15, 1997 (b) June 08, 1996 (c) July 27,1997(d) February 28, 1996 (e) February 08, 1997 (f) at 0.00 UTC,[wind velocity (m/sec)].

demonstrate the impact of wind fields in modifying the shapes and magnitude of IPV. The westerly winds in Feb. 28, 1996 and Feb. 08, 1997 have similar wind pattern between $60 - 70^0$N (see Fig. 5.17). It looks like a large scale disturbance propagation along the direction indicated.

These characteristics are similar to what would have been observed in the presence of Rosbby waves. Quasi-stationary Rossby waves are the most significant vertically propagating mode in the extra tropics [Holton, 1980]. The waves occur only under certain atmospheric conditions, they are most prominent in the northern hemisphere winter under weak westerly wind conditions [Charney and Drazin, 1961]. Charney and Drazin [1961] first explained the confinement of vertically propagating waves to the winter hemisphere.

As Holton [1975] points out, the 'guiding' of the Rossby waves into the region of strong mean zonal winds is one of the most important features to the dynamics of the winter

stratosphere. The waveguide should be thought of as a channel, which the waves are directed through and allowed to propagate higher than the troposphere. In contrast to the much more quiescent summer hemisphere, the wintertime stratosphere is dominated by large-amplitude, planetary-scale Rossby waves propagating upward from the troposphere. Intermittently, these waves break, stirring air more or less isotropically across large distances of the winter stratosphere within a region that has become known as the surf zone [Plumb, 2002].

Since the two events considered here are winter time events we may see signals that indicate the presence of waves. Therefore, we want to investigate the presence. If exist, to assess their impact on IPV, and the resulting ozone distribution. One of the indicator or diagnostic tool for Rossby wave occurrence is zonal vertically upward propagating wind. Fig. 5.18 illustrate meridional cross-sections of zonal wind fields at 30^0 E for the six events considered.

The presence of vertically upward propagating zonal wind observed only during Feb.28, 1996 and Feb. 08, 1997. The westerly zonal wind from $40-50^0$ N and $50-60^0$ N at 900 and 1000 hPa moved up to a latitude band covering an area within $45-75^0$ N to altitude range of 200 -1 hPa as shown in the Fig. 5.18 c and d. The strength of the zonal wind increases upwards from 10 m s^{-1} to 70 m s^{-1} on Feb. 28, 1996 and to 90 m s^{-1} on Feb. 08, 1997.

Westerly zonal winds centered about 450 hPa are also seen in all the four events over the poles and mid latitude regions. At the pole, they are all occur closer to the tropopause and stronger during winter, 70 m/sec compared to 30 m/sec observed in April and June in panels a and b of Fig. 5.18. Easterly winds seen at about $60-70^0$ N, for Feb. 28, 1996 and Feb. 08, 1997, which are stronger in the later day. From the above observations it is apparent that the distribution and concentration of ozone are greatly influenced by zonal winds and Rossby waves which are active during NH winter seasons.

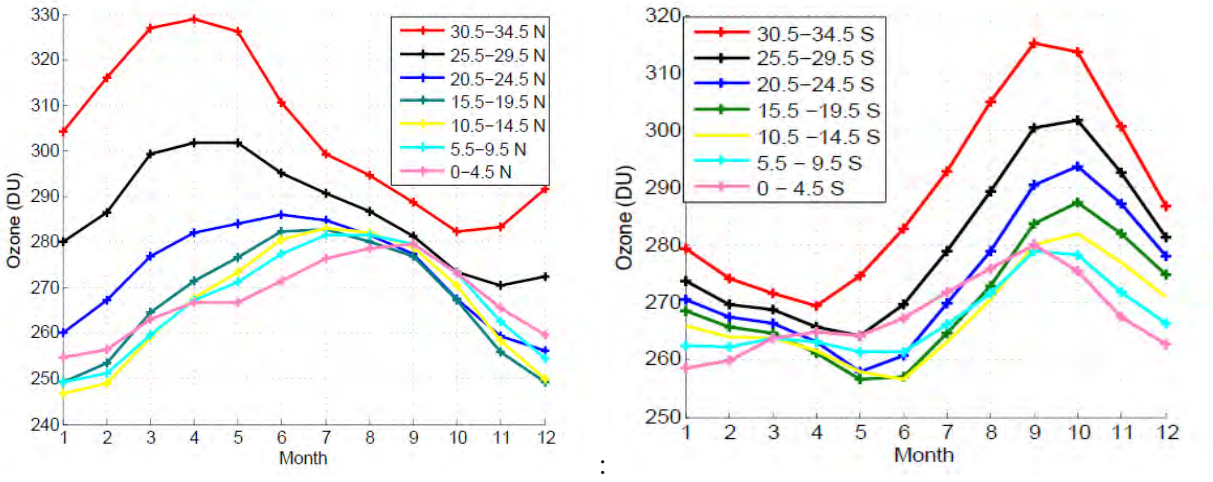

Figure 5.19: Seasonal and spatial variability of ozone (monthly average from January 1979 to January 1992). Within $0 - 34.5^0$ N (left panel) and $0 - 34.5^0$ S (right panel) latitude.

5.3 Spatial and seasonal variability of ozone over Africa

The methodology used to analyze TOC data from Nimbus-7 has already been described in methodology section of Chapter 4. The focus of this study is to investigate the seasonal and spatial distribution of ozone.

Fig. 5.18 shows the seasonal variability of mean ozone for the twelve months of the year in the study period from January 1979 to January 1992 (14 years) for both north and south of the equator. The regions are divided into seven zones each as shown in the left and right panels of the figure. In both cases TOC concentration increases towards higher latitude from the equator. At the northern tip of Africa, ozone concentration peaks in April, and shifts from April to September near the equator. Ozone concentration peaks during the period from June to October, and decreases afterwards over Southern Africa.

The spatial variation of ozone with season mainly related with the position of the sun (see Appendix A.1). Appendix A.1 shows daily mean solar insolation as a function of latitude and seasons [Liou,K. N., 2002]. There is high solar insolation in the northern hemisphere from March to September which peaks on June. From September to March

the sun insolation is higher in the southern part of Africa with its peak insolation in December. In Fig. 5.18 (left panel) ozone concentration also increases between March and September following the position of the sun in northern hemisphere. In the southern hemisphere, ozone concentration starts to increase from June and peaks between August and November. The peak ozone concentrations change from 280 DU in the latitude band $0 - 19.5^0$ N to 330 DU within $30.5^0 - 34.5$ N. Similarly in the southern hemisphere the peak ozone concentration changes from 280 DU in the latitude band $0 - 14.5^0$ S to 316 DU within $30.5^0 - 34.5^0$N. Since more than 90% of ozone is found in the stratosphere TOMS ozone record is mainly stratospheric origin. It is apparent that from the discussion in Chapter 3, stratospheric ozone is produced due to photochemical reaction. Therefore, the amount of ozone concentration is related with the position of the sun. From the above analysis it is clearly evident that TOMS observation shows no O_3 enhancement over northern (sub-Saharan) Africa during the biomass burning season between December and March. This contrasts with ozone concentration observation at the boundary layer.

Seasonal variability of mean ozone over Africa were studied by Akinyemi [2007] using EPTOMS TOC data for the period 1997 to 2002. The region was deviled into twelve zones, each 5 degree latitude range, between $0 - 30^0$ S and $0 - 30^0$ N. A noticeable increase in seasonal ranges and annual mean of ozone concentration observed as one moved farther away from the equator. Ozone variability was attributed to overall ozone dynamics in the atmosphere that he referred as a transport process and differs from photochemical processes that actually create and destroy ozone. For the southern tropics $10^0 - 30^0 S$ seasonal ranges varied between 16.7DU and 34.8DU and for the northern tropics $10^0 N - 30^0$N, it varied between 34.7DU and 42DU. While the annual means varied between 262.7 DU and 278 DU, 264.6 DU and 279.6 DU respectively .

Seasonal ranges were more pronounced in the northern tropics than in the south. For zones $10^0 - 30^0$S well defined seasonal maxima occurred around September/October while the seasonal minima were not well defined, but a long stretch from February to June. For

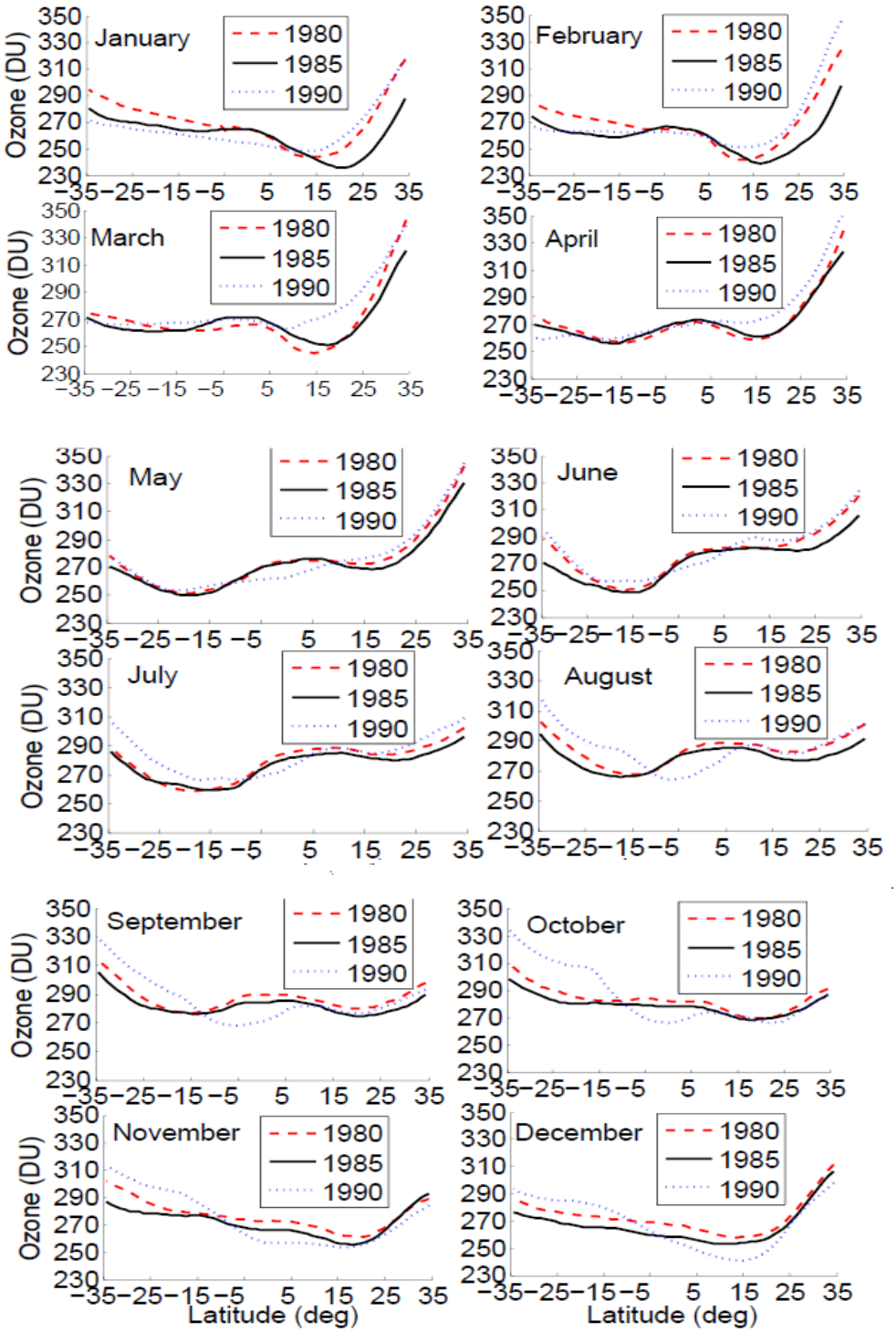

Figure 5.20: Latitudinal seasonal variation of ozone minimum and maximum in the years 1980, 1985 and 1990.

zones 10^0N-30^0N seasonal maxima varied between April to August, and seasonal minima between December and January Akinyemi [2007]. These outcomes are in agrement with our results.

The spatial seasonal variability of ozone is also shown in Fig. 5.19. As can be seen from the figure, from December to June ozone concentration is higher at the northern Africa between 20^0 N and 34.5^0 N, while from July to November in the southern Africa between 20^0 and 34.5^0S. This observation is similar with the case described in Fig. 5.18. It also exhibited a seasonal sea-saw in ozone concentration peak between September to march and April to August. Two local minimum centered at 20^0 N and 20^0 S are also observed which could be related to dynamical factors such as convection. There is strong ozone variability between 20^0-34.5^0 for both north and south of the equator. Ozone in the central latitude region, in a latitude band 5^0S-5^0 N, also changes between 270-290 DU.

Chapter 6

Conclusion

The impact of dynamical factors that affect stratospheric and tropospheric ozone distribution such as intrusion, convection and Rossby waves are thoroughly investigated and discussed. On top of this, variation of Total ozone column and stratospheric ozone with season are presented. First we have introduced relevant previous works related to ozone and the objectives of our study. The dynamical factors that affect the distribution of tropospheric and stratospheric ozone are reviewed. Ozone is one of the key trace gas, which has an important role in atmospheric chemistry and climate change. In light of this we have presented an extensive discussion on ozone and its precursors chemistry.

Ozone dynamics over equatorial and north Africa and seasonal variability of ozone over Africa are presented. We have observed ozone and relative humidity spikes exceeding 100 ppbv and 100% respectively over equatorial Africa. Stratospheric intrusion coupled to convection are found to be the key physical process that attributed to spiky ozone VMR and relative humidity observations. Potential vorticity values exceeding 2 PVU observed below the tropopause level confirm stratospheric intrusion. Convection was investigated using proxy parameters. The vertical wind field (ω) and low daily mean OLR value ($<$ 220 W/m^2) indicate the presence of deep convection. Very high latent heat release and cloud liquid water transport indicate the existence of thunderstorm activity over the area of deep convective regions. Using ozone from ECMWF ERA-interim, the possible ozone distribution within the troposphere during these two dynamical events was observed. Very

low ozone VMR within the deep convective regions resulted in low ozone. It is the main mechanism that decreases ozone concentration mainly at the boundary layer. Very high ozone of stratospheric origin (> 200 ppbv) is introduced during PV intrusion to upper troposphere equatorial Africa. The intruding stratospheric ozone was able to make its way down to boundary layer. These processes have resulted in ambient air pollution with O_3 VMR exceeding the proposed WHO guideline limit of 60 ppbv.

Enhanced MOZAIC ozone events are analyzed over North Africa on the cruse flights between Johannesburg to Vienna. We have also investigated their source and regions of discharge using various diagnostic tools. The study has revealed that all MOZAIC enhanced ozone observations are measured within lower stratosphere. This is mainly due to the strong variation in the dynamic tropopause with time. Meridional cross section of PV, IPV on isentropic surface and ozone mass mixing ratio revealed large scale subsidence from the stratosphere at the polar and mid-latitude regions. Some of subsidence at mid-latitude led to cross tropopause enhanced ozone transport to upper troposphere.

Zonal wind fields and Rossby waves have strong contribution in modifying IPV and ozone concentration and distribution. This study has revealed that large scale air mass transport from high latitude to mid-tropics, particularly North Africa, is captured by a high resolution but in few MOZAIC observations. This was consistent with dynamics exhibited in ECMWF reanalysis data. These observations clearly show that polar and mid latitudes are intense STE regions. Enhanced stratospheric ozone transported from these regions to upper troposphere North Africa would have a significant effect on chemistry, climate and radiative forcing.

The total column ozone analysis from TOMS satellite data shows a distinct seasonal and spatial variation. The concentration increases with latitude from the equator. Generally TOC increases in the northern hemisphere from January to June and peaks in April between $30.4^0 - 34.5^0$ N and shift to August in the latitude band $0^0 - 4.5^0$ N. In the southern Africa the concentration increases from June to October the peak being in

September and October then decreases afterwards. This variation is mainly related to the position of the sun and hence photochemical reaction. Low total column ozone concentration around 20^0 N and 20^0 S was observed which could be related to dynamical factors such as convection. This result is in agrement with that reported by Akinyemi [2007].

Appendix

A.1 Solar Radiation at the Top of the Atmosphere

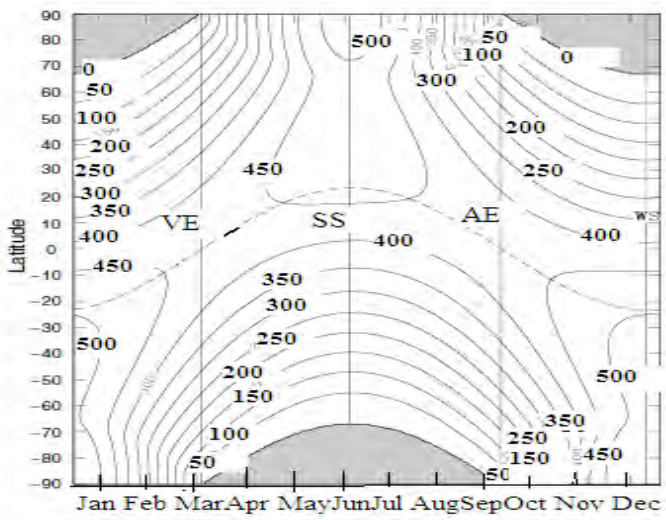

Daily mean solar insolation (Q/24 hr) as a function of latitude and day of year in units of Wm^{-2} based on a solar constant of 1366 Wm^{-2}. The shaded areas denote zero insolation. The position of vernal equinox (VE), summer solstice (SS), autumnal equinox (AE), and winter solstice (WS) are indicated with solid vertical lines. Solar declination is shown with a dashed line [Liou,K. N., 2002].

A.2 Summery of ozone chemistry

Chemical process	Process description	Reaction number
	Chapman chemistry	
$O_2 + h\nu \rightarrow 2O$		R1
$O + O_2 + M \rightarrow O_3 + M$		R2
$O_3 + h\nu \rightarrow O_2 + O(^1D)$		R3
$O(^1D) + M \rightarrow O + M$		R4
$O_3 + h\nu \rightarrow O_2 + O$		R5
$O + O + M \rightarrow O_2 + M$		R6
$O + O_3 \rightarrow 2O_2$		R7
	Illustrative odd Hydrogen Catalytic cycles	
$O + OH \rightarrow O_2 + H$		R8
$H + O_2 + M \rightarrow HO_2 + M$		R9
$O + HO_2 \rightarrow O_2 + OH$		R10
$Netcycle1 : O + O + M \rightarrow O_2 + M$		R6
$OH + O_3 \rightarrow HO_2 + O_2$		R11
$HO_2 + O_3 \rightarrow OH + 2O_2$		R12
$Netcycle2 : 2O_3 \rightarrow 3O_2$		R13
	Illustrative odd nitrogen Catalytic cycles	
$NO + O_3 \rightarrow NO_2 + O_2$		R14
$O + NO_2 \rightarrow NO + O_2$		R15
$Netcycle3 : O + O_3 \rightarrow 2O_2$		R7
	Illustrative odd Chlorine Catalytic cycles	
$Cl + O_3 \rightarrow ClO + O_2$		R16
$ClO + O \rightarrow ClO + O_2$		R17
$Netcycle4 : O + O_3 \rightarrow 2O_2$		R7
$Cl + O_3 \rightarrow ClO + O_2$		R16
$ClO + ClO + M \rightarrow Cl_2O_2 + N$		R18
$Cl_2O_2 + h\nu + M \rightarrow Cl + ClO_2$		R19
$ClO_2 + M \rightarrow Cl + O_2 + M$		R20
$Netcycle5 : 2O_3 \rightarrow 3O_2$		R13
	Illustrative Cl-Br Catalytic cycles	
$Cl + O_3 \rightarrow ClO + O_2$		R16
$Br + O_3 \rightarrow BrO + O_2$		R21
$BrO + ClO \rightarrow Br + ClO_2$		R22
$ClO_2 + M \rightarrow Cl + O_2 + M$		R20
$Netcycle6 : 2O_3 \rightarrow 3O_2$		R13
	Some Important Coupling and Reservior Reactions	
$ClO + NO \rightarrow Cl + NO_2$		R23
$Cl + CH_4 \rightarrow HCl + CH_3$		R24
$HO_2 + ClO \rightarrow HOCl + O_2$		R25
$Cl + CH_4 \rightarrow HCl + CH_3$		R26
$OH + NO_2 + M \rightarrow HNO_3 + M$		R27
	Key Hetrogeneous Reactions	
$HCl + ClONO_2 \rightarrow HNO_3 + Cl_2$		R28
$N_2O_5 + H_2O \rightarrow 2HNO_3$		R29
$ClONO_2 + H_2O \rightarrow HNO_3 + HOCl$		R30
$HCl + HOCl \rightarrow H_2O + Cl_2$		R31
$BrONO_2 + H_2O \rightarrow HNO_3 + HOBr$		R32
$HCl + BrONO_2 \rightarrow HNO_3 + BrCl$		R33
$HCl + HOBr \rightarrow H_2O + BrCl$		R34

Key chemical Processes and Catalytic Cycles (Susan Solomon,1999).

Bibliography

[1] Aghedo, A.M., Schultz, M.G. Rast, S., *The influence of African air pollution on regional and global tropospheric ozone* , Atmos. Chem. Phys., 7, 1193-1212, 2007.

[2] Akinyemi , M. L, *The Influence of Some Atmospheric Phenomena on Total Ozone Concentration over the Tropics*, Australian Journal of Basic and Applied Sciences, 1(4), 497-505, 2007.

[3] Allan, R. P., Shine, K. P., Slingo, A. and Pamment, J. A., *The dependence of clear-sky outgoing long-wave radiation on surface temperature and relative humidity*, Q. J. R. Meteorol., Soc., 125, 2103-2126, 1999.

[4] Andrews, D. G.,Holton J. R., and Leovy, C. B., *Middle Atmosphere Dynamics*, Academic, San Diego, Calif., 1987.

[5] Appenzeller, C., Holton, J.R. Rosenlof, K.H., *Seasonal variation of mass transport across the tropopause* , J. Geophys. Res., 101(D10), 1507-15078, 1996.

[6] Auvray, M., Bey, I., *A modeling study of the background ozone over europe: Origin and interannual variability*, J.Geophys. Res. 110 (D10), D11303, 2005.

[7] Bates, D. R. and Nicolet ,M., *Atmospheric hydrogen*, Publ.Astron. Soc. Pac., 62, 106-110, 1950.

[8] Brewer, A.M., *Evidence for a world circulation provided by the measurements of helium and water vapor distribution in the stratosphere*, Q. J. R. Meteorol. Soc., 75, 3, 51-63, 1949.

[9] Butchart, N., and A. A. Scaife, *Removal of chlorofluorocarbons by increased mass exchange between the stratosphere and troposphere in a changing climate*, Nature, 410, 799- 802, 2001.

[10] Carl McCalla, *Objective Determination of the Tropopause, Using WMO Operational Definitions*, U.S, Department of commerce national oceanic and atmospheric administration national weather service national metrological center, Office note 246, 1981.

[11] Charney, J. G. and Drazin,P. G., *Propagation of planetary-scale disturbances from the lower into the upper atmosphere*, J. Geophys. Res., 66, 83-109, 1961.

[12] Chen, P., *Isentropic cross-tropopause mass exchange in the extra tropics*, Geophys. Res.100, 6, 661-16, 673, 1995.

[13] Clough, S. A., Iacono, M. J. and Moncet, J.-L., *Line-by-line calculations of atmospheric fluxes and cooling rates: Application to water vapor*, J. Geophys. Res., 97, D14, 15761-15785, 1992.

[14] Clough, S. A. and Iacono, M. J, *Line-by-line calculation of atmospheric fluxes and cooling rates, 2: Application to carbon dioxide, ozone, methane, nitrous oxide and the halocarbons*, J. Geophys. Res., 100, D8, 16519-16535, 1995.

[15] Cornu, A., *Observation de la limite ultraviolette du spectre solaire adiverses altitudes*, C. R. Hebd. Seances Acad. Sci., 89, 808, 1879.

[16] Crutzen, P. J., *Influence of nitrogen oxides in the atmospheric ozone content*, Q. J. R. Meteorol. Soc., 96, 320-325, 1970.

[17] Danielsen, E.F., Hiskind, R.S., Gaines, S.E., Sachse, G.W., Gregory, G.L. Hill, G.F., *Three dimensional analysis of potential vorticity associated with tropopause folds and observed variations of ozone and carbon monoxide.*, J. Geophys. Res., 92, 2103-2111, 1987.

[18] Danielsen, E. F., *A dehydration mechanism for the Stratosphere*, Geophys. Res. Lett., 9, 605-608, 1982.

[19] Danielsen, E.F., Stratospherisco urcef or unexpectedllya rgev alues of ozone measured over the Pacific Ocean during Gametag, August1 977, J. Geophys, Res., 85, 401-412, 1980.

[20] Danielsen, E.F., *Stratospheric-tropospheric exchange based on radioactivity, ozone and potential vorticity*, J. Atmos. Sci., 25, 502-528, 1968.

[21] Dee, D. P, et al., *The ERA-Interim reanalysis: configuration and performance of the data assimilation system,*, Q. J. R. Meteorol. Soc. 137: 553597, April 2011 A.

[22] Dessler, A., Hintsa, E., Weinstock, E., Anderson, J., Chan, K.,*Mechanisms controlling water vapor in the lower stratosphere: A tale of two stratospheres.*, J. Geophys. Res., 100, 23,167-23,172, 1995.

[23] Dessler, A.E. Sherwood, S.C., *Simulation of tropical upper tropospheric humidity*, J. Geophys. Res., 105, 20155-20163, 2000.

[24] Dobson, G. M. B, *Origin and distribution of polyatomic molecules in the atmosphere*, Proc. R. Soc., London, Ser. A, 236, 187-193, 1956.

[25] Douglas R, A, Noboru N, *Tracer Equivalent Latitude: A Diagnostic Tool for Isentropic Transport Studies*, Journal of the Atmospheric Sciences, 60, 287-304, 2003.

[26] Duncan, B. N., Bey, I., *A modeling study of the export pathways of pollution from europe: Seasonal and interannual variations (1987-1997)*, J. Geophys. Res. 109 (08301), 2004.

[27] Duncan, B. N., West, J., Yoshida, Y., Fiore, A. M., Ziemke, J. R., *The influence of european pollution on ozone in the near east and northern Africa*, Atmos. Chem. Phys. Discuss. 8, 1913 - 1950, 2008.

[28] Dunkerton, T., *Nonlinear Hadley circulation driven by asymmetric differential heating* , J. Atmos.Sci., 46, 2325-2333, 1989.

[29] ECMWF Newsletter, *ECMWF,Shinfield Park*, No. 113, G2 9AX, England, Autumn 2007.

[30] ECMWF Website, uk, $http://wcrp.ipsl.jussieu.fr/Workshops/Reanalysis2008/Documents/V1-102_ea.pdf$.

[31] Eisinger, M. and Burrows, J. P, *Tropospheric Sulfur Dioxide observed by the ERS-2 GOME Instrument*, Geophys. Res. Lett., 25, 4177-4180, 1998.

[32] Eluszkiewicz, J.E., Crisp,D., Zurek,R., Elson L., Fishbein E., Froidevaux, L., Waters, J., Grainger, R., Lambert, A., Harwood, R., and Peckham, G., *Residual circulation in the stratosphere and lower mesosphere as diagnosed from Microwave Limb Sounder data*, J. Atmos. Sci., 53, 217-240, 1996.

[33] Ertel, H., *Ein neuer hydrodynamischer Erhaltungssatz. Die Naturwissenschaften*, 36, 543-544, 1942a.

[34] Ertel, H, *Über hydrodynamischer Wirbelstze.* Physikalische Zeitschrift Leipzig, 43, 526-529, 1942b.

[35] Ertel, H., *Ein neuer hydrodynamischer Wirbelsatz.* Meteorologische Zeitschrift, 59, 277-281, 1942c.

[36] Fishman, J. and P. Crutzen, *The origin of ozone in the troposphere*, Nature, Vol.274, 855-858, 1978.

[37] Franzblau, E., *Electrical discharges involving formation of NO, NO_2, HNO_3, and O_3*, J. Geophys. Res., 96, 22, 337-22, 345, 1991.

[38] Forster, P. M. de F. and Shine, K. P.,*Radiative forcing and temperature trends from stratospheric ozone changes*, J. Geophys. Res.102, 10841-10857, 1997.

[39] Fortuin, J.P.F., and Kelder, H., *An ozone climatology based on ozonesonde and satellite measurements*, J. Geophys. Res., 103, 31,709-31,734, 1998.

[40] Gettelman, A. Forster de F., P.M., *A climatology of the tropical tropopause layer*, Journal of the Meteorological Society of Japan, 80(4B), 911-924, 2002.

[41] Goering, M. A., W. A. Gallus Jr., M. A. Olsen, and J. L. Stanford, *Role of stratospheric air in a severe weather event: Analysis of potential vorticity and ozone*, J. Geophys. Res., 106(D11), 11,813- 11, 823, 2001.

[42] Gouget, H., Cammas, J.-P., Marenco, A., Rosset, R., Jonquieres, I., *Ozone peaks associated with a subtropical tropopause fold and with a tread wind inversion: a case study from the airborn campain tropoz ii over the Caribbean in winter*, J.Geophys. Res. 101, 25,979 - 25,993, 1996.

[43] Gouget, H., Vaughan, G., Marenco, A. Smit, H., *Decay of a cut-off low and contribution stratosphere-troposphere exchange.* Q.J. R. Meteorol. Soc., 126, 1117-1141, 2000.

[44] Graedel, T.E. and Crutzen, P.J., *Atmospheric trace constituents,in: The Earth as Transformed by Human Action*,Eds.B.L. Turner II et al., Cambridge University Press, 295-311, 1990.

[45] Graninger, J.F., and Ring,J., *Anomalous Fraunhofer line profiles* , Nature, 193, 762, 1962.

[46] Grewe, V, *Impact of climate variability on tropospheric ozone*, Sci. Total Environ., 374, 167- 181, 2007.

[47] Hansen. J, Sato .M, and Kuedy, K, *Radiative forcing and Climate response,*, J.Geophy.Res., 6831-6864, 1997.

[48] Harries, J. E, *The greenhouse earth: A view from space.*, Q. J. R. Meteorol. Soc., 122, 799-818, 1996.

[49] Harries, J. E, *Atmospheric radiation and atmospheric humidity*, Q. J. R. Meteorol. Soc., 123, 2173-2186, 1997.

[50] Hartley, W. N., *On the probable absorption of solar radiation by atmospheric ozone*, Chem. News, 42, 268, 1880.

[51] Haynes, P.H., Marks, C.J., McIntyre, M.E., Shepherd T.G., and Shine K.P., *On the downward control of extratropical diabatic circulations by eddy induced mean zonal forces,* J. Atmos. Sci., 48, 651- 678, 1991.

[52] Hegels, E., Crutzen, P., upfel, T., Perner, D., and Burrows, J. P., *Global distribution of atmospheric bromine monoxide from GOME on Earth observing satellite ERS-2*, Geophys. Res. Lett., 25, 3127-3130, 1998.

[53] Held, I.M., and Hou, A.Y., *Nonlinear axially symmetric circulations in a nearly inviscid atmosphere,*, J. Atmos. Sci., 37, 515-533, 1980.

[54] Held, I. M., and Schneider.T., *The surface branch of the zonally averaged mass transport circulation in the troposphere,*,J. Atmos. Sci., 56, 1688-1697, 2000.

[55] Hewitt, C.N. Andrea, Jackson, V (Editors) *Handbook of Atmospheric Science Principles and Applications*, by Blackwell Science Ltd, 2003.

[56] Hegels, E., Crutzen, P. J., Upfel Kl , Perner T, and Burrows, J. P., *Global distribution of atmospheric bromine monoxide from GOME on Earth observing satellite ERS-2*, Geophys. Res. Lett., 25, 3127-3130, 1998.

[57] Hill, R.D., Rahmim, I. Rinker, R.G., *Experimental study of the production of NO, N_2O, and O_3 in a simulated corona*, Ind. Eng. Chem. Res., 27, 1264-1269, 1988.

[58] Hoerling, M.P., *Diabatic sources of potential vorticity in the general circulation*,J. Atmos. Sci., 49, 2282-2292, 1992.

[59] Holton, J. R., *The Dynamic Meteorology of the Stratosphere and Mesosphere*, Meteor. Monogr., No. 37, Amer. Meteor. Soc., 218, 1975.

[60] Holton, J. R., *Wave propagation and transport in the middle atmosphere*, Phil. Tran. Roy. Soc. Lon. Math. Phys. Sci., 296, 73-85, 1980.

[61] Holton , J R., Hayne, P. H , Mcintyre, M, E, Douglas, A, R, Rood, R.B, Fister, L, P, *stratosphere-troposphere exchange*, Rev. Geophys, 33, 4, 403-439, 1995.

[62] Hoskins, B. J., M. E. McIntyre, and A. W. Robertson ,*On the use and significance of isentropic potential vorticity maps*, Q. J. R. Meteorol. Soc., 111, 877-946, 1985.

[63] Hsu, N., Christina, R. D, McPeters, C. J, Seftor, and Thompson, A. M., *The Effect of An Improved Cloud Climatology on the TOMS Total Ozone Retrieval*, J. Geophys. Res., 102, 4247-4255, 1997.

[64] Hughes, W.L, *"Numerical Forecasts Of Tropopause And Maxwind'", International Civil Aviation Organization, Area Forecast Panel Second Meeting, Montreal*, 21st September to 9th October, 1981.

[65] IPCC, Climate change, *the scientific basis, Contribution of Working Group I to the Third Assessment Report of theIntergovernmental Panel on Climate Change*, Cambridge University Press, Cambridge, 2001.

[66] John M. Wallace, Peter V. Hobbs, *Atmospheric Science an Introductory Survey*, Elsevier, 2006.

[67] John P. Burrows, Mark Weber, Michael Buchwitz, Viadimir Rozanov, Annette Ladstatter-Weibenmayer, Andreas Richter, Rudiger Debeek, Ricarda Hoogen Klaus Bramstedt, Kai-uwe eichmann, Michael Eisinger, *Global ozone monitoring experiment (GOME): Mission concept andfirst scientific results*, J. Atmos. Sci. 56, 151-175, 1999.

[68] Johnston, H. S. *Reduction of stratospheric ozone by nitrogen oxide catalysts from supersonic transport exhaust.*, Science, Vol. 173, 517-522, 1971.

[69] Joiner, J., Bhartia P. K., Cebula R. P., Hilsenrath E., and McPeters R. D., *Rotational Raman Scattering (Ring Effect) in Satellite Backscatter Ultraviolet Measurements*, Applied Optics, 34, 4513-4525, 1995.

[70] Junge, C. E., *Air chemistry and radioactivity*, Volume 4 of Internat., Geophys Ser.New York, London: Academic Press., 1963.

[71] Katie A. Read, Anoop S. Mahajan, Lucy J. Carpenter, Mathew J. Evans, Bruno V., Faria, Dwayne E. Heard, James R. Hopkins, James D. Lee, Sarah J. Moller, Alastair C. Lewis, Luis Mendes, James B. McQuaid, Hilke Oetjen, Alfonso Saiz-Lopez, Michael J. Pilling, John M.C. Plane, *Extensive halogen-mediated ozone destruction over the tropical Atlantic Ocean*, Nature, 453, 1232-1235, 2008.

[72] Kiladis, G.N., *Observations of Rossby waves linked to convection over the eastern tropical Pacific*, J. Atmos. Sci., 55, 321-339, 1998.

[73] Kiehl, J. T. and Trenberth, K. E. *Earth's annual global mean energy budget*, Bull. Am. Meteorol, Soc., 78(2), 197-208, 1997.

[74] Klenk, K. F., Bhartia, P. K. ,Hilsenrath, E. and Fleig, A. J. *Standard Ozone Profiles From Balloon and Satellite Data Sets*, J. Climate Appl. Meteorol., 22, 2012 - 2022, 1983.

[75] Kneizys, F.X., Shettle, E.P., Abreu, L.W., Chetwynd, J.H, Anderson, G.P., Galley, W.O., Selby, J.E.A, and Clough S.A., *User guide to LOWTRAN, Tech. Rep. Afgltr-88-0177*, Air Force Geophys.Lab.,Bedford, Mass., 1988.

[76] Kodera, K., Yamazaki, K., Chiba, M. and Shibata, K., *Downward propagation of upper stratospheric mean zonal wind perturbation to the troposphere*, Geophys. Res. Lett., 17, 1263-1266, 1990.

[77] Koh, T.-Y., *Isentropic diagnostics of mid-latitude circulation and transport*,Ph. D. thesis, M. I. T., 287, 2001.

[78] Kurosu, T., Rozanov V.V. , and Burrows, J.P., *Parameterization schems for teresterial water cloud in the radiative transfer model GOMETRAN*, J. Geophys. Res., 102, 21, 809-21,823, 1997.

[79] Kuze, A., and Chance, K.V., *Analysis of cloud top height and cloud coverage from satellite using O_2 A and B bands*, J. Geophys. Res., 99, 4481-14991, 1994.

[80] Lamarque, J.F. Hess, P.G., *Cross-tropopause mass exchange and potential vorticity budget in a simulated tropopause folding.*, J. Atmos. Sci., 51, pp. 2246-2269, 1994.

[81] Land, C., Meloen, J., Papayannis, A., Priller ,A., Seibert, Sprenger ,Roelofs, P.,M.,Scheel G. J., Schnabel, H. E.,C., Siegmund, Tobler , P., Trickl, L.,Wernli,T., Wirth , H., Zanis, V., and Zerefos, C , *Stratosphere-troposphere exchange: Areview, and what we have learned from STACCATO, J. Geophys. Res,.(108), D12,*, 1-15, 2003.

[82] Leue, C., Wenig, M., Wagner, T., Klimm, O., Platt, U., and Jahne, B., *Quantitative Analysis of NO_x emissions from Global Ozone Monitoring Experiment satellite image sequences,*, J.Geophys. Res.,106, 5493-5505, 2001.

[83] Li, Q., Jacob, D., Bey, I., *Transatlantic transport of pollution and its effect on surface ozone in Europe and North America.J.Geophys*,Res.107(D13) (4166), 363 - 377, 2002.

[84] Liou, K. N, *An introduction to atmospheric radiation*, Second Edition, Elsevier Science, 2002.

[85] Marenco, et al.,Thouret, V., Nedelec, P., et al., *Measurement of ozone and water vapour by airbus in-service aircraft: The mozaic airborne programme, an overview*, J. Geophys. Res. 103(D13), 25, 631 25, 642, 1998.

[86] McElroy, M. B.,Salawitch, R. J. ,Wofsy, C. S., and Logan, J. A. ,*Reductions of Antarctic ozone due to synergistic interactions of chlorine and bromine* , Nature, Vol.321, 759-762, 1986.

[87] McIntyre, M.E., and Palmer, T.N. *Breaking planetary waves in the stratosphere*, Nature, 305, 593-594, 1983.

[88] McKinley A and Deffey BL,*A reference action spectrum for ultraviolet induced erythema in human skin." in Humen Exposure to Ultraviolet Radiaton: Riskes and Regulations, (W.F. Passchier and B.F.M. Bosnajakovic, eds.)*, International Congress Series, Elsevier, Amsterdam, The Netherlands, 1987.

[89] Mengistu Tsidu G., Stiller G. P., von Clarmann T., Funke B., Hopfner M., Fischer H., Glatthor N., Grabowski U., Kellmann S., Kiefer M., Linden A., Lopez-Puertas M., Milz, M., Steck, T., 1and Wang D. Y, *NO_y from Michelson Interferometer for Passive Atmospheric Sounding on Environmental Satellite during the Southern Hemisphere polar vortex split in September/October 2002*, J. Geophys. Res. 110, 1-20, 2005.

[90] Mengistu Tsidu. G., von Clarmann T., Stiller G. P., Hopfner M., Fischer H., Glatthor. N, Grabowski U., Kellmann S., Kiefer M., Linden A., Milz M., Steck T., and Wang D. Y., *Stratospheric N2O5 in the austral spring 2002 as retrieved from limb emission spectra recorded by the Michelson Interferometer for Passive Atmospheric Sounding (MIPAS)*, J. Geophys. Res., 109, D18301, 1-15, 2004.

[91] Mirador, *Website: NASA Goddard,http://mirador.gsfc.nasa.gov.*

[92] Molina, L. T. and Molina , M. J.,*Production of Cl_2O_2 from the self reaction of the ClO radical*, J. Phys. Chem., Vol. 91, 433, 1987.

[93] Molina, L.T and Rowland , F., *Stratospheric sink for chloroumethanes: chlorine atom catalyzed destruction of ozone*, Nature, Vol.249, 820-822, 1974.

[94] Neal, B., Ellis, E, R, *The area of the stratospheric polar vortex as a diagnostic for tracer transport on an isentropic surface*, Journal of the Atmospheric Sciences, 43, 1319-1339, 1986.

[95] Neeman, B,U and Alpert , P, *Visualizing Atmospheric Fields on Personal Computer: Application to potential Vorticity*, AMS, 154-160, 1990.

[96] NOAA Interpolated Outgoing Longwave Radiation (OLR), website: *http : //www.esrl.noaa.gov/psd/data/gridded/data.interp$_O$LR.html*.

[97] Noxon, J.F., *Tropospheric NO_2*,J. Geophys. Res., 83, 3051-3057, 1978.

[98] Prather, M. Ehhalt, D., *Atmospheric chemistry and greenhouse gases. Climate Change the Scientifi c Bases*,eds J.T. Houghton et al., Cambridge University Press: Cambridge, 2001.

[99] Plumb, R.A, *Stratospheric Transport* , J. Meteor. Soc. Japan, 80, 793-809, 2002.

[100] Plumb, R. A., and Eluszkiewicz, J. *The Brewer-Dobson circulation: dynamics of the tropical upwelling*, J. Atmos. Sci., 56, 868-890, 1999.

[101] Price, C. Asfur, M., *Can lightning observations be used as an indicator of upper-tropospheric water vapor variability ?*, AMS, 87(3), 291298, 2006.

[102] Reed, R. J. , *A study of a characteristic type of upper level frontogenesis,J. Meteorol.*, 12, 226-237, 1955.

[103] Ricarda Hoogen, Vladimir V. Rozanov, and John P.Burrows, *Ozone profile from GOME satellite data: Algorithm description and first validation* , J. Geophy. Res. Lett., Vol 104, D7,8263-8280, 1999.

[104] Rinsland, C. P., M. R. Gunson, R. J. Salawitch, M. J. Newchurch, R. Zander, M. M. Abbas, M. C. Abrams, G. L. Manney, H. A. Michelsen, A. Y. Chang, and A. Goldman ATMOS measurements of H2O + 2CH4 and total reactive nitrogen in the November, 1994 *Antarctic stratosphere: Dehydration and denitrifcation in the vortex*. Geophys. Res. Lett., Vol. 23, 2397-2400, 1996.

[105] Rosenlof, K.H., *Seasonal cycle of the residual mean meridional circulation in the stratosphere*. J.Geophys. Res., 100, 5173-5191, 1995.

[106] Salby, M. L, *Fundamentals of atmospheric physics. Vol. 61 of International Geophysics Series*, Academic Press, 1996.

[107] Sauvage B., Thouret V., Cammas J.-P., Gheusi, F., Athier G., and Nedelec P., *Tropospheric ozone over Equatorial Africa: regional aspects from the MOZAIC data*, Atmos. Chem. Phys. Discuss., 4, 3285-3332, 2004.

[108] Sauvage. B. Gheusi, F. Thouret, V., Cammas J.-P., Duron J. Escobar, J. Mari, C. Mascart, P., and Pont, V.,*Medium-range mid-tropospheric transport of ozone and precursors over Africa: two numerical case studies in dry and wet seasons* , Atmos. Chem. Phys.,7, 5357-5370, 2007.

[109] Scott, R.K and Cammas, J. P., *Wave Breaking and Mixing at the Subtropical Tropopause*, American Meteorological Society, 2002.

[110] Seinfeld, J. and Pandis, S.,*Atmospheric Chemsity and Physics.* , Hoboken, N.J.: John Wiley, 1997.

[111] Seinfeld ,J., Pandis, S., *Atmospheric Chemistry and Physics, From Air Pollution to Climate Change*, John Wiley Sons, inc, Second ed., 2006.

[112] Semeniuk, K., and Shepherd, T. G., *Mechanisms for tropical upwelling in the stratosphere.* , J. Atmos. Sci., 2002a.

[113] Semeniuk, K., and Shepherd, T. G., *The middle atmosphere Hadley circulation and equatorial inertial adjustment*, J. Atmos. Sci., 2002b.

[114] Sheperd, T. G., *Large-Scale Atmospheric Dynamics for Atmospheric Chemists.*, Chem. Rev., Vol. 103, 4509 -4531, 2003.

[115] Shibata, K, and Deushi, M, *Long range variations and trends in the simulation and trends in the simulation of middle atmosphere 1980-2004 by the chemistry climate model of the Meteorological Research Institute*, Ann. Geophysics, 26, 1299-1326, 2008.

[116] Sinha, A. and Harries, J. E. *Water vapor and greenhouse trapping the role of far-infrared absorption*, J. Geophys. Res., 22, 2147-2150, 1995.

[117] Sobel, A.H., and Plumb, R.A. *Quantitative diagnostics of mixing in a shallow-water model of the stratosphere.*, J. Atmos. Sci., 56, 2811-2829, 1999.

[118] Staehelin,J , Harris, N. R. Appenzeller ,P., C., and Eberhard ,J., *Ozone trends: a review*, Geophysics, 39, 231-290, 2001.

[119] Stohl, A., Eckhardt, S., Forster, C., James, P., Spichtinger, N., *On the pathways and timescales of intercontinental air pollution transport*, J. Geophys. Res. 107, 4684, 2002.

[120] Susan Solomon, *Stratospheric ozone depletion: A review of concepts and history*, Rev, Geophys, 37, 1999.

[121] Von Bargen, A. and Thomas, W.,*GOME GDP Update Report for GDP 0-to-1 Version 2.0 and GDP 1-to-2 Version 2.7, ER-TN-DLR-GO-0043*, (Issue 1/A),DLR/DFD, Oberpfaffenhofen, Germany, 1999.

[122] Waugh, D.W., *Impact of potential vorticity intrusions on subtropical upper tropospheric humidity*, J. Geophys. Res., 110, D11305,doi:10.1029/2004JD005664, 2005.

[123] Wickert J,A., Gobiet, G. Beyerie, A.K, Steiner,G, Kirchengast, U., Foelsche, and Schmidt,T, *GPS radio occultation with CHAMP: Comparision of atmospheric profiles from GFZ Postsdam and IGAM Graz, in Eatth observation with CHAMP: Coparison of atmospheric profiles from GFZ potsdam and IGAM Graz,in Earth observation with CHAMP - Results from three years in orbit,*, C. Reigber, H. Lhr,P.

Schwintzer, and J.Wickert (Eds.), Springer, Berlin-Heidelberg-New York, 525-530, 2005.

[124] Woods, T. N., et al., *Validation of the UARS Solar Ultraviolet Irradiance: Comparison With the Atlas 1-2 Measurements*, J. Geophys. Res., 1996.

[125] World Meteorological Organization, *WMO Statement on the status of the Global Climate in 2003*,WMO-No. 966, 2004.

[126] Yienger, J. and H. L. II, *Empirical model of global soil-biogenic NO_x emissions*, Geophys. Res., Vol. 100, 11447-11464, 1995.

[127] Zachariasse, M.,Smit, H. G. J.,van Velthoven, P. F. J. , and Kelder, H., *Crosstropopause and interhemispheric transports into the tropical free troposphere over the Indian Ocean,*, J. Geophys. Res.,06, 28,441- 28,452, 2001.

[128] Zbinden, R. M., Cammas, J. P., Thouret, V., Nedelec, P., Karcher, F., Simon, P., *Mid-latitudetropospheric ozone columns fromthe mozaic program: climatologyand interannualvariability*, Atmos. Chem. Phys. Discuss. 6, 1053 -1073, 2006.

[129] Zeldovich, Y. and Raizer, Y., *Rates of relexation processes in gases (8/9)* , Physics of Shock Waves and High-Temperature Hydrodynamic Phenomena, Vol. 1, 374-382, 1967

Declaration

This thesis is my original work, has not been presented for a degree in any other University and that all the sources of material used for the thesis have been dully acknowledged.

Name: Kassahun Ture

Signature:

Place and time of submission: Addis Ababa University, July 2011

This thesis has been submitted for examination with my approval as University advisor.

Name: Dr. Gizaw. Mengistu

Signature: